Andean Geology 47 (2): 207-255. May, 2020
doi: 10.5027/andgeoV47n2-3118

Andean Geology
www.andeangeology.cl

Stratigraphic and provenance analysis of Triassic rock units between 28-29° S, northern Chile: implications on the tectonic and paleogeographic evolution of the southwestern margin of Gondwana

[*]Esteban Salazar[1], Paulina Vásquez[1], Daniela Vallejos[2], Christian Creixell[1], Verónica Oliveros[3], Mihai N. Ducea[4, 5]

[1] *Servicio Nacional de Geología y Minería, Santa María 0104, Santiago, Chile.*
esteban.salazar@sernageomin.cl; paulina.vasquez@sernageomin.cl; christian.creixell@sernageomin.cl
[2] *Empresa Nacional del Petróleo, Casilla 247, Punta Arenas, Chile.*
daniela.vallejos.t@gmail.com
[3] *Departamento de Ciencias de la Tierra, Universidad de Concepción, Edmundo Larenas 129, Casilla 160-C, Concepción, Chile.*
voliveros@udec.cl
[4] *Departament of Geosciences, University of Arizona, 1040 E 4th Street, Tucson, AZ 85721, USA.*
ducea@email.arizona.edu
[5] *Faculty of Geology and Geophysics, University of Bucharest, 010041, Bucharest, Romania.*

** Corresponding author: esteban.salazar@sernageomin.cl*

ABSTRACT. Triassic rock units of northern Chile (28-29° S) record the transition, both in time and space, between two major orogenies that affected the southwestern margin of South America, the Gondwanian and Andean orogenies. The geodynamic configuration of the margin during this transition is still a matter of debate, particularly whether subduction was interrupted or continued under different parameters in between the orogenies. In order to evaluate these hypotheses by understanding the paleogeographic evolution of the margin, this work synthesizes recent stratigraphical, structural and geochronological data from northern Chile (28-29° S), along with detrital zircon analysis and detritus characterization of the two main siliciclastic Triassic basins present in the area. A detailed study of the evolution of the San Félix and the Canto del Agua basins, their source areas, and exhumation processes of the margin recognizes two stages of intra-arc/forearc basins system development separated by a Carnian unconformity. The first stage (Lopingian-uppermost Middle Triassic) develops an eastern intra-arc basin, which is represented by the volcaniclastic rocks included in the Guanaco Sonso Formation and the roots of the volcanic arc represented by Chollay Plutonic Complex, bounded to the east by a Pennsylvanian-Cisuralian basement block. The forearc basin for this stage is constituted by two graben depocenter, separated by a topographic high, of marine to transitional depositional environment and proximal sediment sources. The eastern graben is filled by conglomerates and turbiditic rocks grouped in Members M1 to M4 of the San Félix Formation, and the western graben, by sedimentary and volcanic rocks of the lower section of the Canto del Agua Formation. The second stage (Norian-Rhaetian) involves an eastern intra-arc basin, represented by the volcanic rocks of the La Totora Formation that seals the exhumed roots of the magmatic arc developed in the previous stage, and a marine to transitional forearc basin to the west, represented by the sedimentary rocks of M5 member of the San Félix Formation and the upper section of the Canto del Agua Formation. These two successions show basal fluvial conglomerates unconformably overlying Anisian prodelta deposits of the first stage, recording a major base level drop of the forearc basin.

Keywords: Triassic, Gondwana, Paleogeography, Intra-arc basin, Forearc basin, Carnian unconformity.

RESUMEN. Análisis estratigráfico y de proveniencia de unidades de rocas triásicas entre los 28-29° S, norte de Chile: implicancias en la evolución tectónica y paleogeográfica del margen suroccidental de Gondwana. Las unidades de roca triásicas del norte de Chile registran la etapa transicional entre dos orogenias mayores que afectaron el margen suroccidental de Sudamérica, las orogenias Gondwánica y Andina. Aún no existe consenso respecto de la configuración geodinámica del margen durante esta transición, y en particular, si es que la subducción se vio interrumpida o si fue continua, pero con distintos parámetros de convergencia. Con el fin de evaluar estas hipótesis por medio del entendimiento de la evolución paleogeográfica del margen, en este trabajo se realiza una síntesis de los datos estratigráficos, estructurales y geocronológicos del norte de Chile (28-29° S), incluyendo además análisis de circones detríticos y caracterización de detritos de las dos principales cuencas sedimentaria-clásticas del Triásico, presentes en el área. Un análisis detallado de la evolución de las cuencas de San Félix y Canto del Agua, sus áreas fuente y procesos de exhumación del margen, revela el desarrollo en dos etapas del sistema de cuenca de antearco/intrarco, separadas por una discordancia de edad carniense. En la primera etapa (Lopingiense-Triásico Medio alto) se desarrolla una cuenca de intrarco hacia el este, representada por las rocas volcanoclásticas de la Formación Guanaco Sonso y el Complejo Plutónico Chollay que representa las raíces del arco volcánico, limitada al oeste por un bloque de basamento pensilvánico-cisuraliense. El antearco de esta etapa se constituye por depocentros tipo graben, separados por un alto topográfico, de ambiente depositacional marino a transicional y fuentes de aporte sedimentario proximales. El graben oriental está relleno de rocas conglomerádicas y turbidíticas agrupadas en los miembros M1 a M4 de la Formación San Félix, mientras el graben occidental, de rocas sedimentarias y volcánicas de la sección inferior de la Formación Canto del Agua. La segunda etapa (Noriense-Rhaetiense) involucra una cuenca de intrarco, representada por las rocas volcánicas de la Formación La Totora que sella las raíces exhumadas del arco volcánico que se desarrolló en la etapa anterior, y una cuenca de antearco de ambiente marino a transicional, representada por las rocas sedimentarias del Miembro M5 de la Formación San Félix y la sección superior de la Formación Canto del Agua. Estas dos sucesiones presentan conglomerados fluviales basales que cubren discordantemente depósitos de prodelta de edad anisiana de la etapa anterior, registrando una gran caída del nivel de base en el antearco durante el carniense.

Palabras clave: Triásico, Gondwana, Paleogeografía, Cuenca de intrarco, Cuenca de antearco, Discordancia del Carniense.

1. Introduction

In the southwestern South American margin Early Triassic to Early Jurassic rock units record the transition, both in time and space, between two major orogenies, the Gondwanean and the Andean. The changes that occurred between these orogenies include: westward shift of the magmatic locus, modifications in deformation style, magmatism and metamorphism (Fig. 1). These changes reveal an important contrast in the geodynamical configuration of the continental margin. The current hypotheses about the geodynamic setting of northern Chile during this period are divergent (Fig. 1 inset). On one hand, one model postulates continental rifting and arrested subduction (Mpodozis and Kay, 1992). For this model, some authors propose that during the Triassic-Lower Jurassic there were extensional basins with fast subsidence characterized by continental and marine sedimentation with abundant volcanoclastic rocks of felsic to intermediate composition (Fig. 1; Charrier, 1979; Uliana and Biddle, 1988; Franzese and Spalletti, 2001). The NW-SE to NNW-SSE orientations of these basins would be controlled by the reactivation of Paleozoic structures inherited from the accretionary history of the margin (Ramos, 1994; Franzese and Spalletti, 2001). On the other hand, recent studies based on geochemical data postulate a setting with continuous subduction under extensional or transtensive tectonic regime (Vásquez *et al.*, 2011; Del Rey *et al.*, 2016; Coloma *et al.*, 2017). Most of these hypotheses are used as generalized models for the whole southwestern Gondwana margin; nevertheless, stratigraphical and geochronological data to support both hypotheses is rather limited.

In northern Chile, between the 28° and 29° S, Permian to Lower Jurassic rocks crop out widely from the coastline to the Andean water divide (*i.e.*, Chile-Argentina international border, Fig. 1). These rock units include clastic sedimentary successions, volcanic successions, and plutonic and metamorphic complexes (Reutter, 1974; Moscoso and Covacevich, 1982; Ribba *et al.,* 1988; Mpodozis and Kay, 1992; Welkner *et al.,* 2006; Murillo *et al.,* 2013; Salazar *et al.,* 2013; Salazar and Coloma, 2016; Figs. 2 and 3). Such wide variety of Permian-Triassic rocks offers a unique record for the surface and subsurface geological processes that took place in the Gondwanean margin during the end of the Gondwanides and the birth of the early Andean Orogenic Cycle.

In this contribution, we present a complete revision of the Permian to Triassic stratigraphy of northern

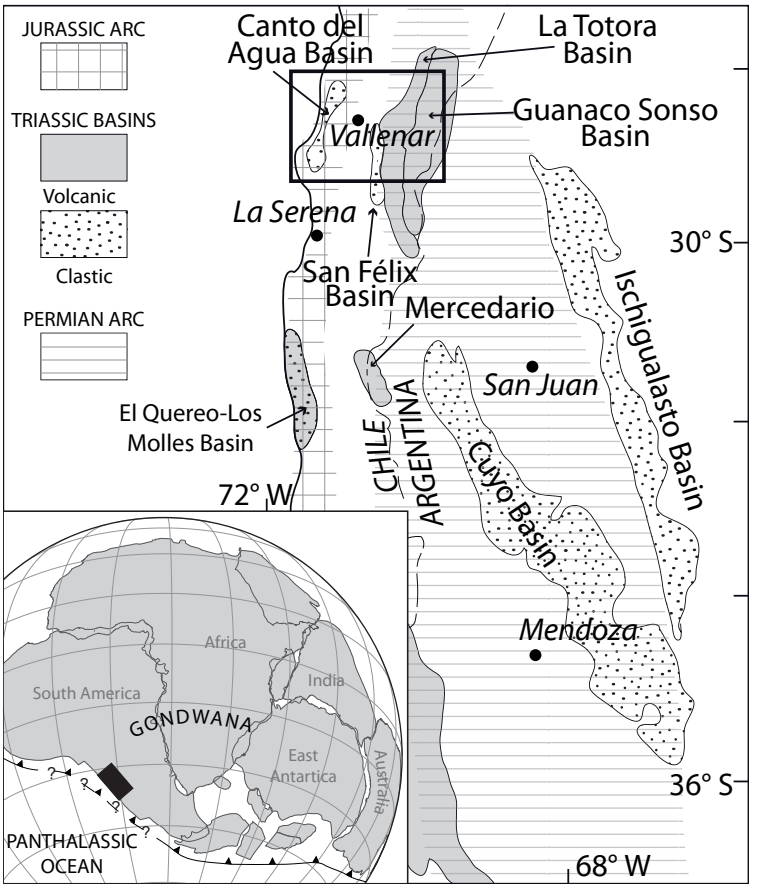

FIG. 1. Location and regional geological context of the study area. Features distribution in Chile and Argentina modified from Charrier *et al.* (2007) and Franzese and Spalletti (2001), Gondwana reconstruction modified from Torsvik and Cocks (2013) and Castillo *et al.* (2017) and references therein. .

Chile between 28° and 29° S, both in the Frontal and Coastal cordilleras. Then, through U-Pb detrital zircons analysis and sediment characterization, we study their depositional ages, possible sources and genetic relationship between different basins, to then elucidate the exhumation history of the margin. Finally, we study the paleogeographic evolution in this area through a comparison between the different Triassic rock units and evaluate the possible geodynamic configuration of the margin.

2. Pre-Triassic Stratigraphy

The oldest rocks in the study area are of Paleozoic age. These units outcrop as N-S oriented belts both in the Frontal and Coastal Cordilleras. Pre-Triassic rock units on the Frontal Cordillera constitute the basement where the San Félix, Guanaco Sonso and La Totora basins developed, while the ones outcropping in the Coastal Cordillera nested the Canto del Agua basin.

2.1 Frontal Cordillera

2.1.1. Ordovician-Missisipian

The oldest rock in the studied segment correspond to those included in the El Cepo and El Tránsito Metamorphic Complexes (ECMC and ETMC, respectively), cropping out in the western part of Frontal Cordillera, and the Las Placetas Formation, in the eastern part (Fig. 2). The ECMC is exposed as small isolated xenoliths of phyllites and mica schists within Pennsylvanian plutons in the southernmost part of the study area (Fig. 2) whose maximal depositional age is Ordovician (Ortiz and Merino, 2015; Table 1).

The Las Placetas Formation is composed of a 500 m thick pile of low grade metagrawackes

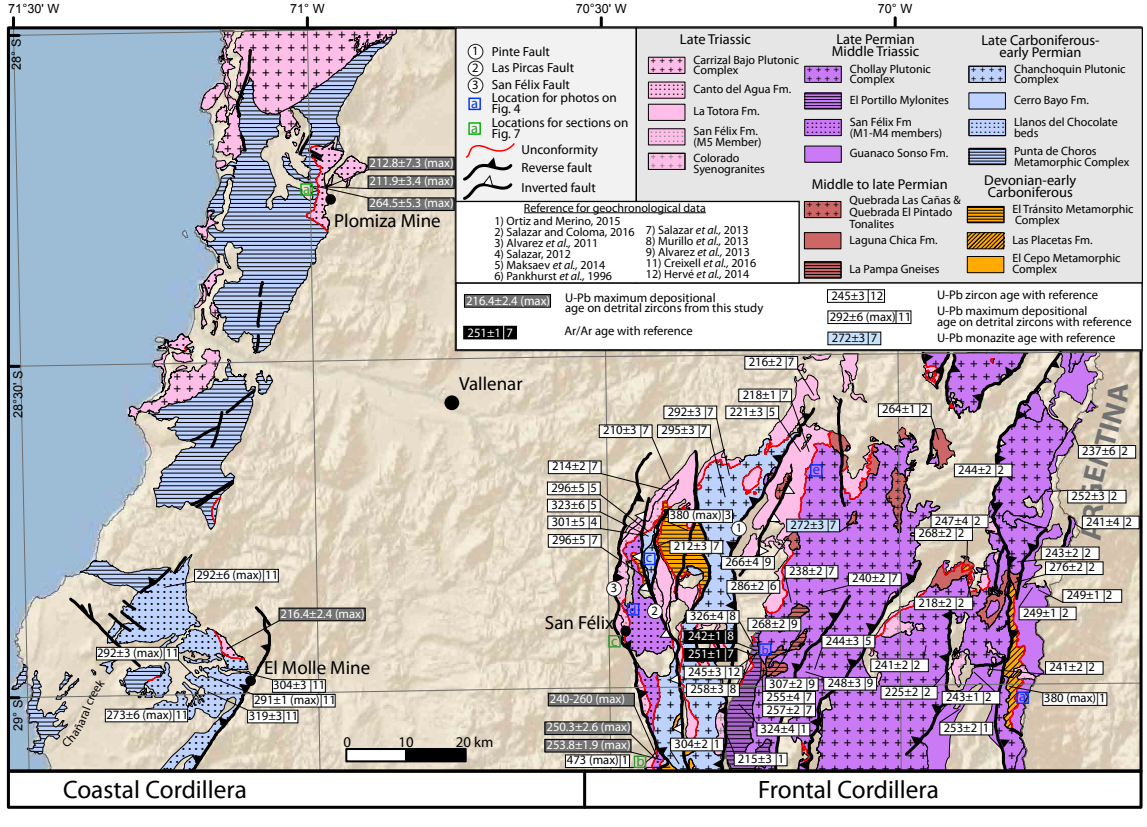

FIG. 2. Distribution of Paleozoic to Triassic Units in the study area and geochronological data referenced in the text. Modified from Arévalo and Welkner (2008), Salazar *et al.* (2013), Ortiz and Merino (2015), Creixell *et al.* (2016) and Salazar and Coloma (2016).

TABLE 1. PUBLISHED GEOCHRONOLOGICAL DATA AND LITHOLOGICAL CHARACTERISTIC OF POTENTIAL ZIRCON SOURCES FOR THE TRIASSIC CLASTIC BASINS.

	Units	Lithology	Age	Main Stratigraphic relationship
Frontal Cordillera	El Cepo Metamorphic Complex	Xenoliths of phyllites and mica schists	U-Pb zircon maximum depositional age for the protolith: 450-490 Ma. Other populations: 1.3-1.6 Ga, 990-1100 Ma, *ca.* 640 Ma *ca.* 520 Ma (1)	-
	Las Placetas Formation	Low grade metagrawackes and metapelites	U-Pb zircon maximum depositional age of 377 Ma. Other Populations: 1.8-2 Ga, 1.2-1.3 Ga, 0.9-1.2 Ga, 750-520 Ma, 520-420 Ma (1 and 2)	Unconformable covered by the Guanaco Sonso and Laguna Chica Fms.
	ETMC (El Tránsito Metamorphic Complex)	Metabasites, quartz-mica schists, nodular albite-schists, quartzites and marbles	U-Pb zircon maximum depositional age: *ca.* 380 Ma. Other populations: 3 Ga; 2.7 Ga; 2 Ga; 1.7 Ga; 1.1 Ga; 867 Ma; 662 Ma; 626 Ma; 596 Ma; 569 Ma; 554 Ma; 535 Ma; 504 Ma; 492 Ma; 464 Ma; 390-380 Ma (3)	Unconformably covered by the San Félix Fm.
	Cerro Bayo Formation	Dacitic and rhyolitic volcaniclastic rocks	crystalization U-Pb zircon ages: 301±5 Ma (4); 325±4 Ma; 323±6 Ma (5).	Unconformably covered by the San Félix Fm.
	Chanchoquín Plutonic Complex	Granodiorites, monzogranites, tonalities and diorites	crystallization U-Pb zircon ages: 286±2 Ma (6); 292±3 Ma; 296±5 Ma; 295±3 Ma (7); 304±2 Ma (1)	Unconformably covered by the San Félix Fm.
	EPM (El Portillo Mylonites)	Metadiorites and metatonalites	Protolith U-Pb zr ages: 324±4 Ma (1); 326±4 Ma; 258±3 Ma (8). Deformation Ar/Ar amphibole age: 251±1 Ma (7). Deformation Ar/Ar white mica age 242±1 Ma (8)	Unconformably covered by the La Totora Fm.
	Laguna Chica Formation	Dacitic and rhyolitic volcaniclastic rocks.	crystallization U-Pb zircon ages: 264±1 Ma; 268±2 Ma; 276±2 Ma (2)	Unconformably covered by the Guanaco Sonso Fm. Unformably covers the Las Placetas Fm.
	Quebrada El Pintado Tonalite	Biotite bearing tonalite	crystalization U-Pb monazite age: 272±3 Ma (7); U-Pb zr age 266±4 Ma (9)	-
	Quebrada Las Cañas Tonalite	Amphibole and biotite bearing tonalite	crystallization U-Pb zircon ages: 257±2 Ma; 255±4 Ma (7)	-
	La Pampa Gneiss	Sillimanite and cordierite gneisses	crystallization U-Pb zircon protolith age: 307±2 Ma (9). U-Pb zircon metamorphic peak age: 268±2 Ma (9)	-
	Guanaco Sonso Formation	Rhyolitic welded tuffs and dacitic volcanic rocks with minor siliciclastic rocks	crystallization U-Pb zircon age: 237±6 Ma; 241±4 Ma; 241±2 Ma; 243±1 Ma; 247±4 Ma; 249±1 Ma; 249±1 Ma; 252±3 Ma (2), 253±2 Ma (1)	Unconformably covers the Las Placetas and Laguna Chica Fms.
	Chollay Plutonic Complex	Amphibole-and biotite-bearing monzogranites, gabbros and tonalites	crystallization U-Pb zircon ages: 244±2 Ma; 241±2 Ma; 243±2 Ma (2); 240±2 Ma; 247±3 Ma; 237±2 Ma (7); 242±3 Ma; 248±3 Ma (9); 244±3 Ma (5)	Covered by the La Totora Fm.
	Pastos Blancos Formation (*)	Rhyolitic to dacitic tuffs and lavas and minor andesites	crystallization U-Pb zircon ages: 222±2 Ma; 224±2 Ma; 232±2 Ma (5); 216±2 Ma; 221±2 Ma; 222±1 Ma; 230±1 Ma; 232±1 Ma (1)	Unconformably covers the Chollay Plutonic Complex
	Colorado syenogranites	Syenogranites	crystallization U-Pb zircon age: 225±2 Ma (2)	-
	La Totora Formation	Andesitic lavas and tuffs	crystallization U-Pb zircon ages: 210±3 Ma; 216±2 Ma; 218±1 Ma (7); 221±3 Ma (5); 218±2 Ma (2)	Unconformably covers the Chollay Plutonic Complex and the EPM
Coastal Cordillera	PCMC (Punta Choros Metamorphic Complex)	Micaschist, metaturbidites and metabasites.	U-Pb zr protolith age: 334±6 Ma (10). Metamorphic Ar/Ar amphibole age: 319±1 Ma (11). Metamorphic Ar/Ar white mica age: 260.7±1 Ma (11).	Unconformably covered by the Llanos del Chocolate Beds. Covered in onlap by the Canto del Agua Fm.
	Llanos del Chocolate Beds	Conglomerates, sandstones, mudstones, limestones and locally dacites and tuffs	Crystallization U-Pb zircon ages: 304±3 Ma and 319±3 Ma (11). U-Pb zircon maximum depositional age: 292±6 Ma; 292±3 Ma; 291±1 Ma; 273±6 Ma (11).	Covers the Punta de Choros Metamorphic Complex and is covered by the Canto del Agua Fm.

(**1**) Ortiz and Merino, 2015; (**2**) Salazar and Coloma, 2016; (**3**) Álvarez *et al*., 2011; (**4**) Salazar, 2012; (**5**) Maksaev *et al*., 2014; (**6**) Pankhurst *et al*., 1996; (**7**) Salazar *et al*., 2013; (**8**) Murillo *et al*., 2013; (**9**) Álvarez *et al*., 2013; (**10**) Navarro, 2013; (**11**) Creixell *et al*., 2016; (*) exposed immediately south of the study area.

and metapelites with quartz, muscovite, chlorite and biotite as main minerals, whose fossil content indicates a Late Devonian to early Carbonifeous age (*Haplostigma furquei* Frenguelli) which is consistent with published maximum depositional ages (Table 1; Salazar and Coloma, 2016) and contact relationships (Fig. 4A).

The ETMC is composed of metabasites, quartz-mica schists, nodular albite-schists, quartz-amphibole schists, quartzites and marbles and has been interpreted as a petrotectonic association of an accretionary prism (Ribba *et al.,* 1988) with a maximum depositional age of 370 Ma (Table 1; Álvarez *et al.*, 2011). Bahlburg *et al.* (2009) also reported U-Pb ages on detrital zircon rims for the ETMC from an uncertain location, between 250 and 370 Ma. This younger age distribution is more similar to that obtained from the overlying Triassic San Félix Formation (see section 3.2.1), and therefore this data is not considered in the discussion.

2.1.2. Pennsylvanian to Cisuralian

Rock units of this age crop out in the western part of the Frontal Cordillera forming a NS belt of plutonic and volcanic rocks, defined as the Chanchoquín Plutonic Complex, the Quebrada Pinte Diorites (protolith of the El Portillo Mylonite) and the Cerro Bayo Formation (Fig. 2; Salazar *et al*., 2013). The Cerro Bayo Formation is composed of rhyolitic to dacitic volcaniclastics with U-Pb zircon ages ranging from 301 to 325 Ma (Table 1; Salazar 2012; Maksaev *et al*., 2014), and is intruded by the penecontemporaneous Chanchoquín Plutonic Complex, composed by coarse grained granodiorites, monzogranites and foliated tonalites with U-Pb zircon ages from 286 to 296 Ma (Table 1; Fig. 2; Pankhurst *et al*., 1996; Salazar *et al*., 2013). The easternmost remnant of this plutonism is the Quebrada Pinte Diorites, outcropping east of the Pinte fault (Fig. 2), with U-Pb zircon ages of 324 and 326 Ma (Table 1; Ortiz and Merino, 2015; Murillo *et al*., 2013) which is one of the protoliths of Middle Triassic El Portillo Mylonites (Table 1; Fig. 3; Murillo *et al*., 2013).

2.1.3. Cisuralian to Lopingian

Eastward of the Carboniferous magmatic belt a Permian N-S trending magmatic belt crops out composed by isolated outcrops or rhyodacitic pyroclastic rocks (Laguna Chica Formation), tonalitic intrusives (Quebrada El Pintado and Quebrada Las Cañas tonalites) and metamorphic rocks as xenoliths within the Triassic Chollay Plutonic Complex (La Pampa Gneisses; Fig. 2; Table 1). The Laguna Chica Formation is a dacitic to rhyolitic volcaniclastic unit that lies unconformably on the Las Placetas Formation rocks, is intruded by the Triassic Chollay Plutonic Complex, and has reported U-Pb zircon ages between 264 and 276 Ma (Salazar and Coloma, 2016). Middle to upper Permian tonalitic units have U-Pb zircon ages ranging from 255 to 270 Ma (Salazar *et al.*, 2013), commonly show penetrative magmatic foliation marked by orientation of plagioclase, amphiboles and biotite crystals and also constitute a protolith of the El Portillo Mylonites. Metamorphic rocks of this age are assigned to the La Pampa Gneisses (Ribba, 1985; Salazar *et al.*, 2013), sillimanite and cordierite bearing gneisses where Álvarez *et al.* (2013) interpreted a peak of metamorphic conditions between 5.1 and 5.6 kbar and 709-779 °C at 268±2 Ma (Fig. 2).

2.2. Coastal Cordillera

2.2.1. Pennsylvanian to Cisuralian

The pre-Triassic basement in the Coastal Cordillera in the studied segment is composed by two units, the Punta de Choros Metamorphic Complex (PCMC, Carboniferous) (Creixell *et al.*, 2012) and the sedimentary rocks of the Llanos del Chocolate Beds (Carboniferous-Permian) (Welkner *et al.*, 2006; Creixell *et al.,* 2016). The PCMC consists of an association of mica schist, metaturbidites and metabasites with a very low to low grade of metamorphism up until greenschist facies with local occurrences of amphibolites facies (Creixell *et al.*, 2012; Navarro, 2013). The former reports a metamorphic peak at 319±3 Ma, based on amphibole Ar/Ar age and a U-Pb detrital zircon maximum depositional age of 334±6 Ma for its protolith, which indicates a deposition age during the Carboniferous. The Llanos del Chocolate Beds is preserved directly to the east of the PCMC as a thick (*ca*. 1,300 m) sedimentary sequence (Creixell *et al.,* 2016). This unit is composed by conglomerates, sandstones, mudstones, limestones and locally exposed dacite domes and tuffs with minor or no metamorphism (Creixell *et al.,* 2016). Two crystallization zircon U-Pb ages obtained from dacite lavas of 304±3 and 319±3 Ma and four zircon U-Pb detrital maximum

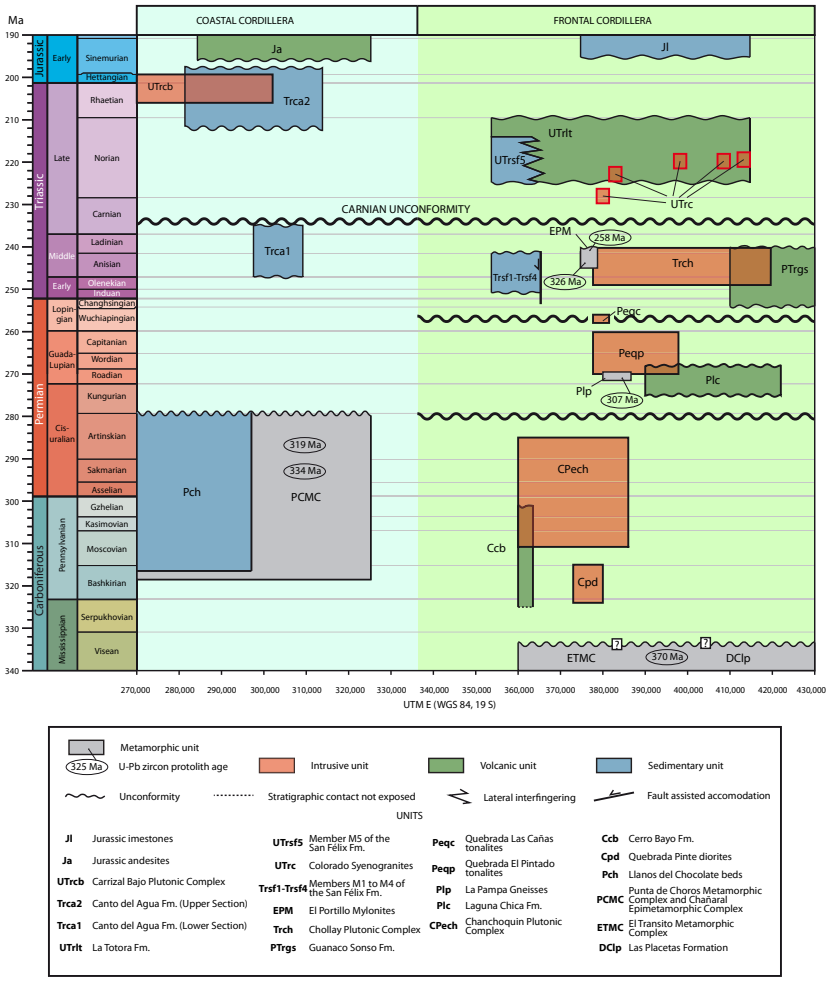

FIG. 3 Chronostratigraphic scheme of the Paleozoic and Triassic units from the Coastal and Frontal Cordilleras in the study area. Based on Cohen *et al.* (2013).

depositional ages between 273 and 292 Ma indicate an upper Carboniferous to Permian age for the sequence (Creixell *et al.,* 2016). These ages are consistent with Permian brachiopod fauna recognized near to the base of this unit (Welkner *et al.*, 2006).

3. Triassic basins in Chile at 28-29° S

3.1. San Félix basin

3.1.1. Stratigraphy

The filling of this basin is exclusively made up by the sedimentary rocks of the San Félix Formation, a NS-striking siliciclastic wedge, reaching up to 6 km in thickness, that crops out along the Del Carmen River (Fig. 4; Reutter, 1974; Ribba, 1985; Salazar, 2012) and is composed by 5 members, M1 through M5, from bottom to top (Ribba, 1985). Members M1 and M5 are dominantly conglomeratic, though the latter also include volcanic intercalations, members M2 and M4 are turbiditic successions, and M3 is composed of sandstones and conglomerates.

Northward and southward of its type locality, the San Félix town, the thickness of the San Félix Formation dramatically diminishes as its members M1 to M4 progressively onlap onto the metamorphic basement (Figs.1 and 4). To the west, the San Félix Formation is truncated by the Late Cretaceous to Tertiary west vergent San Félix Thrust (Salazar *et al.*, 2013) while, to the east,

its thickness is abruptly reduced, as the uppermost member M5 lies directly over the ETMC, east of the high angle Las Pircas fault (Figs. 2, 3 and 4C). The topmost member of the San Félix Formation unconformably overlies the M4 Member (Fig. 4D) and the ETMC (Fig. 4C), to the west and east of the Las Pircas fault, respectively, and it laterally interfingers towards the northeast with the lower section of the La Totora Formation.

Fossil marine fauna from member M4 indicate an Anisian age (Fig. 4; Zeil, 1958; Barthel, 1958), which is consistent with the Norian age assigned to the M5 Member by Salazar *et al.* (2013). The only constraint for the initiation of deposition of the San Félix Formation previous to this work is the underlying Pennsylvanian Cerro Bayo Formation (Fig. 4C). Two U-Pb crystallization zircon ages and one detrital zircon age indicate a Norian (middle Upper Triassic) age for the M5 member (Table 1), which is also consistent with paleoflora age determinations (Mohr and Schöner, 1985; Salazar *et al.,* 2013).

3.1.2. Basin evolution and depositional environment

The areal distribution and stratigraphic relationships of the different members of the San Félix Formation led Salazar *et al.* (2013) to differentiate a rift sequence, composed by Member M1 to M4, from a post-rift sequence, represented by the M5 Member. Moreover, to the east of Las Pircas fault the M5 member lies directly on metamorphic basement (Figs. 2 and 4C, Table 1), implying that this fault accommodated members M1 through M4 of the San Félix Formation during the Early and Middle Triassic, ending its activity in the Late Triassic, when it was covered and sealed by the M5 Member and the La Totora Formation (Fig. 3), hence representing the eastern border fault of the San Félix basin.

Sedimentological studies interpret the San Félix Formation (Triassic) as a marine fan delta depositional system, where conglomeratic members M1 and M5 correspond to delta plain fluvial system, fine grained M2 and M4 members correspond to prodelta environments and the sandy to conglomeratic M3 member as the upper part of the delta slope, with episodic subaerial exposure (Reutter, 1974; Ribba, 1985; Bell and Suárez, 1994; Padel *et al.,* 2012; Salazar *et al.,* 2013). Published geochronological data show a depositional gap between members M4 and M5 of at least 20 Ma (Zeil, 1958; Barthel, 1958; Ribba, 1985; Salazar *et al.,* 2013; Fig. 3) which suggests that the topmost M5 member of the formation represents a fluvial system within a different geological context, likely influenced by the volcanic processes related to the La Totora Formation, since these two units laterally interfinger (Table 1).

3.2. Guanaco Sonso basin

3.2.1. Stratigraphy

The units involved in the configuration of this basin are the Guanaco Sonso Formation, the Chollay Plutonic Complex and the El Portillo Mylonites. The volcaniclastic Guanaco Sonso Formation corresponds to the filling of the basin, which is contemporaneous and partially intruded by the granitic Chollay Plutonic Complex. Both of these units are bounded to the west by the mylonitic NS trending belt of the El Portillo Mylonites.

Guanaco Sonso Formation. The Guanaco Sonso Formation (Martin *et al.*, 1999) consists in a volcaniclastic succession cropping out in the eastern part of the Frontal Cordillera (Fig. 2). It covers, in an angular unconformity, the Late Devonian Las Placetas Forma-tion (Fig. 4A) and the Guadalupian Laguna Chica Formation, and is intruded by penecontemporaneous granites of the Chollay Plutonic Complex. It is best exposed close to the Chile-Argentina international border, where it reaches nearly 300 m in thickness and is unconformably covered by Paleocene to Miocene strata. It is composed of basalts at the base, and dacitic to rhyolitic tuffs and lavas with sandstones, conglomerates and mudstone intercalations towards the top (Salazar and Coloma, 2016).

The Guanaco Sonso Formation was originally assigned a Guadalupian (middle Permian) age, based on multigrain U-Pb zircon ages (Martin *et al.*, 1999; Charchaflié, 2003), however, recently, a series of single grain LA-ICP-MS U-Pb zircon ages obtained by Ortiz and Merino (2015) and Salazar and Coloma (2016), including an age in its type locality, allowed these authors to reassign this unit to an age range between 254 and 237 Ma, arguing that the presence of inherited populations of Cisularian to Guadalupian age identified in their analysis, would account for the older multigrain ages previously published.

Chollay Plutonic Complex. The Chollay Plutonic Complex is the most widely exposed unit in the Chilean

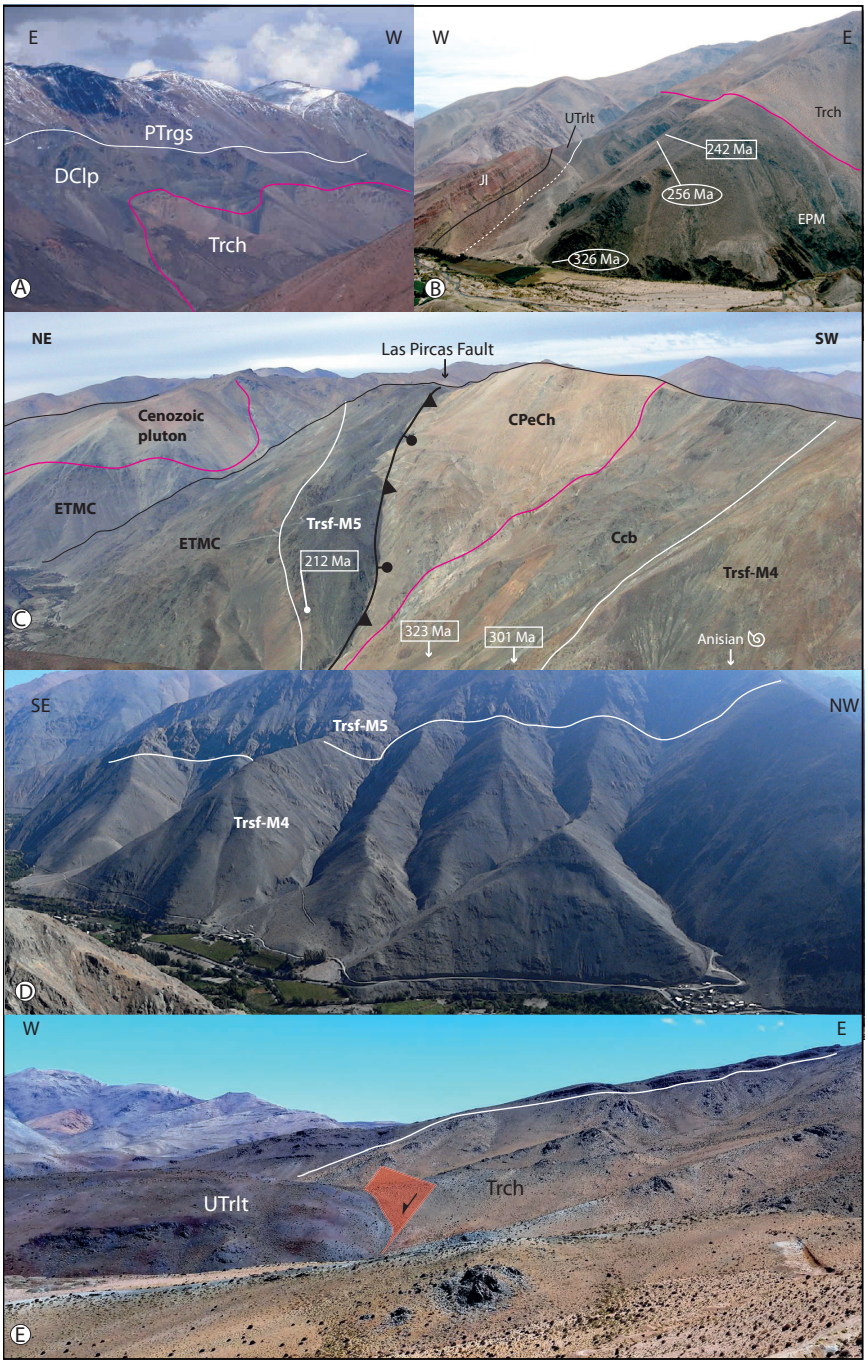

FIG. 4. Field photographs of main contact relationships mentioned in the text. Photographs are taken from areas shown in figure 2 and they are also indicated in the block diagrams of figure 8. Pink lines are intrusion contact and white lines are unconformities. Units abbreviation same as in figure 3. **A.** Valeriano river, highest peaks constitute the Chile-Argentina international border; **B.** Northeastern slope of the El Tránsito river, el Portillo locality. Ovals and square show protolith and deformation ages, respectively, obtained by Murillo *et al.* (2013); **C.** Southern slope of the El Tránsito river, near the conjunction with the Del Carmen river. Square show tuff U-Pb ages by Salazar *et al.* (2013); **D.** Del Carmen river, western slope. Unconformity between members M4 and M5 of the San Félix Formation; **E.** Eastern slope of the La Totora creek, red polygon represents a normal fault synchronous with the deposition of the La Totora Formation.

Frontal Cordillera (Fig. 2). It intrudes Devonian metasediments of the Las Placetas Formation (Fig. 4A) and, in a minor extent, the penecontemporaneous Guanaco Sonso Formation. This plutonic complex is intruded by Late Triassic Plutons of the Colorado syenogranites and Cenozoic granitoids, as is unconformably covered by the Late Triassic La Totora Formation and younger stratified units (Fig. 2; Salazar *et al.*, 2013; Salazar and Coloma, 2016).

It is composed of diorites, tonalities, granodiorites, monzogranites and syenogranites, being monzogranites the dominant lithology, which is commonly coarse-grained with abundant graphic and perthitic textures. Biotite and amphibole are the dominant ferromagnesian phases (Salazar *et al.*, 2013; Salazar and Coloma, 2016).

Nine U-Pb zircon ages obtained by several authors in the study area (Álvarez *et al.*, 2011; Salazar *et al.*, 2013; Maksaev *et al.*, 2014; Salazar and Coloma, 2016) allows to constraint the construction of this plutonic complex between 248 and 237 Ma (Lower-Middle Triassic) (Table 1).

El Portillo Mylonites. El Portillo Mylonites, was described by Ribba *et al.* (1988) as a thin 10 km long fringe of mylonitic rocks located east of the Pinte fault trace (Fig. 2). This unit includes mylonitized portions of the Quebrada Pinte Diorites and Las Cañas Tonalites (Salazar *et al*., 2013), which are host rocks of the Chollay Plutonic Complex, and is unconformably covered by the Late Triassic La Totora Formation (Fig. 4B).

Lithologically, it is composed by bands of metadiorites, metatonalites and metagranodiorites crosscut by granitic bands, all of these present variable degrees of mylonitization and with a dominant vertical and NS oriented foliation with left-lateral shear sense (Murillo *et al.*, 2013).

Two SHRIMP U-Pb ages on zircon nuclei, obtained by Murillo *et al.* (2013), of 326±4 and 256±3 Ma are consistent with the age range of the protoliths Quebrada Pinte Diorites (*ca.* 324 Ma) and Las Cañas Tonalites (255-257 Ma; Table 1). On the other hand, Hervé *et al.* (2014) obtained a 245±2.3 Ma SHRIMP U-Pb zircon age in the granitic band near the intrusive contact with the Chollay Plutonic Complex, very similar to an Ar/Ar age of 241.9±0.5 Ma reported by Murillo *et al.* (2013) from dynamically deformed muscovite, indicative of left lateral shear sense, and to the U-Pb age range published for the Chollay Plutonic Complex (248-237 Ma; Salazar *et al.*, 2013; Table 1), which supports a genetic relationship between the last mylonitization event recorded in the El Portillo Mylonites and the construction of the Chollay Plutonic Complex.

3.2.2. Basin depositional environment

Published studies focused on depositional processes and environment for the rocks of the Guanaco Sonso Formation (Lower to Middle Triassic) are scarce (López *et al.,* 2015; Salazar and Coloma, 2016). Based on volcanic and siliciclastic facies analysis, López *et al.* (2015) interpreted a continental environment with fluvial, alluvial and lacustrine facies associations carrying fossil remains of hydrophilic flora. The volcanic deposits, rhyolitic to basaltic-andesite in composition, evidence hydromagmatic eruptive mechanisms and a strong control exerted by a syndepositional set of bivergent normal fault system of low displacement and wavelength (~15 m and ~50 m, respectively), as the result of low elastic thickness for the basement of the studied volcanic pile during its accumulation (López *et al.*, 2015; Salazar and Coloma, 2016). The latter is interpreted by these authors as consequence of the shallow emplacement of granitic magma bodies of the contemporaneous Chollay Plutonic Complex (Fig. 3; Table 1), which is consistent with the intrusion relationship observed between these two units in some places (Fig. 2) and the section exposed at the Valeriano river (Fig. 4A). These features are characteristic of caldera environments developed over batholith construction sites (Zimmerer and McIntosh, 2012; Branney and Acocella, 2015), as is drainage isolation represented by the lacustrine environment. The Chollay Plutonic Complex, underlying the Guanaco Sonso basin, is bounded to the west by the contemporaneous El Portillo Mylonites (EPM, Table 1), which is a 251-240 Ma left-lateral shear zone (Murillo *et al.,* 2013; Salazar *et al.,* 2013; Hervé *et al.,* 2014) affecting older Carboniferous to Permian plutons (Fig. 2; Table 1).

3.3. La Totora basin

3.3.1. Stratigraphy

La Totora Formation (Reutter, 1974), represents the filling of this basin. It is an andesitic volcanic succession up to 700 m thick. It unconformably covers the ETMC (Late Devonian-Missisipian), Cisularian Granitoids, Guadalupian gneisses and

volcanics, the Chollay Plutonic Complex (Early to Middle Triassic; Fig. 4E) and the El Portillo Mylonites (Middle Triassic; Fig. 4B). In its westernmost outcrops it laterally interfingers and covers the uppermost member of San Félix Formation (M5 Member). It is unconformably covered by Jurassic marine and volcanic rocks (Reutter, 1974; Ribba, 1985; Salazar *et al.*, 2013; Salazar and Coloma, 2016).

This unit is composed of andesitic lavas with aphanitic, amygdaloidal and porphyritic texture, andesitic breccia and minor tuffs.

U-Pb zircon ages range from 210 to 221 Ma (Salazar *et al.*, 2013; Maksaev *et al.*, 2014; Salazar and Coloma, 2016; Table 1) and are consistent with the contact relationships described above. Older U-Pb zircon ages in a basaltic tuff of the basal layer yielded Carboniferous and Early Triassic populations (Maksaev *et al.*, 2014), however, the contact relationships of the unit and composition of the sampled rock, suggest these are inherited ages, not reflecting a depositional age for the unit.

The La Totora Formation is slightly younger than both the Colorado syenogranites, within the study area (Fig. 3 and Table 1; Salazar and Coloma, 2016), and the rhyolitic and dacitic rocks of the Pastos Blancos Formation (232 and 221 Ma; Ortiz and Merino, 2015), located a few km further south.

3.3.2. Basin Configuration

The La Totora basin is a NS elongated depocenter infilled by the dominantly andesitic volcanics of the La Totora Formation (Upper Triassic; 210-221 Ma) and accommodated by normal faults (Fig. 4E; Salazar *et al.,* 2013). The maximum accommodation of this basin occurs as a NS trending axis, immediately east of the Pinte fault (Fig. 2). Along this maximum accommodation domain the volcanic rocks of the La Totora Formation unconformably covers the mylonitic contact (El Portillo Mylonites) between the Chollay Plutonic Complex (Lower to Middle Triassic), to the east, and Carboniferous to early Permian intrusives to the west (Fig. 2). West of the Paleozoic block, the La Totora Formation laterally interfingers with the fluvial sedimentary M5 member of the San Félix Formation, which unconformably covers the prodelta deposits of Anisian (Middle Triassic) M4 Member (Bell and Suárez, 1994; Salazar *et al.,* 2013). Along the eastern shoulder of the La Totora basin the volcanic rocks of the La Totora Formation covers mostly the Chollay Plutonic Complex, while further east, near the international border, it locally covers the volcanics of the Guanaco Sonso Formation (Salazar and Coloma, 2016).

3.4. Canto del Agua basin

3.4.1. Stratigraphy

The Canto del Agua Formation (Moscoso and Covacevich, 1982) consists of a marine, clastic and volcanic succession, with their outcrops discontinuously distributed along the Coastal Cordillera between the 28°30' and 29°10' S. At its type locality, it was described as a 2,100 m thick succession, carrying Anisian, Norian and Early Jurassic fossil fauna, that lies unconformably on the Punta de Choros Metamorphic Complex (Carboniferous) and is covered by andesites and basaltic andesites of Jurassic age (La Negra Formation). At the base of a succession originally assigned to this unit at the Chañaral Creek (29° S), Welkner *et al.* (2006) described Permian brachiopod fauna that led them to define a restricted basal section as Llanos del Chocolate Beds. Recently the contact between Llanos del Chocolate Beds and Canto del Agua Formation has been displaced further upsection at the Chañaral Creek, based on Carboniferous to Permian U-Pb zircon ages obtained by Creixell *et al.* (2016). The latter implies a major stratigraphic discontinuity between Llanos del Chocolate beds and the Canto del Agua Formation which has not been recognized before nor characterized on outcrop.

3.4.2. Basin depositional environment

This unit was initially described by Moscoso (1979) as a marine sequence, on the basis of its lithology and fossil fauna. The distribution of the unit along two localities in the study area suggests it was deposited in distinct depocenters. In the type locality, Moscoso and Covacevich (1982) estimated a total thickness of 2,100 m, whereas in the south, near El Molle mine (29º S), thickness estimations remain under doubt since Creixell *et al.* (2016), on the basis of new U-Pb geochronology, demonstrated that an important portion of the sequence first assigned to this unit, is older and attributed to the Carboniferous to Permian Llanos del Chocolate Beds (Table 1). According to Suárez and Bell (1992), the Canto del Agua basin was developed in a submarine section of a coarse-grained fan delta, and Arévalo and Welkner (2008) proposed that the basin was bounded by two normal faults of WNW strike, active during deposition.

4. Detritus characterization

4.1. Clast and grain composition

4.1.1. San Félix Formation

Fully developed thickness of the San Félix Formation is exposed exclusively in the hanging wall of the west vergent San Félix fault (section location c in Fig. 2), while only a condensed 350 m thick section is exposed in the footwall of the same fault, at the southernmost part of the Carmen river (section location b in Fig. 2), which was sampled for detrital zircon analysis (Figs. 6, 7). The latter section is directly overlying late Carboniferous acid volcanics of the Cerro Bayo Formation (Fig. 2; Table 1). From bottom to top this sequence is made of a basal section of tabular pebbly sandstones, arkosic to lithic in composition, whose lithic component include volcaniclastic, metamorphic and felsic intrusive lithologies and a silicic lithic ash tuff bed. Towards the top of this basal section, the conglomeratic component increases forming clast supported cobbly conglomerates lenses, with concave erosive bases, rounded to subrounded clasts of mainly felsic tuffs and intrusives, and minor metamorphic rocks. Overlying this section there are 70 m of alternating dark mudstones and grey sandstones, the latter occasionally showing groove marks, mudclasts and centimetric diagenetic calcareous nodules. Feldspathic litharenites and wackas cover the former section in an angular unconformity, varying to conglomeratic sandstones towards the top. The lithic component of these sandstones is mainly felsic volcaniclastics, schists and andesites, and the minerals are quartz, plagioclase and muscovite. These beds also carry fossil flora remnants of *Dicroidium odontoperoides* and *Dicroidium zuberi*. A younger section of alternating beds of mudstones and sandstones covers previous sandstones, with a middle section of sandstones and pebbly sandstones, with filled channels structures, cross stratification, mudclasts and abundant felsic volcaniclastics and intrusives and minor metamorphic clasts. Finally this section ends with beds of clast supported conglomerates and sandstones, with abundant concave erosive bases and clasts of felsic composition (volcanic and intrusive) and of polycrystalline quartz. Sandstones are more abundant towards the top, and they are coarse grained, with angular grains and abundant quartz and amphibole.

4.1.2. Canto del Agua Formation

In its type locality, near de Plomiza mine (Fig. 2), this unit onlaps the metamorphic basement (Fig. 2; Table 1). From bottom to top, the section is composed of parallel laminated muddy sandstone with mudstone intercalations bearing Daonella sp.; covered by a section of brown conglomeratic sandstone with subrounded metapelitic clasts (Fig. 5). The upper part of the section is composed of glassy lapilli tuffs and fine-grained sandstone lenses, covered by polimictic orthoconglomerates with clasts of metapelites, acid volcanics and andesites, bearing minor reworked fossil trunks of Calamites sp. Over the conglomerates lies a rhythmic sequence of fissile mudstones that vary to sandstones towards the top, followed by mudstones with minor intercalations of altered volcanic rocks and sandstone to the roof. Above that, there are recrystallized limestones with abundant fossils fragments such as echinoderms, brachiopods, indeterminate shell fragments, allochemical clasts, peloids and minor terrigenous quartz fragments. The top of the section corresponds to a rhythmic sequence of mudstone and muddy sandstone with parallel lamination and flame structures. The sandstones present allochemical components such as peloids, shell fragments and terrigenous components such as feldspar and quartz fragments.

The base of the section of the Canto del Agua Formation at the El Molle mine (Fig. 2) is made up of matrix-supported conglomerates with acid volcanic clasts and a coarse grained sandstone matrix, intercalated with minor conglomeratic and coarse grained sandstones. Clast-supported conglomerate with rounded to sub/rounded, imbricated, poorly-sorted clasts cover the previous strata and are intercalated with centimetric lenses of coarse-grained sandstones. Clasts correspond to rhyolites, acid volcanic rocks, tuffs, microdiorites and metamorphic quartz. The upper beds are coarse-grained cross-bedding sandstone and conglomerates, with clasts of acid volcanics, tuffs and metamorphic lithics. At the top, sandstones and mudstones with parallel lamination, normal-graded and trough cross-bedding bearing bivalves and indeterminate fossils of pelecypodes crop out. The sandstones are composed of tuffaceous and metamorphic lithics, quartz, plagioclase and white mica.

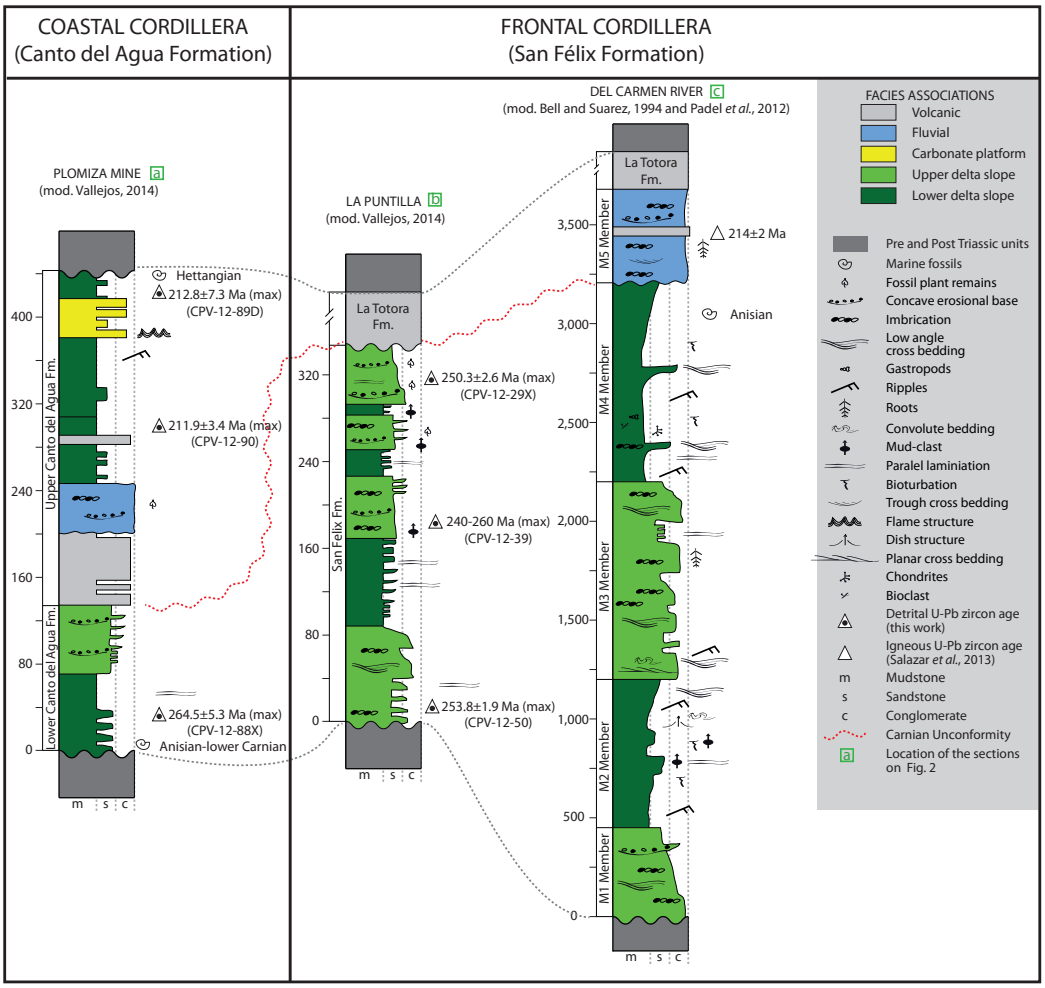

FIG. 5. Stratigraphic sections of the San Félix and Canto del Agua Formations.

4.2. Detrital zircon U-Pb Geochronology

U-Pb data and methodology are included in the supplementary material (Supplementary material 1 and 2, respectively), while concordia and density population diagrams are shown in figures 6 and 7.

4.2.1. Chilean Frontal Cordillera

Detrital zircon U-Pb ages were obtained on samples from the base (CPV-12-50), middle (CPV-12-39) and top sections (CPV-12-29X) of the San Félix Formation exposed at the la Puntilla locality (section b in Figs. 2 and 5).

Detrital zircons (n=98) from a lithic arkose (CPV-12-50) yielded ages between 242 and 339 Ma, with one single older age of 1842.3± 3.7 Ma and three unmixed populations of 253.8± 1.9 Ma, 294.5±0.7 Ma and 329.4±2.1 Ma (Figs. 6 and 7).

Ages from the sample at the middle section (n=95; sample CPV-12-39), a feldspathic litharenite, do not show well defined peaks (Fig. 7), but there is considerable grouping between 240 and 332 Ma, with three poorly defined peaks at 240-260, 280-300 and 310-335 Ma, and isolated results at 478, 849, 995, 1,182 and 1,755 Ma. For the sample from the top of the section, a lithic arkose, detrital zircon U-Pb age populations (n=97; sample CPV-12-29X) range between 341 and 242 Ma and display three well defined peaks at 250.3±2.6, 288.3±2.6 and 328.2±3.1 Ma.

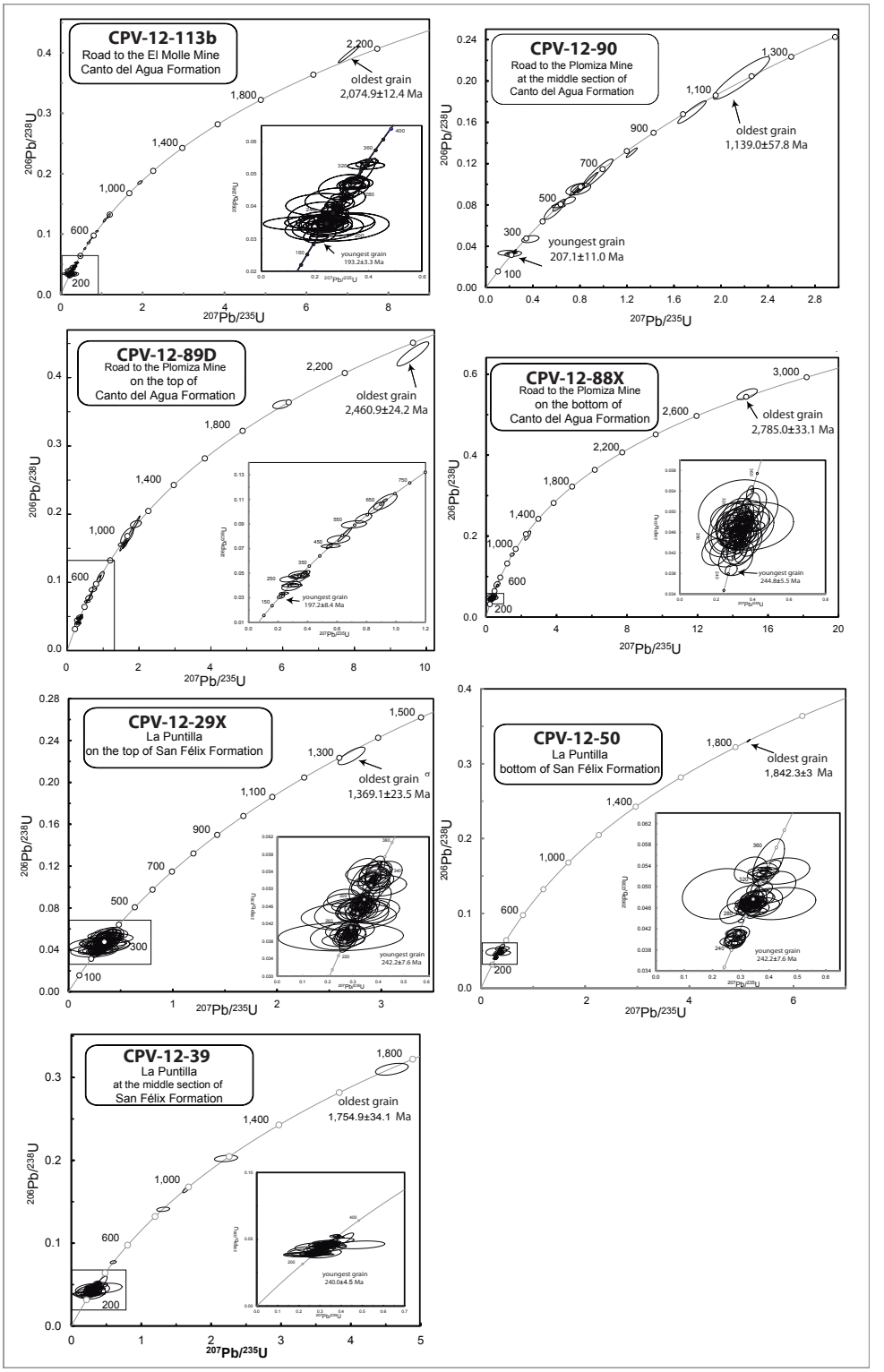

FIG. 6. U-Pb concordia diagrams of analyzed samples with youngest and oldest age indication. Data-point error ellipses are 68.3% confidence (1 σ).

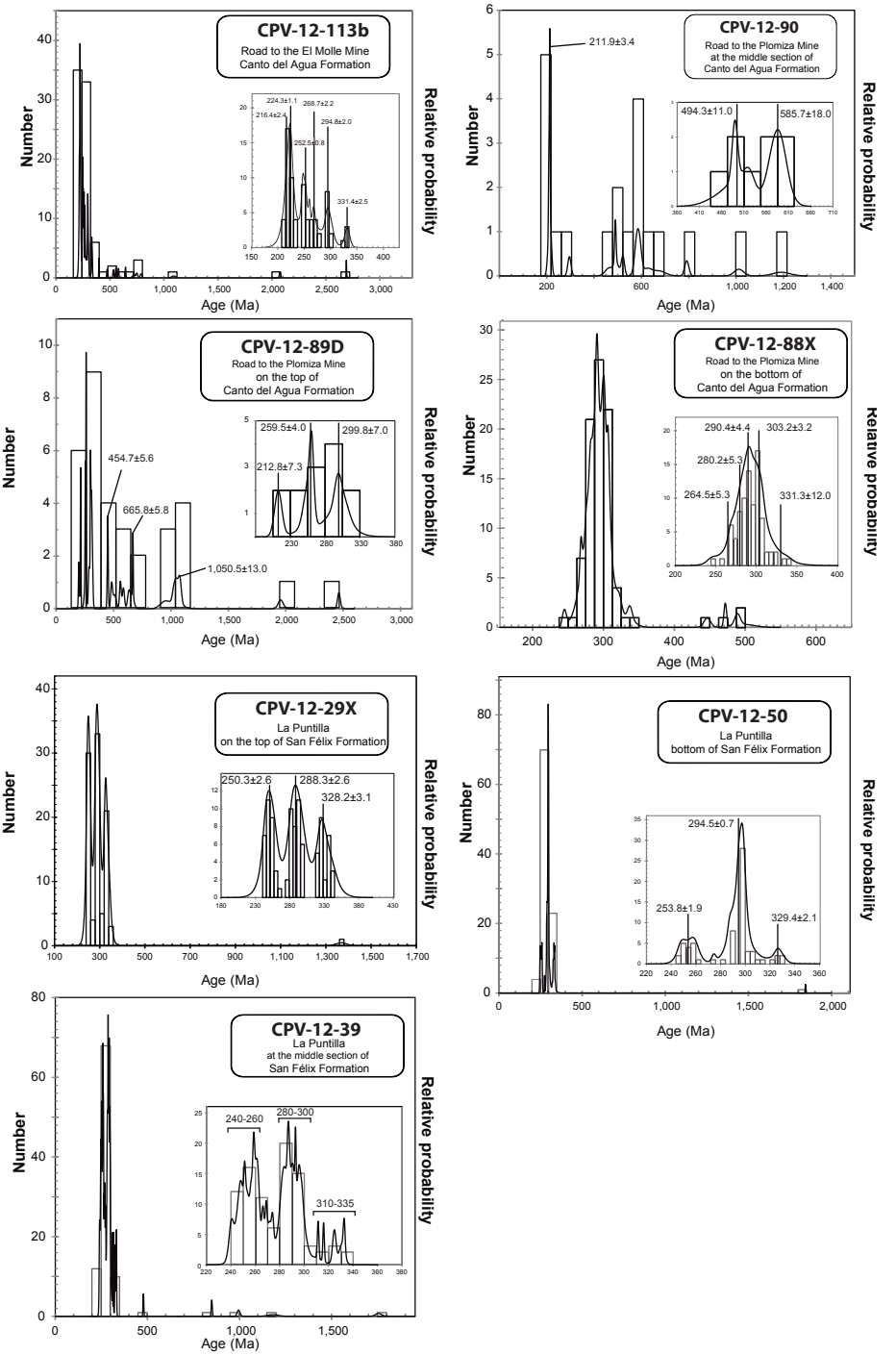

FIG. 7. Detrital zircon U-Pb probability density plot for analyzed samples. Reported maximum depositional ages were determined by the unmix tool of ISOPLOT (Ludwig, 2003) using the following fractions (f) of total analysed grains (n): CPV-12-113b (f=0.12; n=146); CPV-12-89D (f=0.16; n=33); CPV-12-88X (f=0.05; n=94); CPV-12-29X (f=0.33; n=97); CPV-12-50 (f=0.19; n=98). For sample CPV-12-90, maximum depositional age was calculated as the weighted mean for the younger population made up of 6 zircons.

4.2.2. Coastal Cordillera

Detrital zircon U-Pb ages were obtained on four samples from the Canto del Agua Formation. Samples CPV-12-88X, CPV-12-90 and CPV-12-89D belong to the bottom, middle and top segments of the type locality section (Plomiza mine), respectively (Figs. 2 and 5), and CPV-12-113b belongs to the El Molle mine section (Fig. 2).

A sandstone from the bottom of the type locality section (CPV-12-88X) yielded five unmixed Permian-Carboniferous age peaks (n=94): 264.5±5.3, 280.2±5.3, 290.4±4.4, 303.2±3.2 and 331.3±12 Ma (Fig. 7), and four dispersed zircons between 450 and 500 Ma.

Zircon age distribution (n=20) from an arkose of the middle section (CPV-12-90) show well-defined peaks of 211.9±3.4 Ma, 494.3±11.0 and 585.7±18.0 Ma (Fig. 7). At the top of the type section (CPV-12-89D), the U-Pb age populations (n=33) from an arkose are 212.8±7.3, 259.4±4.0, 299.8±7.0, 454.7±5.6, 665.8±5.8 and 1,050.5±13.0 Ma (Fig. 7). A litharenite from the El Molle mine section (CPV-12-113b) shows well-defined peaks (n=95) at 216.4±2.4 Ma, 224.3±1.1, 252.5±0.8, 268.7±2.2, 294.8±2.0 and 331.4±2.5 Ma (Fig. 7).

5. Depositional age for the San Félix and Canto del Agua Formations

5.1. San Félix Formation

An age range between upper Anisian (~242 Ma) and upper Ladinian (~237 Ma) has been assigned to the M4 member from its fossil content (*Daonella sturi* and *Daonella* lommeli; Zeil, 1958; McRoberts, 2010). Maximum depositional ages from detrital zircons are represented by the youngest age populations of 253.8±1.9 and 250.3±2.6 Ma, from samples at the bottom and top of the La Puntilla section, respectively (Figs. 6 and 7). These results suggest that the deposition of members M1 to M4 of the San Félix Formation began after 255 Ma and extended through the Ladinian (242-237 Ma, Cohen *et al.*, 2013).

5.2. Canto del Agua Formation

At its type locality, the base of the Canto del Agua Formation bear *Daonella*; whose biostratigraphic age varies between upper Anisian through Ladinian (McRoberts, 2010), whereas its topmost part bears *Psiloceras (Calcoceras*) sp. and *Arnioceras* sp. of Hettangian and Sinemurian ages (199-190 Ma; Moscoso and Covacevich, 1982). Maximum depositional ages for three samples on the same section are represented by the youngest detrital zircon age populations of 264.5±5.3 Ma (base) and 211.9± 3.4 Ma (middle) and 212.8±7.3 Ma (top; Figs. 6 and 7). The maximum depositional age for the lower part of the section is consistent with and upper Anisian to Ladinian age of deposition evidenced by its fossil content. Both the biostratigraphical and maximum depositional ages obtained in the upper section are significantly younger, Norian to Sinemurian, than the lower part of this formation. These contrasting ages would allow dividing the unit in two different sequences, the first deposited in the Middle Triassic and a youngest deposited in the Norian to Hettangian. Further south, at the El Molle mine locality (Fig. 2), a maximum depositional age of 216.4±2.4 Ma was obtained in the middle part of the exposed section. This age is consistent with the upper part of the section exposed in the type locality.

5.3. Stratigraphic correlations

Maximum depositional age of 255 Ma, along with the marine to transitional depositional environments and the absence of Upper Triassic detrital ages in the La Puntilla section, suggest that members M1 to M4 of the San Félix Formation can be correlated to the lower section of the Canto del Agua Formation at the Coastal Cordillera (Fig. 5). On the other hand, coincident geochronological data from the upper section of Canto del Agua Formation and the Member 5 of San Félix Formation allows us to correlate the regression evidenced by the establishment of fluvial depositional systems during the Late Triassic on both areas (Fig. 5).

6. Discussion

6.1. Sediment provenance for the Triassic fore-arc basins

6.1.1. San Félix basin

San Félix Formation shows, along the whole sequence, a relatively homogenous lithic component for sandstones and conglomerates, with variable amounts

of metamorphic rocks, felsic tuffs, intrusives and minor andesites. Sandstones are texturally immature to submature, which indicates relatively local sources. The detrital zircon U-Pb age distributions also show similar age patterns along the sequence, which consists of three well defined age populations of 240-260, 280-300 and 310-335 Ma, with scarce older ages in the middle of the section (Fig. 7).

The zircon pattern distribution for the older than 335 Ma ages is similar to those found in the El Tránsito Metamorphic Complex (ETMC; Álvarez *et al.,* 2011), which is unconformably covered by the San Félix Formation (Fig. 2 and Table 1), hence representing the most probable source for such zircons and for the ubiquitous metamorphic lithic fragments. The age population between 310 and 335 Ma suggests a detrital zircon contribution from the underlying Cerro Bayo Formation (301-325 Ma, Table 1) and the EPM protolith (324-326 Ma, Table 1), although volcanic felsic rocks of similar age have been reported further east, in northwestern Argentina (Zappettini *et al.,* 2015). However, the rocks of the EPM are unconformably covered by the Totora Formation (Fig. 4B, Table 1), indicating they were exhumed before the Norian, probably providing Carboniferous zircons to the Triassic drainage systems. The lower Permian age population is the most important component throughout the La Puntilla section and it most likely reflects the erosion of the Chanchoquín Plutonic Complex (285-304 Ma), which is unconformably covered by the San Félix Formation (Fig. 2 and Table 1) and constitutes the footwall of the eastern border fault of the San Félix basin (Las Pircas fault). The third and youngest age population (240-260 Ma) is broadly contemporaneous with the Guanaco Sonso Formations (Fig. 3 and Table 1). The abundant felsic volcaniclastic component of the Guanaco Sonso Formation indicates highly explosive eruptions, which may have contributed juvenile zircons to the basin.

In summary, sources for sediment to the San Félix basin are located eastward of the San Félix Formation, and furthermore, non-contemporaneous sources can be constrained to the basement block bounded by the Las Pircas fault, in the west, and the EPM in the east.

6.1.2. Canto del Agua basin

At its type section at Plomiza Mine the detrital zircon ages of the Canto del Agua Formation are grouped in a major population between 300 and 260 Ma (Fig. 7), with minor clusters around 330 and 480 Ma, while the nature of the lithic components is dominated by metapelitic clasts and quartz grains. The most prominent age population correlates with the age range of the Llanos del Chocolate Beds (Table 1), which are exposed 80 km south of this locality (Fig. 2). The interbedded felsic volcanics present in the Llanos del Chocolate Beds could have contributed to the subarkosic nature of the sandstones. The 330 Ma and older ages are most likely populations inherited from the metamorphic complexes underlying the Canto del Agua Formation (Punta de Choros Metamorphic Complex or PCMC in table 1; Bahlburg *et al.,* 2009; Álvarez *et al.,* 2011).

The middle and top parts of the type section roughly show the same age peaks recognized at the bottom of the section, though less prominent and with a Late Triassic age population. Given that no Late Triassic volcanic units have been recognized in the Coastal Cordillera, a possible source for such population could be the tuffaceous deposits underlying the analyzed horizons (Fig. 5). A volcanic input to the basin is evidenced by the increased contribution of felsic and andesitic volcanic fragments up section. The section exposed at the El Molle mine locality shows the same age populations than the upper part of the type section, with the exceptions of a Lopingian to Lower Triassic population (*ca*. 259-247 Ma), absent in the type locality, and that the Late Triassic population is slightly older (216-224 Ma). The former cannot be related to any known source of such age in the Coastal Cordillera. In the Frontal Cordillera, stratigraphic relationships show plutonic and volcanic rocks of this age (Chollay Plutonic Complex and Guanaco Sonso Formation; Fig. 3). These rock units were exhumed before the Norian (Table 1), therefore, providing a possible source for this population of zircons. The Norian population could be attributed to acidic volcanism in the Frontal Cordillera exposed immediately south of the study area (Pastos Blancos Formation; Table 1).

In conclusion, the sediment contribution for the Canto del Agua Formation is dominated by local sources. An exception, are the rocks cropping out near El Molle locality, which are equivalent to the upper part of the type section and suggest some contribution from the Frontal Cordillera, both by drainage processes and by atmospheric transport from volcanic eruptions.

6.2. Gondwana margin evolution during the Triassic at 28-29° S

Triassic basins in the southwestern Gondwanean margin have been previously interpreted as a continuous NNW oriented horst and graben system encompassing both Argentinian Ischigualasto and Cuyo basins and Chilean marine to transitional Triassic basins distributed along the margin (Charrier, 1979). However such scenario is not completely compatible with the presence of a NS trending magmatic belt in the Frontal Cordillera, composed of granitic batholiths (Chollay Plutonic Complex), a volcaniclastic basin (Guanaco Sonso Formation), both with continental magmatic arc isotopic and geochemical signatures (Del Rey *et al.,* 2016; Coloma *et al.,* 2017), and with the presence of NS mylonitic shear zones (EPM). These features suggest the mechanical decoupling of the clastic rift basin systems located west (Chile) and east (Argentina) of the magmatic belt. On the other hand, Early to Middle Triassic basins located west of the arc, are bounded by contemporaneous N-S faults (such as the Las Pircas fault and El Portillo Mylonites) rather than by the NNW orientation of Argentinean basins (Fig. 1). Under such considerations, in the studied segment, Triassic volcanic basins located in the present Frontal Cordillera and Triassic sedimentary basins in Chile are more likely to have developed as NS trending intra-arc and forearc basins respectively. This is consistent with the structural style shown in offshore seismic reflection studies at 31-33° S (Contreras-Reyes *et al.,* 2014, 2015), where, in spite that the ages of the reflectors are poorly constrained, the sedimentary cover fills a series of N-S trending grabens and hemigrabens in the upper slope, that were tectonically inverted in recent (Andean) compressive pulses and gravitational collapses.

Geochronological data and stratigraphic relationships exposed above (Fig. 3) identify two stages during the Triassic evolution of the study area, separated by a regional unconformity of Carnian age, a first latest Permian-Anisian stage and a second Late Triassic stage (Fig. 3). Such unconformity coincides with the Middle to Late Triassic exhumation of mélanges between 26 and 42° S along the Chilean coastline (Kato and Godoy, 2015).

6.2.1. First stage

Between the Lopingian and the uppermost Middle Triassic (Ladinian), the studied segment presented three depocenters separated by two topographic highs. The eastern depocenter, an intra-arc basin, accommodated the Guanaco Sonso Formation, a mainly volcaniclastic succession whose well developed lacustrine facies relate to a closed drainage network and a local base level (Fig. 8). This depocenter was developed penecontemporanously with the incremental construction of the Chollay Plutonic Complex conforming the coupled magmatic system of a caldera type volcanic complex (Salazar and Coloma, 2016; López *et al.,* 2015). The Chollay Plutonic Complex is flanked westward by the EPM (Fig. 4B), a ductile shear zone with left-lateral displacement recorded at 242 Ma (Murillo *et al.,* 2013; Table 1) and whose surface expression could have been the structures bounding the Guanaco Sonso basin to the west (Fig. 8).

The San Félix forearc basin is bounded to the east by the Las Pircas fault and the western block of the EPM, which is composed of Pennsylvanian to Cisuralian igneous rocks (Chanchoquín Plutonic Complex) intruding the ETMC. This block is the footwall of the Las Pircas normal fault, hence, it constitutes a relatively uplifted block and the main source for the sedimentary rocks of the San Félix basin, as depicted by lithic components, detrital zircon patterns and textural maturity of the San Félix Formation sedimentary rocks. Lopingian to Middle Triassic (Ladinian) detrital zircon input to this unit is interpreted as the contribution of highly explosive eruptions related to the Guanaco Sonso basin evolution that could have episodically poured juvenile zircons into the drainage system feeding the San Félix basin (Fig. 8). Maximum accommodation of Members M1 to M4 is reached between Las Pircas and the San Félix faults (Fig. 2), suggesting these faults could have been initially bounding a graben structure (Fig. 8) but they were reversely reactivated during Andean orogenesis.

Sedimentary provenance analysis on the San Félix and the lower Canto del Agua Formations evidences local sources for both depocenters, which suggests emerged landmasses offshore from the San Félix basin coastline (Fig. 8). Possible present-day analogues for such landmasses can be recognized as longitudinal island belts or bathymetric highs exhumed as footwalls of normal faults developed in the inner wedge of some accretionary prisms (*e.g.*, Wang and Hu, 2006; Gallen *et al.,* 2014).

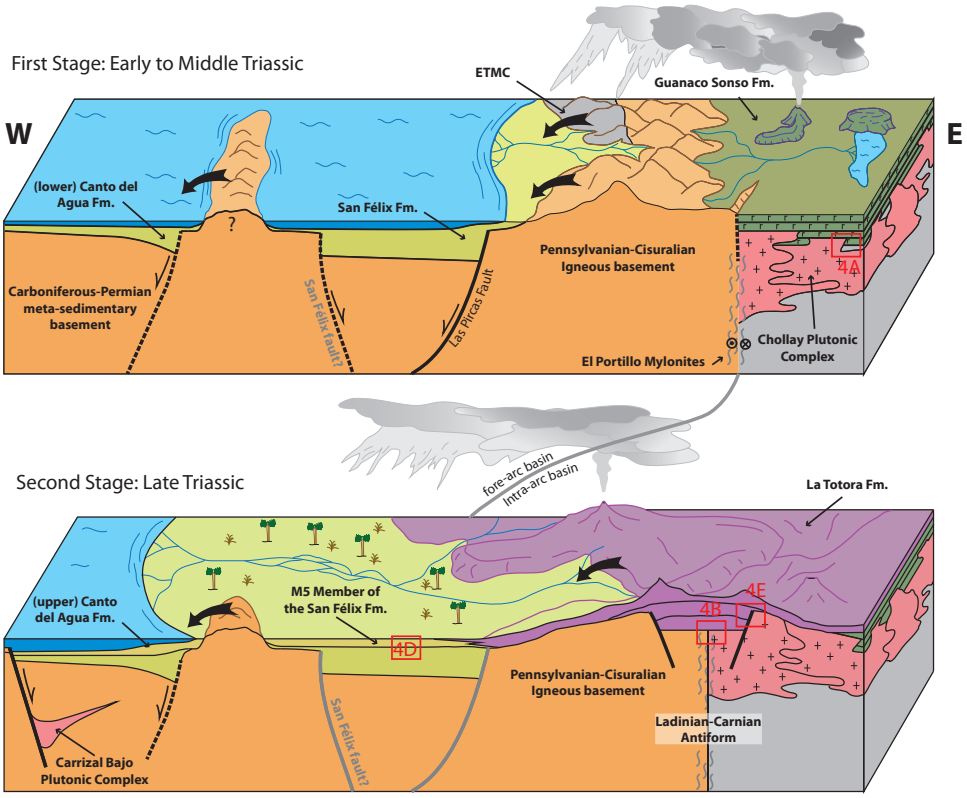

FIG. 8. Paleogeographic block diagramas for the first and second evolutionary stages of the Triassic basins discussed in text. Thick black arrows indicate sediment inputs to the basins, red squares show contact relationship shown in photographs of figure 4. **ETMC**: El Tránsito Metamorphic Complex.

6.2.2. The Carnian unconformity

The regional unconformity documented at the base of the Upper Triassic units in the study area evidences a regional exhumation event taking place after the Anisian.

In the Coastal Cordillera, the unconformity between the fluvial upper section of the Canto del Agua Formation (Norian) and the underlying Anisian-Ladinian delta deposits of the Lower section reveals only a minor exhumation that doesn't expose deep crustal levels. In the Frontal Cordillera, however, the unconformity documented at the base of the La Totora and the M5 Member of the San Félix Formation reveals marked EW variations in magnitude of exhumation. West of the Paleozoic block, the exhumation is similar to the observe in the Coastal Cordillera as it exposes Anisian marine sediments, while to the east, the exhumation is maximum, exposing Anisian intrusives and mylonites. Further east, exhumation gradually diminishes to expose Lopingian to Anisian volcanics. This lateral variation is similar to the one described for the Pastos Blancos Formation (233-221 Ma) immediately south of the study area, where its maximum thickness is located covering the contacts between Paleozoic intrusives to the west and Triassic intrusives to the east, and Triassic volcanics in its easternmost outcrops (Ortiz and Merino, 2015).

The E-W variation on exhumation magnitude in the Frontal Cordillera evidences the growth of a regional NS trending antiform. The axis of this antiform follows a regional shear zone along the contact between the Chollay and the Chanchoquín plutonic complexes (Figs. 2 and 8). Along the hinge of this antiform, the volcanotectonic depression of the La Totora basin is later developed during the second stage (Fig. 8). This antiform could be explained by passive rift extension, that is, thermal bulging by heat input from the mantle leading to normal faulting and magmatism. Such scenario is consistent with

the mantle like magma source for Late Triassic magmatism described at the study area (Hervé *et al*., 2014; González *et al.,* 2018).

On the other hand, in the Coastal Cordillera, this unconformity has been related to a transpressional exhumation event between Middle to Late Triassic along the Chilean coast (Kato and Godoy, 2015; Godoy, 1985). The latter is consistent with a major shift on the global motion of Gondwana at around 230 Ma, from a counterclockwise rotation with an Euler pole located in northernmost South America to a westward drift of the whole supercontinent (Torsvik *et al.,* 2012; Matthews *et al*., 2016).

6.2.3. Second stage

During the Norian and Rhaetian, andesitic lavas and tuffs of the La Totora Formation were accommodated within a volcanotectonic depression at the present-day Frontal Cordillera (Fig. 4E), as part of the intra-arc basin (Fig. 8). These deposits seal the activity of two major structural features developed in the previous stage, the Las Pircas fault (Fig. 4C) and the El Portillo Mylonites shear zone (Figs. 8 and 4B). In the forearc basin, its volcanic deposits laterally interfingers with the M5 Member fluvial deposits (Fig. 8), hence, recording a westward migration of the coastline towards the Canto Del Agua depocenter (Fig. 8). On the other hand, the volcanic activity that took place in the Frontal Cordillera is recorded as felsic pyroclastic deposits in the Coastal Cordillera, probably derived from the Pastos Blancos Formation related volcanism, located a few km south of the study area (Table 1). During this stage, the facies arrangement in the Canto del Agua depocenter shows a local transgression, not evidenced in the San Félix Depocenter (Fig. 7). Such transgression may be related to local extensional tectonism evidenced in the contemporaneous fault assisted emplacement of the Carrizal Bajo Plutonic Complex (Fig. 8; Grocott *et al.,* 2009).

6.3. Major unconformities and their regional correlations

The Carboniferous to Triassic stratigraphic record of the outward Pangea margin shows global discontinuities that mark major shifts in the geodynamic configuration of the supercontinent at 280, 260 and 230 Ma (Riel *et al*., 2018). In the studied segment of the southwestern margin of Gondwana, recent studies and the results of this work allow to better constraint the timing and distribution of these unconformities (Fig. 9).

The Cisuralian unconformity that places the Laguna Chica Formation over deformed Devonian sediments in the Frontal Cordillera correlates well with a regional unconformity defined in the San Rafael Block (Argentina), where Cisuralian volcanics of the Choiyoi Group overlie deformed Carboniferous sediments (Rocha-Campos *et al*., 2011; Fig. 9). This unconformity has been referred to as the San Rafael tectonic phase (Azcuy and Caminos, 1987), and has been well documented also in the Argentine Frontal Cordillera and Precordillera provinces (Fig. 9). Its presence in the Coastal Cordillera is uncertain, however, it might be represented in the unconformity by which the Llanos del Chocolate beds cover the penecontemporaneous PCMC near the Chañaral Creek, in an structurally complex accretionary prism environment (Figs. 2 and 9; Creixell *et al*., 2016).

A Lopingian-Triassic unconformity is described in the Chilean Frontal Cordillera, by which members M1 to M4 of the San Félix Formation overlie Carboniferous-Cisuralian igneous rocks and Devonian metasediments in the west, and the Guanaco Sonso Formation covers Devonian metasediments and Guadalupian volcanics, in the east (Figs. 2 and 9). This unconformity correlates with the one described at the base of the Cuyo and Uspallata groups in Argentina, where rift related clastic sediments cover Permian volcanics of the Choiyoi Group (Fig. 9). Its presence in the Argentine Frontal Cordillera is not clear since Late Triassic Rancho de Lata Formation directly overlies volcanic rocks assigned to the Choiyoi Group, although the age of the latter is poorly constrained in that area (Fig. 9), hence the presence of Triassic volcanics equivalent to the Guanaco Sonso Formation cannot be discarded, nor a discontinuity in this underlying volcanic pile. In the Coastal Cordillera, this unconformity is not well geochronologically constrained, however, in consideration of the Lower to Middle Triassic age assigned in this work to the lower section of the Canto del Agua Formation in the Plomiza mine area (Fig. 2), it should be equivalent to the basal unconformity through which it overlies Carboniferous-Permian metasedimentary rocks (PCMC).

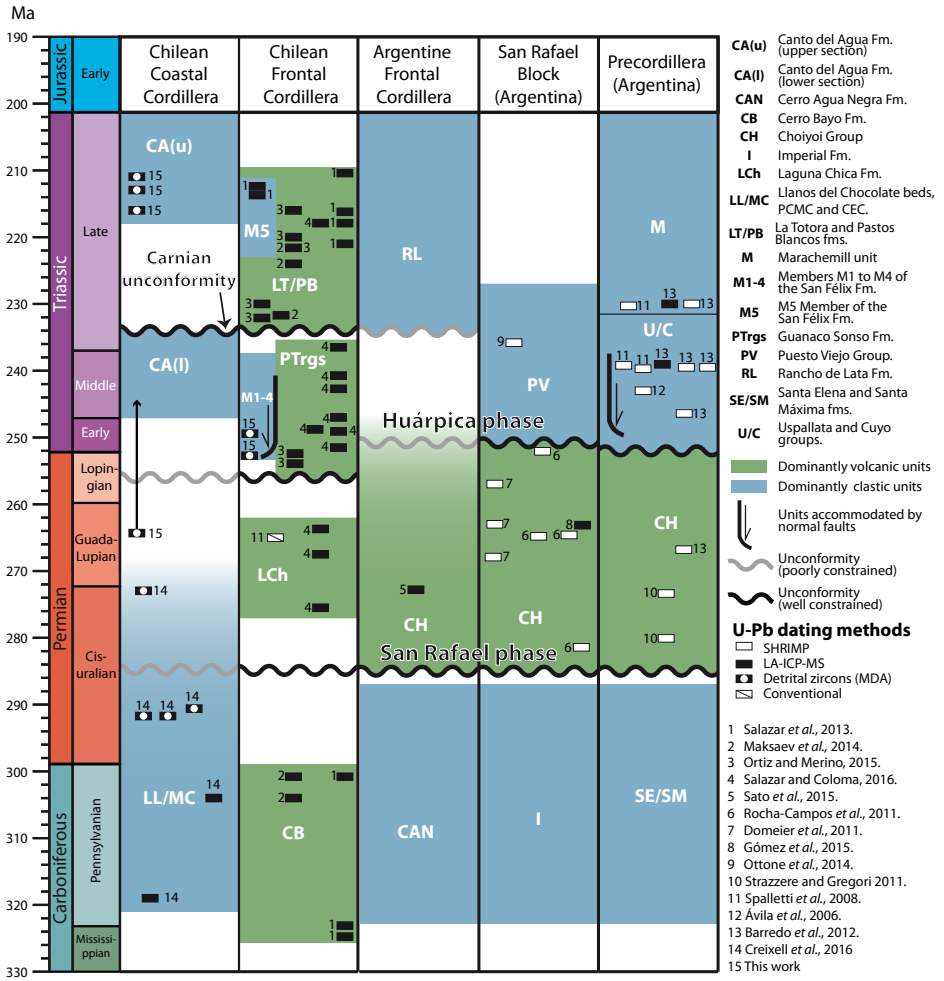

FIG. 9. Regional correlations for lithostratigraphic units and unconformities (based on timescale by Cohen *et al.*, 2013).

Finally, the Carnian unconformity described in this work in the Chilean Coastal and Frontal Cordilleras could be equivalent to the basal unconformity of the Rancho de Lata Formation in the Argentinean Frontal Cordillera (Fig. 9), and to changes on the accommodation structures and environmental conditions in the Precordillera (Cuyo basin) recorded in the Marachemill unit (Barredo *et al.*, 2012). Recently, this unconformity has been well constrained in norther Chile at the base of the Domeyko basin (Espinoza *et al.*, 2018).

This regional framework for the main sequences of the Carboniferous-Triassic rock record, will allow to better study the timing and spatial variations of tectonic processes for each evolutionary stage of the southwestern margin of Gondwana and its possible relationship with global geodynamic events.

7. Conclusions

Between 28° and 29° S, the transition between the Gondwanean and Andean Orogenies during the Triassic is made up of two stages of an intra-arc/forearc basins system, separated by a Carnian unconformity recognized in the Frontal Cordillera and inferred in the Coastal Cordillera in Chile.

During the first stage (Lopingian-uppermost Middle Triassic), the intra-arc basin is represented by the Guanaco Sonso Formation (253-237 Ma), rooted by the Chollay Plutonic Complex (237-248 Ma) and bounded to the west by a left-lateral shear zone recorded in the EPM (242 Ma). The forearc basin is represented by two extensional marine to transitional depocenters separated by topographic highs, the San Félix basin to the east and the Canto

del Agua basin to the west, filled by the homonymous formations. This stage is recorded in members M1 to M4 of the San Félix Formation and in the lower section of the Canto del Agua Formation, both of which carry Anisian fossil fauna and where maximum depositional ages of 254 and 265 Ma were obtained from detrital zircon analyses, respectively. Detrital zircons, clast composition and sediment maturity indicate local sources for both depocenters. Particularly, for the San Félix Formation, the main source of sediment is the Triassic-Paleozoic block located at the footwall of the normal Las Pircas fault that bounds the San Félix basin to the east, with minor inputs from the volcanic activity related to the Guanaco Sonso basin evolution.

The Carnian unconformity shows a major exhumation in the Chilean Frontal Cordillera where it gets to expose the Chollay Plutonic Complex (237-248 Ma) and the El Portillo Mylonites (242 Ma), while in the forearc basin it is recorded by a an erosional unconformity where Norian fluvial deposits overlie Anisian prodelta deposits in both, San Félix and Canto del Agua formations (Fig. 5).

During the second stage (Norian-Rhaetian), lavas and pyroclastic deposits from La Totora Formation and the Member 5 of the San Félix Formation sealed the activity of the Las Pircas fault and the El Portillo Mylonites shear zone. At the Coastal Cordillera, the volcanic activity present in Canto del Agua Formation is recorded by acid pyroclastic deposits probably derived from the Pastos Blancos Formation related volcanism. Furthermore, the upper sedimentary levels of Canto del Agua depocenter recorded a local transgression, which is absent in the San Félix Formation, and coincides with local extensional emplacement of the Carrizal Bajo Plutonic Complex.

Regionally, the Carnian unconformity has not been documented before as such, although it is suggested to correlate with other unconformities at the bases of Late Triassic units in the Frontal Cordillera.

Acknowledgements

This research was funded by the Plan Nacional de Geología of the Servicio Nacional de Geología y Minería (SERNAGEOMIN) and the Fondecyt grant 1120715. F. Coloma, M. Ortiz, R. Merino and I. Murillo are thanked for the fruitful discussions on the updated geological mapping in northern Chile. We thank F. Poblete for facilitating Gondwanean paleogeographic reconstructions and M. Padel for his company and guidance on the field. M.N.D. acknowledges support from United States National Science Foundation grant EAR 1725002 and the Romanian Executive Agency for Higher Education, Research, Development and Innovation Funding project PN-III-P4-ID-PCCF-2016-0014. Finally we thank L. Giambiagi, E. Godoy and an anonymous reviewer for the constructive comments that led to a substantial improvement of the manuscript.

References

Álvarez, J.; Mpodozis, C.; Arriagada, C.; Astini, R.; Morata, D.; Salazar, E.; Valencia, V.A.; Vervoort, J.D. 2011. Detrital Zircons from Late Paleozoic Accretionary Complexes in North-Central Chile (28°-32°S): Possible Fingerprints of the Chilenia Terrane. Journal of South American Earth Sciences 32: 460-476.

Álvarez, J.; Mpodozis, C.; Blanco-Quintero, I.; García-Casco, A.; Arriagada, C.; Morata, D. 2013. U-Pb ages and metamorphic evolution of the La Pampa Gneisses: Implications for the evolution of the Chilenia Terrane and Permo-Triassic tectonics of north Central Chile. Journal of South American Earth Sciences 47: 100-115.

Arévalo, C.; Welkner, D. 2008. Geología del Área Carrizal Bajo-Chacritas, región de Atacama. Servicio Nacional de Geología y Minería, Carta Geológica de Chile, Serie Geología Básica 111: 67 p. Santiago.

Ávila, J.N.; Chemale, F.; Mallmann, G.; Kawashita, K.; Armstrong, R.A. 2006. Combined stratigraphic and isotopic studies of Triassic strata, Cuyo Basin, Argentine Precordillera. Geological Society of America Bulletin 118 (9-10): 1088-1098.

Azcuy, C.L.; Caminos, R. 1987. Diastrofismo. *In* El Sistema Carbonífero en la República Argentina (Archangelsky, S.; editor). Academia Nacional de Ciencias: 239-252. Córdoba.

Bahlburg, H.; Vervoort, J.D.; Du Frane, S.A.; Bock, B.; Augustsson, C.; Reimann, C. 2009. Timing of Crust Formation and Recycling in Accretionary Orogens: Insights Learned from the Western Margin of South America. Earth-Science Reviews 97: 215-241.

Barredo, S.; Chemale, F.; Marsicano, C.; Ávila, J.N.; Ottone, E.G.; Ramos, V.A. 2012. Tectono-sequence stratigraphy and U-Pb zircon ages of the Rincón Blanco Depocenter, northern Cuyo Rift, Argentina. Gondwana Research 21 (2): 624-636.

Barthel, L. 1958. Eine Marine Faunula Aus Der Mittleren Trias Von Chile. Neues Jahrbuch für Geologie und Paläontologie, Abhandlungen 106: 352-382.

Bell, C.M.; Suárez, M. 1994. The sedimentation and tectonics of a marine fan-delta developed on an active

continental margin: the Triassic San Félix Formation in the Andes of northern Chile. Journal of South American Earth Sciences 7: 403-413.

Branney, M.; Acocella, V. 2015. Chapter 16-Calderas. *In* The Encyclopedia of Volcanoes, 2nd edition (Sirgudsson, H.; editor). Academic Press: 299-315. Nueva York.

Castillo, P.; Fanning, C.M.; Fernández, R.; Poblete, F.; Hervé, F. 2017. Provenance and age constraints of Paleozoic siliciclastic rocks from the Ellsworth Mountains in West Antarctica, as determined by detrital zircon geochronology. Geological Society of America Bulletin 129 (11-12): 1568-1584. doi: 10.1130/B31686.1.

Charchaflié, D. 2003. Geological, structural and geochronological framework of the Veladero north area, cordillera frontal, Argentina. MSc. Thesis (Unpublished), University of British Columbia: 137 p. Vancouver.

Charrier, R. 1979. El Triásico en Chile y regiones adyacentes de Argentina: una reconstrucción paleogeográfica y paleoclimática. Universidad de Chile, Departamento de Geología, Comunicaciones 26: 1-37.

Charrier, R.; Pinto, L.; Rodríguez, M.P. 2007. Tectonostratigraphic evolution of the Andean Orogen in Chile. *In* The Geology of Chile (Moreno, T.; Gibbons, W.; editors). The Geological Society: 21-114. London.

Cohen, K.M.; Finney, S.C.; Gibbard, P.L.; Fan, J.X. 2013. The ICS (International Commission on Stratigraphy) international chronostratigraphic chart. Episodes 36 (3): 199-204.

Coloma, F.; Valin, X.; Oliveros, V.; Vásquez, P.; Creixell, C.; Salazar, E.; Ducea, M.N. 2017. Geochemistry of Permian to Triassic igneous rocks from northern Chile (28º-30º15'S): Implications on the dynamics of the proto-Andean margin. Andean Geology 44 (2): 147-178. doi: 10.5027/andgeoV44n2-a03.

Contreras-Reyes, E.; Becerra, J.; Kopp, H.; Reichert, C.; Díaz-Naveas, J. 2014. Seismic structure of the north-central Chilean convergent margin: Subduction erosion of a paleomagmatic arc. Geophysical Research Letters 41 (5): 1523-1529.

Contreras-Reyes, E.; Ruiz, J.A.; Becerra, J.; Kopp, H.; Reichert, C.; Maksymowicz, A.; Arriagada, C. 2015. Structure and tectonics of the central Chilean margin (31°-33° S): Implications for subduction erosion and shallow crustal seismicity. Geophysical Journal International 203 (2): 776-791.

Creixell, C.; Ortiz, M.; Arévalo, C. 2012. Geología del Área Carrizalillo-El Tofo, regiones de Atacama y Coquimbo. Servicio Nacional de Geología y Minería, Carta Geológica de Chile, Serie Geología Básica 133-134: 82 p. Santiago.

Creixell, C.; Oliveros, V.; Vásquez, P.; Navarro, J.; Vallejos, D.; Valin, X.; Godoy, E.; Ducea, M.N. 2016. Geodynamics of Late Carboniferous-Early Permian forearc in north Chile (28°30'-29°30' S). Journal of the Geological Society 173 (5): 757-772.

Del Rey, A.; Deckart, K.; Arriagada, C.; Martínez, F. 2016. Resolving the paradigm of the late Paleozoic-Triassic Chilean magmatism: Isotopic approach. Gondwana Research 37: 172-181.

Domeier, M.; Van der Voo, R.; Tohver, E.; Tomezzoli, R.; Vizan, H.; Torsvik, T.; Kirshner, J. 2011. New Late Permian paleomagnetic data from Argentina: Refinement of the apparent polar wander path of Gondwana. Geochemistry, Geophysics, Geosystems 12 (7): Q07002. doi: 10.1029/2011GC003616.

Espinoza, M.; Montecino, D.; Oliveros, V.; Astudillo, N.; Vásquez, P.; Reyes, R.; Celis, C.; González, R.; Contreras, J.; Creixell, C.; Martínez, A. 2018. The synrift phase of the early Domeyko Basin (Triassic, northern Chile): Sedimentary, volcanic, and tectonic interplay in the evolution of an ancient subduction-related rift basin. Basin Research 31: 4-32. doi: 10.1111/bre.12305

Franzese, J.R.; Spalletti, L.A. 2001. Late Triassic-Early Jurassic Continental Extension in Southwestern Gondwana: Tectonic Segmentation and Pre-Break-up Rifting. Journal of South American Earth Sciences 14: 257-270.

Gallen, S.F.; Wegmann, K.W.; Bohnenstiehl, D.R.; Pazzaglia, F.J.; Brandon, M.T.; Fassoulas, C. 2014. Active simultaneous uplift and margin-normal extension in a forearc high, Crete, Greece. Earth and Planetary Science Letters 398: 11-24.

Godoy, E. 1985. Nuevos antecedentes sobre el basamento metamórfico y la fase tectónica infraneocomiana en la Costa del Norte Chico, Chile. *In* Congreso Geológico Chileno, No. 4, Actas 1: 370-384. Antofagasta.

Gómez, A.L.R.; Rubinstein, N.A.; Valencia, V.A. 2015. Gondwanan magmatism with adakite-like signature linked to Cu (Mo)-porphyry deposits from the San Rafael massif, Mendoza Province, Argentina. Chemie der Erde 75: 89-104.

González, J.; Oliveros, V.; Creixell, C.; Velásquez, R.; Vásquez, P.; Lucassen, F. 2018. The Triassic magmatism and its relation with the Pre-Andean tectonic evolution: Geochemical and petrographic constrains from the High Andes of north central Chile (29°30'-30°S). Journal of South American Earth Sciences 87: 95-112.

Grocott, J.; Arévalo, C.; Welkner, D.; Cruden, A. 2009. Fault-Assisted Vertical Pluton Growth: Coastal Cordillera, North Chilean Andes. Journal of the Geological Society 166: 295-301.

Hervé, F.; Fanning, C.M.; Calderón, M.; Mpodozis, C. 2014. Early Permian to Late Triassic Batholiths of the Chilean Frontal Cordillera (28°-31° S): Shrimp U-Pb Zircon Ages and Lu-Hf and O isotope systematics. Lithos 184: 436-446.

Kato, T.; Godoy, E. 2015. Middle to late Triassic mélange exhumation along a pre-Andean transpressional fault system: Coastal Chile (26°-42° S). International Geology Review 57 (5-8): 606-628.

López, N.; Salazar, E.; Franco, C. 2015. Análisis de facies volcanoclásticas y control estructural de una sección de los Estratos de Guanaco Sonso, a los 29°S, Cordillera Frontal, región de Atacama. *In* Congreso Geológico Chileno, No. 14, Actas: 882-885. La Serena.

Ludwig, K. 2003. User's Manual for Isoplot 3.00: A Geochronological Toolkit for Microsoft Excel. Berkeley Geochronology Center, Special Publication 5: 75 p. California.

Maksaev, V.; Munizaga, F.; Tassinari, C. 2014. Timing of the magmatism of the paleo-pacific border of Gondwana: U-Pb geochronology of Late Paleozoic to Early Mesozoic igneous rocks of the north Chilean Andes between 20° and 31°S. Andean Geology 41 (3): 447-506. doi: 10.5027/andgeoV41n3-a01.

Martin, M.W.; Clavero, R.J.; Mpodozis, M.C. 1999. Late Paleozoic to Early Jurassic tectonic development of the high Andean Principal Cordillera, El Indio Region, Chile (29-30°S). Journal of South American Earth Sciences 12: 33-49.

Matthews, K.J.; Maloney, K.T.; Zahirovic, S.; Williams, S.E.; Seton, M.; Müller, R.D. 2016. Global plate boundary evolution and kinematics since the late Paleozoic. Global and Planetary Change 146: 226-250. doi: 10.1016/j.gloplacha.2016.10.002.

McRoberts, C.A. 2010. Biochronology of Triassic Bivalves. Geological Society, Special Publications 334: 201-219. London.

Mohr, B.; Schöner, F. 1985. Eine Obertriassische Dicroidium-Flora Südöstlich Alto del Carmen, Región de Atacama (Chile). Neues Jahrbuch für Geologie, Palaeontologie, Monatshefte 6: 368-379.

Moscoso, R. 1979. Geología de la franja transversal a la Cordillera de la Costa y Cordillera de los Andes a la latitud de Domeyko (29°S), región de Atacama. Memoria de Título (Inédito), Universidad de Chile, Departamento de Geología: 166 p. Santiago.

Moscoso, R.; Covacevich, V. 1982. Las sedimentitas Triásico-Jurásicas al sur de Canto del Agua, Cordillera de la Costa, región de Atacama, Chile: Descripción de la Formación Canto del Agua. *In* Congreso Geológico Chileno, No. 3, Actas 3: F189-F196. Concepción.

Mpodozis, C.; Kay, S.M. 1992. Late Paleozoic to Triassic Evolution of the Gondwana Margin: Evidence from Chilean Frontal Cordilleran Batholiths (28°S-31°S). Geological Society of America Bulletin 104: 999-1014.

Murillo, I.; Álvarez, J.; Montecinos, P.; Creixell, C.; Salazar, E.; Arriagada, C. 2013. Geochronology and kinematics of El Portillo Mylonites: relation with San Rafael Orogeny and Middle Triassic extension in north-central Chile. *In* International Geological Congress on the Southern Hemisphere GEOSUR. Bolletino di Geofisica teorica ed applicata 54, Supplement 2: p. 83. Viña del Mar.

Navarro, J. 2013. Petrotectónica del complejo metamórfico Punta de Choros III-IV Región, Chile. Memoria de Título (Inédito), Universidad de Chile, Departamento de Geología: 110 p.

Nemchin, A.A.; Cawood, P.A. 2005. Discordance of the U-Pb system in detrital zircons: Implication for provenance studies of sedimentary rocks. Sedimentary Geology 182 (1-4): 143-162. doi: 10.1016/j.sedgeo.2005.07.011.

Ortiz, M.; Merino, R. 2015. Geología de las áreas Río Chollay-Matancilla y Cajón del Encierro, regiones de Atacama y Coquimbo. Servicio Nacional de Geología y Minería, Carta Geológica de Chile, Serie Geología Básica 175-176: 234 p. Santiago.

Ottone, E.G.; Monti, M.; Marsicano, C.A.; Marcelo, S.; Naipauer, M.; Armstrong, R.; Mancuso, A.C. 2014. A new Late Triassic age for the Puesto Viejo Group (San Rafael depocenter, Argentina): SHRIMP U-Pb zircon dating and biostratigraphic correlations across southern Gondwana. Journal of South American Earth Sciences 56: 186-199.

Padel, M.; Salazar, E.; Coloma, F. 2012. Arquitectura y evolución tectonoestratigráfica del Depocentro de San Félix, Triásico medio a superior: Resultados Preliminares. *In* Congreso Geológico Chileno, No. 13: T-5. Antofagasta.

Pankhurst, R.J.; Millar, I.L.; Hervé, F. 1996. A Permo-Carboniferous U-Pb Age for Part of the Guanta Unit of the Elqui-Limarí Batholith at Río del Tránsito, Northern Chile. Andean Geology 23 (1): 35-42. doi: 10.5027/andgeoV23n1-a03.

Ramos, V.A. 1994. Terranes of Southern Gondwanaland and Their Control in the Andean Structure (30°-33°S

Latitude). *In* Tectonics of the Southern Central Andes: Structure and Evolution of an Active Continental Margin, Springer: 249-261. Berlin.

Reutter, K. 1974. Entwicklung Und Bauplan Der Chilenischen Hochkordillere im Bereich 29 südlicher Breite. Neues Jahrbuch für Geologie und Paläontologie 146 (2): 153-178.

Ribba, L. 1985. Geología regional del cuadrángulo El Tránsito, región de Atacama, Chile. Memoria de Título (Inédito), Universidad de Chile, Departamento de Geología: 203 p. Santiago.

Ribba, L.; Mpodozis, C.; Hervé, F.; Nasi, C.; Moscoso, R. 1988. El basamento del Valle del Tránsito, cordillera de Vallenar: eventos magmáticos y metamórficos y su relación con la evolución de los andes chileno-argentinos. Andean Geology 15 (2): 129-149. doi: 10.5027/andgeoV15n2-a03.

Riel, N.; Jaillard, E.; Martelat, J.E.; Guillot, S.; Braun, J. 2018. Permian-Triassic Tethyan realm reorganization: Implications for the outward Pangea margin. Journal of South American Earth Sciences 81: 78-86.

Rocha-Campos, A.C.; Basei, M.A.S.; Nutman, A.P.; Kleiman, L.E.; Varela, R.; Llambías, E.; Canile, F.M.; Da Rosa, O. de .C.R. 2011. 30 million years of Permian volcanism recorded in the Choiyoi igneous province (W Argentina) and their source for younger ash fall deposits in the Paraná Basin: SHRIMP U-Pb zircon geochronology evidence. Gondwana Research 19: 509-523.

Salazar, E. 2012. Evolución tectonoestratigráfica de la cordillera de Vallenar: Implicancias en la construcción del oroclino de Vallenar. Tesis de Magíster (Inédito), Universidad de Chile, Departamento de Geología: 126 p. Santiago.

Salazar, E.; Coloma, F. 2016. Geología del área Cerros de Cantaritos-Laguna Chica, Región de Atacama. Servicio Nacional de Geología y Minería, Carta Geológica de Chile, Serie Geología Básica 181: 171 p. Santiago.

Salazar, E.; Coloma, F.; Creixell, C. 2013. Geología del Área El Tránsito-Lagunillas, Región de Atacama. Servicio Nacional de Geología y Minería, Carta Geológica de Chile, Serie Geología Básica 149: 106 p. Santiago.

Sato, A.M.; Llambías, E.; Basei, M.; Castro, C. 2015. Three Stages in the Late Paleozoic to Triassic Magmatism of Southwestern Gondwana, and the Relationships with the Volcanogenic Events in Coeval Basins. Journal of South American Earth Sciences 63: 48-69.

Spalletti, L.A.; Fanning, M.; Rapela, C.W. 2008. Dating the Triassic continental rift in the southern Andes: the Potrerillos Formation, Cuyo basin, Argentina. Geologica Acta 6 (3): 267-283.

Strazzere, L.; Gregori, D. 2011. Estratigrafía y evolución del Grupo Choiyoi entre Rincón de los Vallecitos (Cordillera Frontal) y Pampa de Canota (Precordillera Mendocina) provincia de Mendoza. *In* Congreso Geológico Argentino, No. 18. Asociación Geológica Argentina, Resúmenes en CD. Neuquén.

Suárez, M.; Bell, C.M. 1992. Triassic rift-related sedimentary basins in northern Chile (24-29° S). Journal of South American Earth Sciences 6 (3): 109-121.

Torsvik, T.H.; Cocks, L.R.M. 2013. Gondwana from top to base in space and time. Gondwana Research 24 (3): 999-1030.

Torsvik, T.H.; Van der Voo, R.; Preedenn, U.; Mac Niocaill, C.; Steinberger, B.; Doubrovine, P.V.; Hinsbergen, D.J.J.; Domeier, M.; Gaina, C.; Tohver, E.; Meert, J.G.; McCausland, P.J.A.; Cocks, L.R.M. 2012. Phanerozoic polar wander, palaeogeography and dynamics. Earth-Science Reviews 114 (3-4): 325-368.

Uliana, M.; Biddle, K. 1988. Mesozoic-Cenozoic Paleogeographic and Geodynamic Evolution of Southern South America. Revista Brasileira de Geociencias 18: 172-190.

Vásquez, P.; Glodny, J.; Franz, G.; Frei, D.; Romer, R.L. 2011. Early Mesozoic Plutonism of the Cordillera de la Costa (34-37 S), Chile: constraints on the onset of the Andean Orogeny. The Journal of Geology 119 (2): 159-184.

Wang, K.; Hu, Y. 2006. Accretionary prisms in subduction earthquake cycles: The theory of dynamic Coulomb wedge. Journal of Geophysical Research-Solid Earth 111 (B06410): 16 p. doi: 10.1029/2005JB004094.

Welkner, D.; Arévalo, C.; Godoy, E. 2006. Geología del Área Freirina-El Morado, Región de Atacama. Servicio Nacional de Geología y Minería, Carta Geológica de Chile, Serie Geología Básica 100: 50 p. Santiago.

Zappettini, E.; Coira, B.; Santos, J.; Cisterna, C.; Belousova, E. 2015. Combined U-Pb and Lu-Hf Isotopes from the Las Lozas Volcanics, Chaschuil Valley, Nw Argentina: Evidence of Lower Pennsylvanian Extensional Volcanism in Western Gondwana. Journal of South American Earth Sciences 59: 13-18.

Zeil, W. 1958. Sedimentation in der Magallanes-Geosynklinale mit besonderer Berücksichtigung des Flysch. Geologische Rundschau 47: 425-443.

Zimmerer, M.J.; Mcintosh, W.C. 2012. The geochronology of volcanic and plutonic rocks at the Questa caldera: Constraints on the origin of caldera-related silicic magmas. Geological Society of America Bulletin 124: 1394-1408.

Manuscript received: July 19, 2018; revised/accepted: April 24, 2019; available online: January 31, 2020.

Supplementary material 1

U-Pb analytic data tables

SAMPLE CPV-12-113b.

Analysis	U (ppm)	$^{206}Pb/^{204}Pb$	U/Th	Isotope ratios				Apparent ages (Ma)										
				$^{206}Pb/^{207}Pb$	± (%)	$^{207}Pb/^{235}U$	± (%)	$^{206}Pb/^{238}U$	± (%)	error corr.	$^{206}Pb/^{238}U$	± (Ma)	$^{207}Pb/^{235}U$	± (Ma)	$^{206}Pb/^{207}Pb$	± (Ma)	Best age (¥) (Ma)	± (Ma)
CPV-12-113b-62	256	17.393	1.1	21.0841	17.1	0.0760	17.4	0.0116	3.2	0.18	74.5	2.4	74.4	12.5	70.9	408.4	74.5	2.4
CPV-12-113b-94	648	45.179	0.5	21.1968	4.7	0.0825	4.9	0.0127	1.3	0.27	81.3	1.1	80.5	3.8	58.2	112.5	81.3	1.1
CPV-12-113b-79	571	98.330	9.9	20.4334	5.6	0.1019	5.7	0.0151	1.4	0.25	96.6	1.4	98.5	5.4	144.9	130.5	96.6	1.4
CPV-12-113b-65	443	32.375	1.1	19.5032	4.4	0.1309	4.8	0.0185	1.7	0.36	118.2	2.0	124.9	5.6	253.2	102.2	118.2	2.0
CPV-12-113b-33	473	36.783	3.8	19.2612	8.5	0.1383	8.9	0.0193	2.4	0.27	123.3	3.0	131.5	10.9	281.8	195.3	123.3	3.0
CPV-12-113b-35	189	24.941	0.7	19.8234	10.4	0.1396	10.5	0.0201	1.9	0.18	128.1	2.4	132.7	13.1	215.6	240.5	128.1	2.4
CPV-12-113b-92	249	18.412	0.7	18.1442	12.9	0.1532	13.0	0.0202	1.5	0.11	128.7	1.9	144.7	17.5	416.8	288.8	128.7	1.9
CPV-12-113b-63	78	27.764	1.2	19.6091	10.4	0.2139	10.6	0.0304	1.7	0.16	193.2	3.3	196.8	18.9	240.7	241.0	193.2	3.3
CPV-12-113b-34	260	33.157	1.4	19.7574	10.2	0.2160	10.2	0.0309	0.9	0.08	196.5	1.7	198.6	18.4	223.3	236.2	196.5	1.7
CPV-12-113b-54	61	8.951	1.1	19.6709	17.7	0.2177	18.3	0.0311	4.9	0.27	197.2	9.6	200.0	33.3	233.4	410.2	197.2	9.6
CPV-12-113b-19	28	5.708	1.4	19.6236	40.4	0.2341	41.1	0.0333	7.6	0.19	211.3	15.8	213.6	79.3	239.0	967.4	211.3	15.8
CPV-12-113b-97	52	11.722	1.8	18.3957	22.5	0.2517	23.0	0.0336	4.5	0.20	212.9	9.5	227.9	47.0	386.0	512.0	212.9	9.5
CPV-12-113b-64	25	4.234	1.4	15.6687	39.4	0.2961	40.3	0.0336	8.6	0.21	213.3	18.1	263.3	93.7	735.7	865.6	213.3	18.1
CPV-12-113b-66	61	13.570	1.7	19.4426	18.0	0.2392	18.3	0.0337	3.7	0.20	213.8	7.8	217.8	36.0	260.3	415.7	213.8	7.8
CPV-12-113b-72	159	65.394	0.8	19.4157	7.1	0.2414	7.2	0.0340	1.4	0.19	215.5	2.9	219.5	14.3	263.5	163.4	215.5	2.9
CPV-12-113b-77	57	23.169	1.1	18.4333	17.6	0.2549	17.9	0.0341	3.4	0.19	216.0	7.2	230.6	37.0	381.4	398.5	216.0	7.2
CPV-12-113b-47	52	9.058	1.8	17.8434	18.0	0.2639	18.8	0.0341	5.3	0.28	216.5	11.3	237.8	39.8	454.1	402.4	216.5	11.3
CPV-12-113b-53	90	13.736	1.5	22.2959	17.1	0.2113	17.3	0.0342	2.7	0.16	216.6	5.7	194.6	30.7	-63.7	419.7	216.6	5.7
CPV-12-113b-75	36	16.514	1.6	16.9043	32.8	0.2806	33.6	0.0344	6.8	0.20	218.0	14.7	251.1	74.8	572.8	732.9	218.0	14.7
CPV-12-113b-81	364	48.418	0.4	19.2756	2.9	0.2475	3.8	0.0346	2.4	0.64	219.3	5.2	224.5	7.6	280.1	66.2	219.3	5.2
CPV-12-113b-38	51	14.718	1.1	18.6313	12.1	0.2566	12.5	0.0347	3.2	0.26	219.7	6.9	231.9	25.9	357.3	273.8	219.7	6.9
CPV-12-113b-18	36	5.693	1.7	30.6548	62.5	0.1560	62.6	0.0347	3.9	0.06	219.8	8.5	147.2	86.0	-908.7	1,990.4	219.8	8.5
CPV-12-113b-22	58	24.762	1.3	20.2544	18.7	0.2366	19.4	0.0348	5.2	0.27	220.2	11.3	215.6	37.7	165.5	439.4	220.2	11.3
CPV-12-113b-9	71	23.396	1.2	18.3009	10.9	0.2623	11.8	0.0348	4.4	0.37	220.6	9.6	236.5	24.9	397.6	245.5	220.6	9.6
CPV-12-113b-52	83	36.212	1.0	19.0519	11.0	0.2529	11.7	0.0349	4.0	0.34	221.4	8.7	228.9	24.1	306.7	252.3	221.4	8.7

Sample CPV-12-113b continued.

Analysis	U (ppm)	$^{206}Pb/^{204}Pb$	U/Th	Isotope ratios				Apparent ages (Ma)									
				$^{206}Pb/^{207}Pb$	± (%)	$^{207}Pb/^{235}U$	± (%)	$^{206}Pb/^{238}U$	± (%)	error corr.	$^{206}Pb/^{238}U$	± (Ma)	$^{207}Pb/^{235}U$	± (Ma)	$^{206}Pb/^{207}Pb$	± (Ma)	Best age (¥) (Ma)	± (Ma)
CPV-12-113b-45	125	24.601	1.2	20.0454	7.5	0.2407	8.1	0.0350	3.0	0.37	221.7	6.5	219.0	16.0	189.7	175.8	221.7	6.5
CPV-12-113b-31	59	23.108	1.3	20.9056	22.9	0.2312	23.5	0.0351	5.1	0.22	222.1	11.1	211.2	44.8	91.1	549.8	222.1	11.1
CPV-12-113b-82	56	10.868	1.4	26.4327	34.3	0.1829	34.5	0.0351	3.5	0.10	222.1	7.6	170.5	54.1	-497.0	934.8	222.1	7.6
CPV-12-113b-70	282	50.027	0.7	19.3740	4.0	0.2495	4.2	0.0351	1.3	0.32	222.2	2.9	226.2	8.5	268.4	90.9	222.2	2.9
CPV-12-113b-12	104	22.556	0.8	20.8614	11.7	0.2319	11.8	0.0351	1.5	0.13	222.3	3.4	211.8	22.6	96.1	278.1	222.3	3.4
CPV-12-113b-55	839	252.595	0.5	19.5032	1.1	0.2481	2.1	0.0351	1.8	0.86	222.4	3.9	225.0	4.2	253.2	25.0	222.4	3.9
CPV-12-113b-32	92	11.919	1.2	18.6847	17.0	0.2595	17.1	0.0352	2.0	0.11	222.8	4.3	234.2	35.8	350.9	386.3	222.8	4.3
CPV-12-113b-14	36	10.998	1.1	17.6141	34.7	0.2754	35.1	0.0352	4.8	0.14	222.9	10.6	247.0	77.0	482.7	789.1	222.9	10.6
CPV-12-113b-16	152	57.509	1.1	20.8411	11.3	0.2328	11.4	0.0352	1.6	0.14	222.9	3.4	212.5	21.9	98.4	268.2	222.9	3.4
CPV-12-113b-7	153	39.312	1.3	20.1918	10.5	0.2416	10.7	0.0354	2.0	0.19	224.1	4.4	219.7	21.1	172.7	244.9	224.1	4.4
CPV-12-113b-87	106	6.837	1.2	18.8146	14.5	0.2598	14.8	0.0355	2.8	0.19	224.6	6.2	234.5	31.0	335.2	331.1	224.6	6.2
CPV-12-113b-71	240	120.397	0.9	19.4339	7.6	0.2519	7.8	0.0355	1.3	0.17	224.9	2.9	228.1	15.8	261.3	175.7	224.9	2.9
CPV-12-113b-84	173	54.976	0.8	18.4282	3.3	0.2670	5.8	0.0357	4.7	0.82	226.0	10.5	240.3	12.4	382.0	75.1	226.0	10.5
CPV-12-113b-43	120	41.793	1.4	19.0129	7.6	0.2592	7.8	0.0357	1.5	0.20	226.4	3.4	234.0	16.3	311.4	173.6	226.4	3.4
CPV-12-113b-48	76	6.056	1.5	17.6823	8.8	0.2804	10.6	0.0360	5.9	0.56	227.7	13.1	251.0	23.5	474.2	194.6	227.7	13.1
CPV-12-113b-39	61	56.606	0.7	20.0342	14.5	0.2498	14.6	0.0363	1.6	0.11	229.8	3.7	226.4	29.6	191.0	338.1	229.8	3.7
CPV-12-113b-73	51	9.810	1.7	18.9534	13.2	0.2647	13.6	0.0364	3.2	0.23	230.4	7.2	238.4	28.9	318.5	302.2	230.4	7.2
CPV-12-113b-28	51	7.209	0.5	21.4393	26.2	0.2343	26.5	0.0364	3.7	0.14	230.6	8.3	213.7	51.1	31.0	637.6	230.6	8.3
CPV-12-113b-21	57	13.496	0.8	24.6222	33.8	0.2073	34.7	0.0370	7.7	0.22	234.3	17.7	191.3	60.6	-311.8	888.5	234.3	17.7
CPV-12-113b-24	104	40.922	2.9	19.1038	7.7	0.2708	8.1	0.0375	2.4	0.30	237.4	5.6	243.3	17.5	300.6	176.0	237.4	5.6
CPV-12-113b-17	123	37.705	1.8	20.1275	9.8	0.2657	10.0	0.0388	1.9	0.19	245.3	4.5	239.2	21.3	180.2	228.9	245.3	4.5
CPV-12-113b-40	278	178.548	1.2	19.1661	2.7	0.2798	2.9	0.0389	1.0	0.35	246.0	2.4	250.5	6.4	293.1	61.5	246.0	2.4
CPV-12-113b-30	96	28.736	0.9	20.4254	9.5	0.2631	10.0	0.0390	3.1	0.31	246.5	7.4	237.2	21.2	145.9	223.8	246.5	7.4
CPV-12-113b-50	227	103.717	1.2	18.7639	2.9	0.2874	3.4	0.0391	1.8	0.52	247.3	4.3	256.5	7.8	341.3	66.3	247.3	4.3
CPV-12-113b-69	277	255.800	3.1	19.1055	4.2	0.2825	4.2	0.0391	0.7	0.17	247.5	1.7	252.7	9.5	300.4	95.5	247.5	1.7
CPV-12-113b-46	180	76.730	1.2	20.3082	4.8	0.2665	5.2	0.0392	2.0	0.39	248.2	5.0	239.9	11.2	159.3	112.8	248.2	5.0
CPV-12-113b-4	255	105.147	0.9	19.3021	3.6	0.2815	3.7	0.0394	1.1	0.29	249.1	2.6	251.8	8.3	277.0	82.1	249.1	2.6

Sample CPV-12-113b continued.

Analysis	U (ppm)	$^{206}Pb/^{204}Pb$	U/Th	Isotope ratios					Apparent ages (Ma)									
				$^{206}Pb/^{207}Pb$	± (%)	$^{207}Pb/^{235}U$	± (%)	$^{206}Pb/^{238}U$	± (%)	error corr.	$^{206}Pb/^{238}U$	± (Ma)	$^{207}Pb/^{235}U$	± (Ma)	$^{206}P*/^{207}Pb$	± (Ma)	Best age (¥) (Ma)	± (Ma)
CPV-12-113b-29	140	26.587	0.8	18.9242	4.3	0.2896	4.6	0.0397	1.5	0.32	251.2	3.6	258.2	10.4	322.1	98.3	251.2	3.6
CPV-12-113b-56	227	99.512	0.7	20.0170	4.1	0.2746	4.2	0.0399	0.9	0.21	252.0	2.2	246.4	9.3	193.0	96.4	252.0	2.2
CPV-12-113b-98	452	127.066	3.2	19.4850	2.5	0.2835	2.7	0.0401	1.0	0.38	253.2	2.6	253.4	6.1	255.3	57.7	253.2	2.6
CPV-12-113b-58	102	30.906	1.4	19.6744	11.0	0.2841	11.1	0.0405	1.6	0.14	256.2	3.9	253.9	24.9	233.0	254.0	256.2	3.9
CPV-12-113b-10	43	10.648	1.0	25.5828	38.4	0.2190	38.8	0.0406	5.4	0.14	256.7	13.6	201.1	70.8	-410.8	1,035.5	256.7	13.6
CPV-12-113b-44	579	212.371	5.8	19.3699	2.3	0.2894	2.9	0.0407	1.8	0.61	256.9	4.4	258.1	6.6	268.9	52.3	256.9	4.4
CPV-12-113b-36	345	72.070	1.1	19.3009	2.0	0.2941	2.1	0.0412	0.6	0.29	260.1	1.5	261.8	4.7	277.1	45.0	260.1	1.5
CPV-12-113b-80	255	163.689	1.1	19.0060	3.7	0.2988	4.0	0.0412	1.4	0.36	260.2	3.6	265.5	9.2	312.2	84.2	260.2	3.6
CPV-12-113b-26	118	23.329	1.3	19.4737	10.7	0.2923	11.1	0.0413	3.0	0.27	260.8	7.6	260.4	25.5	256.6	246.9	260.8	7.6
CPV-12-113b-83	34	10.165	1.1	21.1454	26.4	0.2750	27.0	0.0422	5.6	0.21	266.3	14.7	246.6	59.2	64.0	638.5	266.3	14.7
CPV-12-113b-8	216	35.488	0.9	19.0427	2.7	0.3069	2.9	0.0424	1.0	0.34	267.6	2.6	271.8	7.0	307.8	62.3	267.6	2.6
CPV-12-113b-68	547	201.622	0.7	19.2013	1.3	0.3044	1.7	0.0424	1.1	0.64	267.6	2.8	269.8	4.0	288.9	29.3	267.6	2.8
CPV-12-113b-23	138	106.724	0.9	19.7065	9.0	0.3000	9.1	0.0429	1.8	0.20	270.6	4.9	266.4	21.4	229.2	207.1	270.6	4.9
CPV-12-113b-78	680	14.472	0.7	18.7855	1.0	0.3152	2.3	0.0429	2.1	0.89	271.1	5.5	278.2	5.7	338.7	23.6	271.1	5.5
CPV-12-113b-91	98	14.659	1.1	18.4971	7.2	0.3265	7.6	0.0438	2.4	0.32	276.4	6.6	286.9	19.0	373.6	162.6	276.4	6.6
CPV-12-113b-76	200	63.754	0.9	18.5362	5.1	0.3329	5.5	0.0448	2.0	0.37	282.3	5.6	291.8	14.0	368.9	115.5	282.3	5.6
CPV-12-113b-15	42	8.122	1.0	20.6137	19.7	0.3078	20.5	0.0460	5.4	0.27	290.0	15.4	272.5	49.0	124.3	468.7	290.0	15.4
CPV-12-113b-59	90	43.517	1.3	18.7439	5.9	0.3387	7.5	0.0460	4.6	0.62	290.2	13.1	296.2	19.2	343.8	133.4	290.2	13.1
CPV-12-113b-90	167	115.539	1.3	19.0568	7.8	0.3364	8.6	0.0465	3.6	0.42	293.0	10.5	294.5	22.0	306.2	177.6	293.0	10.5
CPV-12-113b-93	119	36.184	2.6	18.6176	8.0	0.3451	8.1	0.0466	1.2	0.15	293.6	3.4	301.0	21.1	359.0	180.8	293.6	3.4
CPV-12-113b-37	76	26.888	1.1	19.6648	9.1	0.3276	9.4	0.0467	2.3	0.24	294.4	6.5	287.7	23.4	234.2	209.8	294.4	6.5
CPV-12-113b-85	106	37.792	0.8	18.6621	6.7	0.3460	6.9	0.0468	1.7	0.25	295.0	4.9	301.7	18.0	353.6	150.8	295.0	4.9
CPV-12-113b-25	89	59.554	1.3	17.9658	10.0	0.3600	10.2	0.0469	2.4	0.23	295.5	6.8	312.2	27.5	438.9	222.1	295.5	6.8
CPV-12-113b-100	78	24.666	1.3	18.6986	10.4	0.3460	10.7	0.0469	2.3	0.21	295.6	6.6	301.7	27.9	349.2	236.2	295.6	6.6
CPV-12-113b-61	221	25.066	1.2	19.0169	2.8	0.3428	3.3	0.0473	1.8	0.54	297.8	5.2	299.3	8.6	310.9	63.9	297.8	5.2
CPV-12-113b-60	100	42.272	1.6	19.0201	7.0	0.3489	7.2	0.0481	1.6	0.22	303.0	4.7	303.9	18.8	310.5	159.3	303.0	4.7
CPV-12-113b-88	288	114.291	14.8	17.8454	3.0	0.3932	5.9	0.0509	5.0	0.86	320.0	15.7	336.7	16.8	453.8	66.3	320.0	15.7

Sample CPV-12-113b continued.

Analysis	U (ppm)	$^{206}Pb/^{204}Pb$	U/Th	Isotope ratios				Apparent ages (Ma)										
				$^{206}Pb/^{207}Pb$	± (%)	$^{207}Pb/^{235}U$	± (%)	$^{206}Pb/^{238}U$	± (%)	error corr.	$^{206}Pb/^{238}U$	± (Ma)	$^{207}Pb/^{235}U$	± (Ma)	$^{206}Pb/^{207}P*$	± (Ma)	Best age (¥) (Ma)	± (Ma)
CPV-12-113b-3	82	20.507	1.4	18.5736	11.7	0.3905	11.7	0.0526	1.3	0.11	330.5	4.3	334.7	33.5	364.3	263.9	330.5	4.3
CPV-12-113b-41	288	195.693	8.2	18.8564	2.4	0.3849	2.8	0.0526	1.4	0.52	330.7	4.6	330.6	7.8	330.2	53.6	330.7	4.6
CPV-12-113b-74	209	53.433	1.0	18.9765	5.7	0.3861	5.9	0.0531	1.3	0.23	333.7	4.4	331.5	16.7	315.7	130.7	333.7	4.4
CPV-12-113b-6	130	46.936	2.1	18.4012	5.2	0.4023	5.4	0.0537	1.2	0.23	337.1	4.1	343.3	15.6	385.3	117.3	337.1	4.1
CPV-12-113b-99	176	81.946	0.9	17.9813	2.8	0.4880	2.9	0.0636	0.9	0.32	397.7	3.6	403.5	9.7	436.9	61.7	397.7	3.6
CPV-12-113b-13	157	86.324	2.0	17.6281	3.0	0.5971	3.5	0.0763	1.8	0.51	474.2	8.1	475.4	13.3	480.9	67.0	474.2	8.1
CPV-12-113b-67	103	76.011	1.1	17.3301	4.1	0.6834	4.4	0.0859	1.7	0.39	531.3	8.7	528.9	18.3	518.5	89.7	531.3	8.7
CPV-12-113b-57	297	155.184	1.2	17.1806	1.1	0.7202	1.8	0.0897	1.4	0.78	554.0	7.4	550.8	7.5	537.5	24.0	554.0	7.4
CPV-12-113b-5	457	246.576	3.9	16.8701	1.0	0.7675	1.7	0.0939	1.4	0.80	578.6	7.5	578.3	7.5	577.3	22.2	578.6	7.5
CPV-12-113b-42	87	91.164	1.6	16.2483	2.8	0.8916	3.0	0.1051	1.1	0.36	644.0	6.7	647.2	14.4	658.3	60.1	644.0	6.7
CPV-12-113b-51	218	356.904	2.7	14.4773	1.7	1.1282	3.0	0.1185	2.6	0.84	721.7	17.4	766.9	16.4	900.9	34.1	721.7	17.4
CPV-12-113b-89	185	152.073	3.0	15.7316	1.8	1.0797	2.8	0.1232	2.1	0.76	748.9	14.9	743.5	14.7	727.2	38.4	748.9	14.9
CPV-12-113b-95	125	110.707	1.4	15.2525	1.8	1.1776	3.0	0.1303	2.4	0.79	789.4	17.6	790.2	16.5	792.4	38.4	789.4	17.6
CPV-12-113b-27	117	152.615	2.3	13.1910	1.9	1.9416	2.3	0.1857	1.3	0.56	1,098.3	13.1	1,095.5	15.7	1,090.0	38.9	1,090.0	38.9
CPV-12-113b-49	74	137.421	1.8	7.7936	0.7	7.0426	3.0	0.3981	2.9	0.97	2,160.2	53.2	2,116.8	26.5	2,074.9	12.4	2,074.9	12.4
CPV-12-113b-20	166	407.705	1.6	5.4334	0.2	11.5861	0.9	0.4566	0.9	0.97	2,424.4	18.5	2,571.6	8.9	2,689.7	4.0	2,689.7	4.0

(¥) The best age considered these $^{207}Pb/^{235}U$ values for zircons older than 1 Ga and $^{206}Pb/^{238}U$ ages values for zircons younger than 1 Ga (Nemchin and Cawood, 2005).

Nemchin, A.A.; Cawood, P.A. 2005. Discordance of the U-Pb system in detrital zircons: Implication for provenance studies of sedimentary rocks. Sedimentary Geology 182 (1-4): 143-162. doi: 10.1016/j.sedgeo.2005.07.011.

SAMPLE CPV-12-29X

Analysis	U (ppm)	$^{206}Pb/^{204}Pb$	U/Th	Isotope ratios							Apparent ages (Ma)							
				$^{206}Pb/^{207}Pb$	± (%)	$^{207}Pb/^{235}U$	± (%)	$^{206}Pb^{*}/^{238}U$	± (%)	error corr.	$^{206}Pb/^{238}U$	± (Ma)	$^{207}Pb/^{235}U$	± (Ma)	$^{206}Pb/^{207}Pb$	± (Ma)	Best age (¥) (Ma)	± (Ma)
CPV-12-29X-1	195	149.129	1.1	19.3574	5.0	0.3328	5.9	0.0467	3.0	0.51	294.4	8.6	291.7	14.9	270.4	115.7	294.4	8.6
CPV-12-29X-3	173	196.551	1.0	19.0603	12.5	0.3935	12.6	0.0544	1.8	0.15	341.5	6.1	337.0	36.3	305.7	286.0	341.5	6.1
CPV-12-29X-4	230	126.042	1.3	20.2889	6.4	0.3222	6.9	0.0474	2.6	0.38	298.6	7.6	283.6	17.1	161.6	149.7	298.6	7.6
CPV-12-29X-5	313	133.861	1.3	18.3265	8.6	0.3585	10.6	0.0477	6.2	0.59	300.1	18.3	311.1	28.4	394.4	192.5	300.1	18.3
CPV-12-29X-6	30	24.999	1.6	19.3872	16.4	0.3655	18.3	0.0514	8.1	0.44	323.1	25.5	316.3	49.8	266.9	379.2	323.1	25.5
CPV-12-29X-7	396	576.581	1.2	19.0551	3.3	0.3370	3.9	0.0466	2.1	0.53	293.4	6.0	294.9	10.0	306.4	75.8	293.4	6.0
CPV-12-29X-8	719	662.635	2.4	18.7659	0.8	0.3990	3.2	0.0543	3.1	0.97	340.9	10.1	340.9	9.1	341.1	17.7	340.9	10.1
CPV-12-29X-9	73	47.682	1.0	21.9111	14.3	0.3394	15.1	0.0539	4.7	0.31	338.7	15.6	296.7	38.8	-21.4	347.9	338.7	15.6
CPV-12-29X-10	331	255.976	1.4	19.3579	5.3	0.2841	6.0	0.0399	2.7	0.45	252.2	6.7	253.9	13.4	270.3	121.9	252.2	6.7
CPV-12-29X-11	89	84.764	2.0	18.5414	15.2	0.3334	15.7	0.0448	4.0	0.25	282.7	10.9	292.2	39.8	368.2	343.4	282.7	10.9
CPV-12-29X-12	564	360.397	1.1	18.9736	2.3	0.3763	2.5	0.0518	1.2	0.46	325.4	3.7	324.3	7.0	316.1	51.3	325.4	3.7
CPV-12-29X-13	197	115.221	1.1	19.4702	7.4	0.3151	7.7	0.0445	2.2	0.29	280.7	6.1	278.1	18.8	257.0	170.2	280.7	6.1
CPV-12-29X-14	105	77.450	0.6	20.4547	11.2	0.2678	11.6	0.0397	3.3	0.28	251.1	8.1	240.9	25.0	142.5	262.5	251.1	8.1
CPV-12-29X-15	83	59.969	1.8	18.8783	13.0	0.3785	13.5	0.0518	3.5	0.26	325.7	11.2	325.9	37.5	327.6	295.6	325.7	11.2
CPV-12-29X-16	552	904.694	4.2	18.6364	1.8	0.3964	3.3	0.0536	2.8	0.84	336.5	9.2	339.0	9.6	356.7	40.8	336.5	9.2
CPV-12-29X-17	366	190.031	1.4	19.1509	3.1	0.3463	4.1	0.0481	2.6	0.63	302.9	7.6	301.9	10.6	294.9	71.9	302.9	7.6
CPV-12-29X-18	385	152.750	1.0	18.8725	4.8	0.3288	5.2	0.0450	1.8	0.35	283.7	5.0	288.6	13.0	328.2	109.9	283.7	5.0
CPV-12-29X-19	96	17.082	0.7	19.4634	27.0	0.2873	27.4	0.0406	4.7	0.17	256.3	11.7	256.4	62.2	257.8	631.5	256.3	11.7
CPV-12-29X-20	102	64.141	1.7	17.8871	10.9	0.3923	11.3	0.0509	2.9	0.26	320.0	9.1	336.1	32.4	448.6	243.2	320.0	9.1
CPV-12-29X-21	101	50.652	0.9	19.6625	20.3	0.2785	20.8	0.0397	4.3	0.20	251.1	10.5	249.5	46.0	234.4	473.7	251.1	10.5
CPV-12-29X-22	129	83.184	0.8	18.5717	10.6	0.3429	10.8	0.0462	2.0	0.19	291.0	5.8	299.3	28.1	364.6	240.6	291.0	5.8
CPV-12-29X-23	165	81.354	1.4	19.7788	8.8	0.3190	9.2	0.0458	2.6	0.28	288.4	7.3	281.1	22.6	220.8	204.7	288.4	7.3
CPV-12-29X-24	328	205.350	1.3	19.1289	2.7	0.3692	3.1	0.0512	1.5	0.48	322.0	4.7	319.1	8.4	297.6	61.7	322.0	4.7
CPV-12-29X-25	176	98.000	0.9	19.5995	11.5	0.2763	12.1	0.0393	3.8	0.31	248.3	9.2	247.7	26.6	241.8	265.6	248.3	9.2
CPV-12-29X-26	308	251.291	1.1	18.9317	4.7	0.3393	5.3	0.0466	2.5	0.48	293.5	7.3	296.6	13.7	321.2	106.1	293.5	7.3
CPV-12-29X-27	119	100.536	1.4	18.6433	11.5	0.3900	11.8	0.0527	2.7	0.23	331.3	8.6	334.4	33.6	355.9	259.7	331.3	8.6
CPV-12-29X-28	410	231.888	1.2	19.1623	3.7	0.3018	5.4	0.0419	3.9	0.72	264.9	10.2	267.8	12.8	293.6	85.5	264.9	10.2

Sample CPV-12-29X continued.

Analysis	U (ppm)	$^{206}Pb/^{204}Pb$	U/Th	Isotope ratios							Apparent ages (Ma)							
				$^{206}Pb/^{207}Pb$	± (%)	$^{207}Pb/^{235}U$	± (%)	$^{206}Pb/^{238}U$	± (%)	error corr.	$^{206}Pb/^{238}U$	± (Ma)	$^{207}Pb/^{235}U$	± (Ma)	$^{206}Pb/^{207}Pb$	± (Ma)	Best age (¥) (Ma)	± (Ma)
CPV-12-29X-29	390	305.604	2.0	18.6425	4.0	0.3859	4.4	0.0522	1.9	0.42	327.9	5.9	331.4	12.5	356.0	90.9	327.9	5.9
CPV-12-29X-30	62	53.009	0.9	22.3594	36.9	0.2409	37.4	0.0391	6.2	0.16	247.0	14.9	219.1	73.9	-70.7	929.9	247.0	14.9
CPV-12-29X-31	138	136.034	2.2	19.2474	10.9	0.3330	11.1	0.0465	2.2	0.20	292.9	6.4	291.9	28.2	283.5	249.8	292.9	6.4
CPV-12-29X-32	120	160.050	1.3	19.1719	12.2	0.3855	12.9	0.0536	4.3	0.33	336.6	14.0	331.1	36.6	292.4	280.0	336.6	14.0
CPV-12-29X-33	516	310.030	1.5	19.4053	2.3	0.2796	3.5	0.0394	2.7	0.76	248.8	6.6	250.3	7.9	264.7	53.1	248.8	6.6
CPV-12-29X-34	241	183.455	1.7	18.0128	4.1	0.3484	4.4	0.0455	1.7	0.38	286.9	4.6	303.5	11.5	433.0	90.7	286.9	4.6
CPV-12-29X-35	102	155.748	0.9	17.5901	13.9	0.4194	14.5	0.0535	4.4	0.30	336.0	14.5	355.6	43.7	485.7	307.2	336.0	14.5
CPV-12-29X-36	267	67.242	1.0	18.4650	7.8	0.2995	8.3	0.0401	2.7	0.33	253.5	6.7	266.0	19.3	377.5	176.0	253.5	6.7
CPV-12-29X-37	90	90.810	2.6	20.0587	17.0	0.3138	17.6	0.0457	4.7	0.26	287.8	13.1	277.2	42.8	188.2	398.0	287.8	13.1
CPV-12-29X-38	226	241.278	0.6	19.4451	6.8	0.3867	8.2	0.0545	4.5	0.55	342.3	15.1	332.0	23.2	260.0	156.7	342.3	15.1
CPV-12-29X-39	145	115.692	1.1	19.1031	4.1	0.3392	5.7	0.0470	3.8	0.68	296.0	11.1	296.5	14.5	300.6	94.6	296.0	11.1
CPV-12-29X-40	89	85.939	1.1	19.7556	13.2	0.3202	13.6	0.0459	3.3	0.24	289.1	9.3	282.0	33.4	223.5	305.6	289.1	9.3
CPV-12-29X-41	432	350.687	1.0	19.0515	1.9	0.3778	2.5	0.0522	1.6	0.65	328.0	5.2	325.4	7.0	306.8	43.4	328.0	5.2
CPV-12-29X-42	140	134.136	1.7	18.2651	12.5	0.3492	12.9	0.0463	3.0	0.24	291.5	8.7	304.1	33.8	402.0	281.1	291.5	8.7
CPV-12-29X-43	37	43.029	0.5	21.4653	80.3	0.2511	80.6	0.0391	6.8	0.08	247.2	16.5	227.4	165.6	28.1	2,369.1	247.2	16.5
CPV-12-29X-44	151	135.425	1.0	20.6103	10.7	0.3399	11.3	0.0508	3.6	0.32	319.5	11.3	297.1	29.2	124.7	253.7	319.5	11.3
CPV-12-29X-45	425	335.265	0.8	18.4118	3.7	0.3911	4.3	0.0522	2.3	0.53	328.1	7.3	335.1	12.3	384.0	82.3	328.1	7.3
CPV-12-29X-46	74	99.465	1.0	17.3981	21.7	0.4022	22.1	0.0508	3.9	0.18	319.2	12.1	343.3	64.4	509.9	483.3	319.2	12.1
CPV-12-29X-47	291	168.730	1.3	19.3938	5.4	0.3216	6.5	0.0452	3.6	0.56	285.2	10.1	283.1	16.0	266.1	123.1	285.2	10.1
CPV-12-29X-48	244	279.861	1.6	18.1565	4.0	0.3413	4.6	0.0449	2.4	0.51	283.4	6.6	298.1	12.0	415.3	89.3	283.4	6.6
CPV-12-29X-49	626	321.340	1.4	19.0890	3.0	0.2804	3.4	0.0388	1.6	0.48	245.5	4.0	251.0	7.7	302.3	68.9	245.5	4.0
CPV-12-29X-50	454	533.799	1.1	18.5394	2.0	0.3802	2.8	0.0511	1.9	0.70	321.4	6.1	327.2	7.8	368.5	44.9	321.4	6.1
CPV-12-29X-51	198	176.140	1.1	19.4324	10.2	0.3311	10.7	0.0467	3.0	0.28	294.0	8.7	290.4	27.0	261.5	235.9	294.0	8.7
CPV-12-29X-52	141	507.049	0.7	11.4429	1.2	2.7147	1.9	0.2253	1.5	0.78	1,309.8	18.0	1,332.5	14.5	1,369.1	23.5	1,369.1	23.5
CPV-12-29X-53	70	69.450	1.6	16.4695	22.6	0.3767	23.1	0.0450	5.1	0.22	283.7	14.1	324.6	64.3	629.2	491.8	283.7	14.1
CPV-12-29X-54	284	340.695	1.4	18.8237	2.3	0.3785	3.4	0.0517	2.5	0.73	324.8	7.9	326.0	9.5	334.1	52.3	324.8	7.9
CPV-12-29X-55	70	36.226	1.3	20.0909	17.4	0.3070	17.9	0.0447	4.3	0.24	282.1	11.9	271.8	42.7	184.4	407.4	282.1	11.9

Sample CPV-12-29X continued.

Analysis	U (ppm)	$^{206}Pb/^{204}Pb$	U/Th	Isotope ratios							Apparent ages (Ma)							
				$^{206}Pb/^{207}Pb$	± (%	$^{207}Pb/^{235}U$	± (%)	$^{206}Pb/^{238}U$	± (%)	error corr.	$^{206}Pb/^{238}U$	± (Ma)	$^{207}Pb/^{235}U$	± (Ma)	$^{206}Pb/^{207}Pb$	± (Ma)	Best age (¥) (Ma)	± (Ma)
CPV-12-29X-56	311	182.778	1.1	19.3344	3.0	0.2876	4.1	0.0403	2.8	0.68	254.9	6.9	256.7	9.3	273.1	68.8	254.9	6.9
CPV-12-29X-57	1.030	478.118	1.8	19.5743	1.2	0.2789	2.8	0.0396	2.5	0.91	250.3	6.2	249.8	6.2	244.8	27.4	250.3	6.2
CPV-12-29X-58	47	40.137	1.0	20.7804	40.2	0.2938	40.8	0.0443	6.7	0.16	279.3	18.4	261.5	94.2	105.3	985.7	279.3	18.4
CPV-12-29X-59	227	127.763	1.1	20.4420	11.1	0.2690	11.3	0.0399	2.0	0.18	252.1	5.0	241.9	24.3	144.0	261.2	252.1	5.0
CPV-12-29X-60	439	864.058	1.1	19.3413	5.1	0.2916	5.5	0.0409	2.0	0.35	258.4	4.9	259.8	12.6	272.3	118.0	258.4	4.9
CPV-12-29X-61	230	151.570	1.2	19.4606	5.6	0.3729	5.9	0.0526	1.6	0.28	330.7	5.2	321.8	16.2	258.2	129.7	330.7	5.2
CPV-12-29X-62	217	117.839	1.4	18.6856	6.9	0.3407	8.1	0.0462	4.3	0.53	290.9	12.3	297.7	21.0	350.8	156.2	290.9	12.3
CPV-12-29X-63	78	51.627	1.5	19.9343	20.1	0.3137	20.6	0.0453	4.8	0.23	285.9	13.4	277.0	50.1	202.7	469.7	285.9	13.4
CPV-12-29X-64	88	48.057	1.5	16.2090	8.4	0.3993	10.5	0.0469	6.3	0.60	295.7	18.1	341.2	30.4	663.5	180.7	295.7	18.1
CPV-12-29X-65	198	94.574	1.4	20.0366	11.4	0.2793	12.2	0.0406	4.3	0.35	256.5	10.8	250.1	27.0	190.8	266.3	256.5	10.8
CPV-12-29X-66	117	65.971	1.5	20.8854	16.8	0.3024	17.1	0.0458	3.2	0.19	288.7	9.1	268.3	40.3	93.3	399.7	288.7	9.1
CPV-12-29X-67	235	179.382	1.0	18.9557	5.9	0.2807	6.1	0.0386	1.8	0.30	244.1	4.4	251.2	13.7	318.2	133.3	244.1	4.4
CPV-12-29X-68	219	404.883	1.5	21.0271	6.9	0.2627	7.3	0.0401	2.6	0.35	253.3	6.4	236.9	15.5	77.3	163.0	253.3	6.4
CPV-12-29X-69	100	138.185	1.3	25.1993	19.9	0.2622	20.2	0.0479	3.5	0.17	301.8	10.3	236.4	42.6	-371.5	519.8	301.8	10.3
CPV-12-29X-70	224	116.219	2.4	19.6123	5.7	0.2808	6.3	0.0399	2.8	0.44	252.5	6.9	251.3	14.0	240.3	130.6	252.5	6.9
CPV-12-29X-71	124	54.425	0.7	20.4521	9.0	0.2752	9.7	0.0408	3.6	0.37	257.9	9.0	246.8	21.2	142.8	211.2	257.9	9.0
CPV-12-29X-72	148	104.110	0.6	18.8256	9.9	0.2810	11.0	0.0384	4.9	0.44	242.7	11.7	251.5	24.6	333.9	224.5	242.7	11.7
CPV-12-29X-73	99	71.075	0.8	19.9103	14.4	0.2684	14.9	0.0388	4.0	0.27	245.2	9.6	241.4	32.1	205.4	335.2	245.2	9.6
CPV-12-29X-74	178	103.074	1.0	19.1937	4.9	0.2799	5.5	0.0390	2.5	0.45	246.4	6.0	250.6	12.2	289.8	111.9	246.4	6.0
CPV-12-29X-75	298	260.625	1.7	18.4614	3.9	0.3521	4.7	0.0471	2.6	0.55	297.0	7.4	306.3	12.3	378.0	87.4	297.0	7.4
CPV-12-29X-76	259	265.820	1.7	19.0282	5.5	0.3147	5.9	0.0434	2.2	0.37	274.1	5.8	277.8	14.4	309.6	125.7	274.1	5.8
CPV-12-29X-77	198	61.082	0.8	18.2948	9.6	0.4014	10.7	0.0533	4.7	0.44	334.5	15.2	342.7	31.1	398.3	216.0	334.5	15.2
CPV-12-29X-78	221	344.622	1.5	19.3147	7.7	0.3243	8.0	0.0454	2.2	0.27	286.4	6.2	285.2	20.0	275.4	177.0	286.4	6.2
CPV-12-29X-79	43	48.648	1.4	21.3366	54.1	0.2826	54.5	0.0437	6.0	0.11	275.9	16.1	252.7	122.4	42.5	1,391.1	275.9	16.1
CPV-12-29X-80	158	109.240	1.2	19.0709	7.3	0.2786	9.7	0.0385	6.4	0.66	243.8	15.3	249.6	21.5	304.4	166.3	243.8	15.3
CPV-12-29X-82	281	128.631	1.3	19.9914	4.8	0.3097	5.1	0.0449	1.8	0.35	283.2	5.0	274.0	12.3	196.0	112.1	283.2	5.0
CPV-12-29X-84	404	395.342	0.9	19.7956	5.4	0.2779	6.9	0.0399	4.3	0.62	252.2	10.5	249.0	15.2	218.8	124.9	252.2	10.5

Sample CPV-12-29X continued.

Analysis	U (ppm)	$^{206}Pb/^{204}Pb$	U/Th	Isotope ratios							Apparent ages (Ma)							
				$^{206}Pb/^{207}Pb$	± (%)	$^{207}Pb/^{235}U$	± (%)	$^{206}Pb/^{238}U$	± (%)	error corr.	$^{206}Pb/^{238}U$	± (Ma)	$^{207}Pb/^{235}U$	± (Ma)	$^{206}Pb/^{207}Pb$	± (Ma)	Best age (¥) (Ma)	± (Ma)
CPV-12-29X-85	74	42.183	1.4	24.7574	24.0	0.2599	24.3	0.0467	4.0	0.17	294.0	11.6	234.5	51.0	-325.8	623.5	294.0	11.6
CPV-12-29X-86	388	240.712	1.0	19.5408	3.4	0.3302	4.3	0.0468	2.5	0.59	294.8	7.3	289.7	10.7	248.7	78.8	294.8	7.3
CPV-12-29X-87	117	107.671	1.4	18.9090	8.0	0.3446	8.8	0.0473	3.6	0.41	297.7	10.4	300.6	22.9	323.9	182.8	297.7	10.4
CPV-12-29X-88	110	91.454	0.8	17.8784	7.9	0.4016	8.8	0.0521	3.9	0.44	327.3	12.3	342.8	25.5	449.7	175.4	327.3	12.3
CPV-12-29X-89	71	98.141	1.6	18.2831	14.1	0.3912	14.5	0.0519	3.5	0.24	326.0	11.0	335.2	41.4	399.8	316.4	326.0	11.0
CPV-12-29X-90	109	116.851	1.0	19.3335	28.1	0.3289	28.3	0.0461	3.0	0.11	290.6	8.5	288.7	71.1	273.2	655.4	290.6	8.5
CPV-12-29X-91	85	79.247	0.9	20.7862	19.5	0.3554	19.7	0.0536	2.9	0.15	336.4	9.4	308.7	52.5	104.6	464.0	336.4	9.4
CPV-12-29X-92	87	49.981	1.0	18.4912	25.2	0.3349	25.6	0.0449	4.5	0.18	283.2	12.5	293.3	65.2	374.3	574.3	283.2	12.5
CPV-12-29X-93	169	155.983	1.2	20.0466	12.3	0.2690	13.0	0.0391	4.1	0.32	247.3	10.0	241.9	27.9	189.6	287.3	247.3	10.0
CPV-12-29X-94	104	131.248	1.4	19.4654	11.4	0.3779	11.8	0.0534	2.7	0.23	335.1	9.0	325.5	32.8	257.6	263.8	335.1	9.0
CPV-12-29X-95	276	140.650	1.3	18.4255	5.0	0.3048	5.6	0.0407	2.6	0.47	257.3	6.6	270.1	13.3	382.4	111.3	257.3	6.6
CPV-12-29X-96	236	76.727	0.9	19.1899	9.7	0.2792	10.5	0.0389	4.2	0.39	245.8	10.0	250.0	23.4	290.3	221.6	245.8	10.0
CPV-12-29X-97	294	131.861	1.1	18.9683	6.0	0.2875	6.6	0.0396	2.7	0.41	250.1	6.6	256.6	14.9	316.7	136.9	250.1	6.6
CPV-12-29X-98	97	41.702	1.0	20.2345	26.1	0.2609	26.3	0.0383	3.2	0.12	242.2	7.6	235.4	55.4	167.8	620.1	242.2	7.6
CPV-12-29X-99	719	505.172	1.0	19.6839	1.9	0.2734	2.7	0.0390	1.9	0.72	246.8	4.7	245.4	5.9	231.9	42.9	246.8	4.7
CPV-12-29X-100	319	172.468	0.8	19.8599	5.1	0.3106	5.4	0.0447	1.8	0.33	282.1	4.9	274.7	12.9	211.3	117.6	282.1	4.9

(¥) The best age considered these $^{207}Pb/^{235}U$ values for zircons older than 1 Ga and $^{206}Pb/^{238}U$ ages values for zircons younger than 1 Ga (Nemchin and Cawood, 2005).

Nemchin, A.A.; Cawood, P.A. 2005. Discordance of the U-Pb system in detrital zircons: Implication for provenance studies of sedimentary rocks. Sedimentary Geology 182 (1-4): 143-162. doi: 10.1016/j.sedgeo.2005.07.011.

SAMPLE CPV-12-89D.

Analysis	U (ppm)	$^{206}Pb/^{204}Pb$	U/Th	Isotope ratios							Apparent ages (Ma)							
				$^{206}Pb/^{207}Pb$	± (%)	$^{207}Pb/^{235}U$	± (%)	$^{206}Pb/^{238}U$	± (%)	error corr.	$^{206}Pb/^{238}U$	± (Ma)	$^{207}Pb/^{235}U$	± (Ma)	$^{206}Pb/^{207}Pb$	± (Ma)	Best age (¥) (Ma)	± (Ma)
CPV-12-89D-1	94	155.973	1.2	17.2063	9.3	0.7257	9.7	0.0906	2.7	0.28	558.9	14.3	554.0	41.4	534.2	204.4	558.9	14.3
CPV-12-89D-2	96	169.739	2.1	13.8548	5.2	1.6877	7.0	0.1696	4.6	0.66	1,009.8	43.4	1,003.9	44.7	991.0	106.8	991.0	106.8
CPV-12-89D-3	384	120.526	1.6	19.5881	4.2	0.2352	4.9	0.0334	2.6	0.52	211.8	5.3	214.4	9.5	243.2	97.1	211.8	5.3
CPV-12-89D-4	373	434.734	2.0	17.1816	1.8	0.6589	6.0	0.0821	5.7	0.96	508.7	28.1	513.9	24.2	537.4	38.3	508.7	28.1
CPV-12-89D-6	60	133.626	1.1	16.6278	4.8	0.7880	5.9	0.0950	3.3	0.57	585.3	18.6	590.1	26.2	608.6	104.3	585.3	18.6
CPV-12-89D-7	89	362.743	3.2	14.2034	3.8	1.5135	4.0	0.1559	1.2	0.29	934.0	10.1	935.8	24.3	940.2	77.8	940.2	77.8
CPV-12-89D-8	180	94.059	0.9	18.2216	10.1	0.3054	10.3	0.0404	2.3	0.22	255.1	5.8	270.6	24.5	407.3	225.5	255.1	5.8
CPV-12-89D-9	203	812.556	2.3	13.4772	1.2	1.8021	8.2	0.1761	8.1	0.99	1,045.9	78.4	1,046.2	53.6	1,046.9	24.0	1,046.9	24.0
CPV-12-89D-10	198	240.230	1.4	19.8579	7.6	0.3290	7.7	0.0474	1.6	0.21	298.4	4.8	288.8	19.4	211.5	175.2	298.4	4.8
CPV-12-89D-11	32	173.422	1.2	8.3350	2.5	5.9692	2.7	0.3608	1.1	0.41	1,986.2	19.0	1,971.4	23.6	1,955.8	44.1	1,955.8	44.1
CPV-12-89D-12	360	502.382	112.2	18.1770	2.0	0.5464	3.1	0.0720	2.4	0.78	448.4	10.4	442.6	11.1	412.8	43.7	448.4	10.4
CPV-12-89D-13	181	197.296	2.0	13.3186	1.5	1.6408	4.0	0.1585	3.7	0.92	948.4	32.6	986.0	25.3	1,070.7	31.0	1,070.7	31.0
CPV-12-89D-14	194	482.201	1.1	16.4433	3.2	0.8655	5.0	0.1032	3.9	0.77	633.2	23.3	633.1	23.7	632.7	69.4	633.2	23.3
CPV-12-89D-15	423	738.101	4.0	16.2923	1.0	0.9242	1.4	0.1092	1.0	0.69	668.1	6.1	664.6	6.8	652.5	21.9	668.1	6.1
CPV-12-89D-17	215	257.449	1.1	18.9487	6.3	0.3004	6.4	0.0413	1.1	0.17	260.8	2.7	266.7	15.0	319.1	143.5	260.8	2.7
CPV-12-89D-19	74	57.661	1.0	22.8557	16.2	0.2729	16.7	0.0452	4.1	0.25	285.2	11.5	245.0	36.4	-124.6	401.9	285.2	11.5
CPV-12-89D-22	137	857.467	0.8	6.2234	1.4	9.6420	3.0	0.4352	2.7	0.88	2,329.1	52.4	2,401.2	28.0	2,462.9	24.2	2,462.9	24.2
CPV-12-89D-24	106	157.624	2.0	18.7519	14.5	0.3511	14.8	0.0478	3.2	0.22	300.7	9.4	305.6	39.1	342.8	328.6	300.7	9.4
CPV-12-89D-29	125	263.461	1.3	19.7539	15.3	0.3399	16.2	0.0487	5.1	0.31	306.5	15.2	297.1	41.7	223.7	356.7	306.5	15.2
CPV-12-89D-31	210	284.351	2.1	13.2722	1.2	1.6176	2.1	0.1557	1.8	0.82	932.9	15.3	977.1	13.5	1,077.7	24.8	1,077.7	24.8
CPV-12-89D-32	81	68.483	1.0	18.4562	19.1	0.3003	19.3	0.0402	2.6	0.13	254.0	6.4	266.6	45.2	378.6	433.3	254.0	6.4
CPV-12-89D-34	73	97.942	1.4	17.3580	9.7	0.6174	10.3	0.0777	3.4	0.33	482.6	16.0	488.2	40.0	515.0	213.9	482.6	16.0
CPV-12-89D-35	208	168.566	1.1	18.4168	6.8	0.3655	7.3	0.0488	2.7	0.36	307.3	8.0	316.3	19.9	383.4	153.4	307.3	8.0
CPV-12-89D-36	97	278.807	1.7	16.0351	5.0	0.9314	7.0	0.1083	4.9	0.70	663.0	30.8	668.4	34.2	686.6	106.2	663.0	30.8
CPV-12-89D-37	115	80.537	1.4	17.4932	5.7	0.3766	9.6	0.0478	7.8	0.81	300.9	22.8	324.5	26.8	497.9	126.1	300.9	22.8
CPV-12-89D-38	111	184.801	0.5	17.7848	9.4	0.5600	9.5	0.0722	1.6	0.17	449.6	6.8	451.5	34.6	461.4	207.9	449.6	6.8

Sample CPV-12-89D continued.

Analysis	U (ppm)	$^{206}Pb/^{204}Pb$	U/Th	Isotope ratios							Apparent ages (Ma)							
				$^{206}Pb/^{207}Pb$	± (%)	$^{207}Pb/^{235}U$	± (%)	$^{206}Pb/^{238}U$	± (%)	error corr.	$^{206}Pb/^{238}U$	± (Ma)	$^{207}Pb/^{235}U$	± (Ma)	$^{206}Pb/^{207}Pb$	± (Ma)	Best age (¥) (Ma)	± (Ma)
CPV-12-89D-39	117	89.615	1.1	13.6191	1.3	1.6010	5.2	0.1581	5.1	0.97	946.4	44.5	970.6	32.6	1,025.7	25.9	1,025.7	25.9
CPV-12-89D-40	189	72.284	1.3	19.1626	10.5	0.2423	10.8	0.0337	2.4	0.22	213.5	5.0	220.3	21.4	293.5	240.6	213.5	5.0
CPV-12-89D-41	116	8.002	0.7	16.5498	16.6	0.3323	18.2	0.0399	7.5	0.41	252.1	18.6	291.3	46.1	618.8	359.7	252.1	18.6
CPV-12-89D-42	478	238.923	0.8	19.4436	2.4	0.2925	2.8	0.0413	1.5	0.55	260.6	4.0	260.5	6.5	260.2	54.0	260.6	4.0
CPV-12-89D-43	101	39.756	1.2	19.0490	8.1	0.2252	9.2	0.0311	4.3	0.47	197.5	8.4	206.3	17.2	307.1	185.4	197.5	8.4
CPV-12-89D-44	327	235.440	1.5	18.3353	2.9	0.3763	4.4	0.0500	3.3	0.75	314.8	10.2	324.3	12.2	393.4	64.9	314.8	10.2
CPV-12-89D-45	54	236.173	1.3	13.3651	4.9	1.9081	5.3	0.1850	1.8	0.35	1,094.0	18.4	1,083.9	35.1	1,063.7	99.4	1,063.7	99.4

(¥) The best age considered these $^{206}Pb/^{207}Pb$ values for zircons older than 1 Ga and $^{206}Pb/^{238}U$ ages values for zircons younger than 1 Ga (Nemchin and Cawood. 2005).

Nemchin. A.A.; Cawood. P.A. 2005. Discordance of the U-Pb system in detrital zircons: Implication for provenance studies of sedimentary rocks. Sedimentary Geology 182 (1-4): 143-162. doi: 10.1016/j.sedgeo.2005.07.011.

SAMPLE CPV-12-39.

Analysis	U (ppm)	$^{206}Pb/^{204}Pb$	U/Th	Isotope ratios							Apparent ages (Ma)							
				$^{206}Pb/^{207}Pb$	± (%)	$^{207}Pb/^{235}U$	± (%)	$^{206}Pb/^{238}U$	± (%)	error corr.	$^{206}Pb/^{238}U$	± (Ma)	$^{207}Pb/^{235}U$	± (Ma)	$^{206}Pb/^{207}Pb$	± (Ma)	Best age (¥) (Ma)	± (Ma)
CPV-12-39-1	139	83.943	1.0	18.5950	6.6	0.3239	6.9	0.0437	2.0	0.29	275.6	5.4	284.9	17.2	361.7	149.4	275.6	5.4
CPV-12-39-2	123	53.160	0.8	19.5573	10.5	0.3317	10.6	0.0471	1.5	0.14	296.4	4.4	290.9	26.9	246.8	242.7	296.4	4.4
CPV-12-39-3	379	121.335	1.5	19.2569	2.1	0.3543	2.1	0.0495	0.4	0.19	311.3	1.3	307.9	5.7	282.3	48.1	311.3	1.3
CPV-12-39-4	54	23.414	0.6	22.4716	30.0	0.2477	30.5	0.0404	5.1	0.17	255.2	12.8	224.7	61.5	-82.9	749.7	255.2	12.8
CPV-12-39-5	49	36.542	0.9	23.9386	34.9	0.2221	35.1	0.0386	3.8	0.11	243.9	9.0	203.6	64.9	-240.1	905.0	243.9	9.0
CPV-12-39-7	83	158.792	2.6	12.5964	3.0	2.2140	3.1	0.2023	0.8	0.26	1,187.5	8.5	1,185.5	21.5	1,181.8	58.8	1,181.8	58.8
CPV-12-39-8	113	31.274	0.5	18.5597	7.0	0.2927	7.2	0.0394	1.4	0.20	249.1	3.5	260.7	16.5	366.0	158.4	249.1	3.5
CPV-12-39-9	141	27.549	0.8	17.9315	8.1	0.3434	8.2	0.0447	1.5	0.18	281.7	4.2	299.8	21.3	443.1	179.7	281.7	4.2
CPV-12-39-10	101	132.837	1.0	14.7864	2.8	1.3134	2.9	0.1409	0.7	0.26	849.5	5.9	851.6	16.6	857.2	57.8	849.5	5.9
CPV-12-39-11	58	281.985	0.9	9.3154	1.9	4.5873	2.1	0.3099	0.9	0.45	1,740.3	14.3	1,747.0	17.4	1,754.9	34.1	1,754.9	34.1
CPV-12-39-12	108	32.069	1.0	18.8064	14.0	0.3272	14.2	0.0446	2.2	0.16	281.5	6.1	287.5	35.5	336.2	319.0	281.5	6.1
CPV-12-39-13	98	32.385	1.3	18.8207	5.8	0.3375	6.1	0.0461	1.6	0.27	290.3	4.6	295.3	15.5	334.5	132.4	290.3	4.6
CPV-12-39-14	128	57.188	1.0	19.7065	13.6	0.3132	13.7	0.0448	2.2	0.16	282.3	6.2	276.6	33.3	229.2	314.5	282.3	6.2
CPV-12-39-15	1.003	274.333	2.2	19.5249	1.8	0.2806	1.9	0.0397	0.6	0.31	251.2	1.4	251.1	4.1	250.6	40.8	251.2	1.4
CPV-12-39-16	183	45.238	1.0	19.1726	4.2	0.3095	4.3	0.0430	1.0	0.23	271.6	2.6	273.8	10.3	292.3	95.2	271.6	2.6
CPV-12-39-17	413	151.939	1.1	19.2485	2.2	0.3267	2.2	0.0456	0.5	0.22	287.5	1.4	287.0	5.6	283.3	50.2	287.5	1.4
CPV-12-39-18	118	42.225	1.5	19.7944	13.0	0.3282	13.5	0.0471	3.6	0.26	296.8	10.3	288.2	33.8	218.9	301.8	296.8	10.3
CPV-12-39-19	211	78.425	1.6	19.4893	5.5	0.3712	5.7	0.0525	1.3	0.22	329.7	4.1	320.5	15.5	254.8	126.8	329.7	4.1
CPV-12-39-20	132	54.059	1.0	19.0382	10.8	0.3260	10.9	0.0450	1.3	0.12	283.8	3.7	286.5	27.1	308.4	246.1	283.8	3.7
CPV-12-39-21	271	59.794	0.8	18.7575	2.7	0.3800	2.8	0.0517	0.8	0.29	324.9	2.6	327.0	7.8	342.1	60.7	324.9	2.6
CPV-12-39-23	117	37.110	1.6	16.7137	5.5	0.4054	10.8	0.0491	9.3	0.86	309.2	28.0	345.5	31.5	597.5	118.4	309.2	28.0
CPV-12-39-25	172	52.708	1.1	18.6475	10.4	0.3527	10.6	0.0477	1.8	0.17	300.4	5.3	306.7	28.1	355.4	236.3	300.4	5.3
CPV-12-39-26	135	60.109	1.0	20.7188	8.5	0.2754	8.7	0.0414	1.4	0.16	261.4	3.5	247.0	19.0	112.3	201.9	261.4	3.5
CPV-12-39-27	430	247.526	1.6	19.0643	1.9	0.3288	2.0	0.0455	0.5	0.24	286.6	1.3	288.6	5.0	305.3	44.1	286.6	1.3
CPV-12-39-28	714	253.719	2.0	18.8521	1.4	0.3873	1.5	0.0530	0.5	0.32	332.6	1.5	332.4	4.2	330.7	31.8	332.6	1.5
CPV-12-39-29	69	11.668	1.6	20.4802	19.8	0.2673	20.1	0.0397	3.5	0.18	251.0	8.7	240.5	43.0	139.6	468.3	251.0	8.7

Sample CPV-12-39 continued.

Analysis	U (ppm)	$^{206}Pb/^{204}Pb$	U/Th	Isotope ratios							Apparent ages (Ma)							
				$^{206}Pb/^{207}Pb$	± (%)	$^{207}Pb/^{235}U$	± (%)	$^{206}Pb/^{238}U$	± (%)	error corr.	$^{206}Pb/^{238}U$	± (Ma)	$^{207}Pb/^{235}U$	± (Ma)	$^{206}Pb/^{207}Pb$	± (Ma)	Best age (¥) (Ma)	± (Ma)
CPV-12-39-30	434	136.303	0.6	19.0689	2.3	0.3360	2.3	0.0465	0.3	0.13	292.8	0.9	294.2	5.9	304.7	52.0	292.8	0.9
CPV-12-39-31	133	44.464	1.5	18.0944	9.9	0.3497	10.2	0.0459	2.5	0.24	289.3	7.0	304.5	26.9	423.0	222.1	289.3	7.0
CPV-12-39-32	160	22.119	0.8	17.7548	6.0	0.3608	6.2	0.0465	1.7	0.27	292.8	4.8	312.8	16.7	465.1	132.6	292.8	4.8
CPV-12-39-33	387	117.853	0.9	19.3232	3.5	0.2799	3.8	0.0392	1.3	0.36	248.1	3.3	250.6	8.3	274.4	80.4	248.1	3.3
CPV-12-39-34	359	26.973	7.7	17.9971	3.6	0.3951	3.7	0.0516	0.9	0.24	324.2	2.8	338.1	10.6	435.0	79.9	324.2	2.8
CPV-12-39-35	341	118.197	1.9	19.4360	2.8	0.2901	2.9	0.0409	0.6	0.22	258.4	1.6	258.7	6.7	261.1	65.3	258.4	1.6
CPV-12-39-36	30	13.421	1.6	12.9393	19.1	0.4885	19.8	0.0458	5.2	0.26	288.9	14.6	403.9	66.0	1,128.6	383.5	288.9	14.6
CPV-12-39-38	147	64.458	1.0	19.4159	8.7	0.3358	8.9	0.0473	2.2	0.24	297.9	6.3	294.0	22.8	263.4	199.3	297.9	6.3
CPV-12-39-39	215	56.764	1.0	19.0393	7.4	0.2987	7.4	0.0412	0.9	0.13	260.5	2.4	265.4	17.3	308.2	167.8	260.5	2.4
CPV-12-39-40	170	49.697	1.2	18.7662	7.4	0.3385	7.4	0.0461	0.9	0.11	290.3	2.4	296.0	19.1	341.1	167.4	290.3	2.4
CPV-12-39-41	107	108.676	1.3	19.2440	7.9	0.2718	8.1	0.0379	1.9	0.23	240.0	4.5	244.1	17.7	283.9	181.2	240.0	4.5
CPV-12-39-42	488	152.206	3.2	18.6207	2.4	0.3718	2.5	0.0502	0.4	0.16	315.8	1.2	321.0	6.8	358.6	55.1	315.8	1.2
CPV-12-39-43	261	111.880	1.7	19.4564	2.9	0.3744	3.1	0.0528	1.2	0.39	331.8	3.9	322.9	8.6	258.7	65.9	331.8	3.9
CPV-12-39-44	237	77.456	1.5	19.0661	4.4	0.3080	4.5	0.0426	0.6	0.13	268.8	1.5	272.6	10.7	305.0	101.0	268.8	1.5
CPV-12-39-45	296	96.402	1.1	19.5060	3.8	0.2935	4.0	0.0415	1.0	0.26	262.3	2.6	261.3	9.1	252.8	88.0	262.3	2.6
CPV-12-39-46	288	67.377	0.9	19.1515	4.5	0.2988	4.6	0.0415	0.9	0.20	262.1	2.4	265.4	10.7	294.8	102.8	262.1	2.4
CPV-12-39-47	68	21.895	1.0	21.3160	14.4	0.2737	15.5	0.0423	5.8	0.37	267.2	15.2	245.7	33.9	44.8	345.6	267.2	15.2
CPV-12-39-48	126	195.887	0.8	18.2889	9.7	0.3084	9.8	0.0409	1.0	0.10	258.4	2.4	272.9	23.4	399.1	218.7	258.4	2.4
CPV-12-39-49	143	76.650	1.1	19.9594	5.4	0.3085	5.6	0.0447	1.6	0.28	281.6	4.3	273.0	13.4	199.7	124.7	281.6	4.3
CPV-12-39-50	348	91.078	1.3	19.3099	2.0	0.2850	2.7	0.0399	1.7	0.65	252.3	4.3	254.6	6.0	276.0	46.2	252.3	4.3
CPV-12-39-52	87	40.542	0.9	18.2676	13.1	0.3427	13.2	0.0454	1.9	0.14	286.2	5.2	299.2	34.3	401.7	294.4	286.2	5.2
CPV-12-39-53	99	28.912	1.4	19.3406	8.2	0.3318	8.3	0.0465	1.6	0.19	293.3	4.6	290.9	21.1	272.4	187.5	293.3	4.6
CPV-12-39-54	96	83.590	1.0	19.0189	10.5	0.3343	10.8	0.0461	2.5	0.23	290.6	7.1	292.8	27.4	310.7	239.3	290.6	7.1
CPV-12-39-55	340	151.003	0.7	19.1980	3.1	0.3372	3.2	0.0469	0.7	0.21	295.8	1.9	295.0	8.2	289.3	71.4	295.8	1.9
CPV-12-39-56	372	69.292	1.0	19.9945	3.8	0.2824	3.9	0.0410	0.6	0.15	258.7	1.5	252.6	8.6	195.7	88.7	258.7	1.5
CPV-12-39-57	271	102.801	2.1	19.3465	3.8	0.3095	3.9	0.0434	0.7	0.17	274.1	1.8	273.8	9.3	271.7	87.6	274.1	1.8
CPV-12-39-58	104	148.046	1.6	13.8268	0.8	1.6435	1.3	0.1648	1.0	0.78	983.5	8.9	987.1	7.9	995.1	15.9	995.1	15.9

Sample CPV-12-39 continued.

Analysis	U (ppm)	$^{206}Pb/^{204}Pb$	U/Th	Isotope ratios							Apparent ages (Ma)							
				$^{206}Pb/^{207}Pb$	± (%)	$^{207}Pb/^{235}U$	± (%)	$^{206}Pb/^{238}U$	± (%)	error corr.	$^{206}Pb/^{238}U$	± (Ma)	$^{207}Pb/^{235}U$	± (Ma)	$^{206}Pb/^{207}Pb$	± (Ma)	Best age (¥) (Ma)	± (Ma)
CPV-12-39-59	191	65.469	1.1	19.4821	7.1	0.2868	7.2	0.0405	1.2	0.17	256.1	3.0	256.1	16.3	255.6	163.0	256.1	3.0
CPV-12-39-60	98	35.608	1.3	18.8356	9.1	0.3328	9.2	0.0455	1.4	0.15	286.6	4.0	291.7	23.3	332.7	206.2	286.6	4.0
CPV-12-39-61	145	54.182	0.8	19.6511	7.6	0.2898	7.7	0.0413	1.4	0.18	260.9	3.6	258.4	17.6	235.8	175.1	260.9	3.6
CPV-12-39-62	180	82.921	1.2	18.6619	5.8	0.3172	6.2	0.0429	2.2	0.35	271.0	5.7	279.8	15.1	353.6	131.2	271.0	5.7
CPV-12-39-63	90	54.947	0.8	21.5799	39.0	0.2474	39.0	0.0387	2.0	0.05	244.9	4.8	224.5	78.8	15.3	969.9	244.9	4.8
CPV-12-39-64	120	11.028	1.2	16.7292	10.9	0.4047	11.3	0.0491	3.0	0.27	309.0	9.1	345.1	33.0	595.4	236.0	309.0	9.1
CPV-12-39-65	627	273.579	1.1	19.3651	3.1	0.3000	3.2	0.0421	0.7	0.21	266.1	1.7	266.4	7.5	269.4	71.8	266.1	1.7
CPV-12-39-66	96	28.493	0.9	20.0201	13.7	0.2763	13.9	0.0401	2.2	0.16	253.6	5.5	247.7	30.6	192.7	320.3	253.6	5.5
CPV-12-39-67	32	7.940	1.1	20.0969	32.4	0.3026	33.0	0.0441	6.6	0.20	278.2	18.1	268.4	78.1	183.7	771.7	278.2	18.1
CPV-12-39-68	95	119.779	1.3	19.1467	6.3	0.3307	6.8	0.0459	2.5	0.37	289.5	7.2	290.1	17.2	295.4	144.4	289.5	7.2
CPV-12-39-69	149	106.445	0.9	19.5825	12.0	0.2990	12.2	0.0425	2.1	0.17	268.1	5.4	265.7	28.4	243.8	276.8	268.1	5.4
CPV-12-39-70	60	31.637	1.1	24.5677	28.4	0.2289	29.4	0.0408	7.4	0.25	257.7	18.6	209.3	55.6	-306.1	740.1	257.7	18.6
CPV-12-39-71	178	75.195	1.1	21.0992	7.4	0.2554	7.6	0.0391	1.6	0.22	247.2	4.0	231.0	15.7	69.2	177.1	247.2	4.0
CPV-12-39-72	489	259.513	0.9	19.3433	3.5	0.2852	3.7	0.0400	1.2	0.32	252.9	2.9	254.8	8.3	272.0	80.2	252.9	2.9
CPV-12-39-73	125	58.526	1.0	19.5813	5.2	0.3236	6.0	0.0460	2.9	0.49	289.6	8.2	284.6	14.9	243.9	120.6	289.6	8.2
CPV-12-39-74	130	62.703	1.3	19.1684	8.8	0.3358	8.9	0.0467	1.5	0.17	294.1	4.3	294.0	22.7	292.9	201.0	294.1	4.3
CPV-12-39-75	150	52.544	0.9	19.3475	10.0	0.3252	10.3	0.0456	2.7	0.26	287.7	7.7	285.9	25.7	271.5	228.7	287.7	7.7
CPV-12-39-76	222	175.653	12.0	17.7516	2.8	0.5985	3.0	0.0771	0.9	0.31	478.5	4.3	476.3	11.3	465.5	62.3	478.5	4.3
CPV-12-39-77	231	182.186	0.9	19.2369	4.1	0.2949	4.2	0.0411	0.9	0.22	259.9	2.4	262.4	9.8	284.7	94.7	259.9	2.4
CPV-12-39-78	176	80.535	1.3	19.7424	7.0	0.2950	7.2	0.0422	1.6	0.23	266.7	4.3	262.5	16.6	225.0	161.8	266.7	4.3
CPV-12-39-79	115	50.732	1.3	18.8645	12.7	0.3320	13.0	0.0454	2.6	0.20	286.4	7.2	291.1	32.8	329.2	289.5	286.4	7.2
CPV-12-39-80	67	35.899	1.6	18.4608	14.2	0.2986	14.9	0.0400	4.3	0.29	252.7	10.8	265.3	34.8	378.1	321.7	252.7	10.8
CPV-12-39-81	76	9.501	0.9	19.6007	15.1	0.2827	15.3	0.0402	2.2	0.14	254.0	5.4	252.8	34.2	241.7	350.1	254.0	5.4
CPV-12-39-82	70	13.844	0.9	18.3303	14.9	0.2957	15.0	0.0393	2.3	0.16	248.6	5.7	263.0	34.9	394.0	334.8	248.6	5.7
CPV-12-39-83	141	36.086	1.0	20.3971	7.5	0.2809	7.6	0.0416	1.5	0.19	262.5	3.8	251.4	17.0	149.1	175.6	262.5	3.8
CPV-12-39-84	134	33.747	1.4	18.3448	7.3	0.3547	7.5	0.0472	1.9	0.26	297.3	5.6	308.3	20.0	392.2	163.6	297.3	5.6
CPV-12-39-85	57	11.232	1.0	17.4328	21.9	0.3124	23.0	0.0395	7.2	0.31	249.8	17.7	276.1	55.8	505.5	486.9	249.8	17.7

Sample CPV-12-39 continued.

Analysis	U (ppm)	$^{206}Pb/^{204}Pb$	U/Th	Isotope ratios							Apparent ages (Ma)							
				$^{206}Pb/^{207}Pb$	± (%)	$^{207}Pb/^{235}U$	± (%)	$^{206}Pb/^{238}U$	± (%)	error corr.	$^{206}Pb/^{238}U$	± (Ma)	$^{207}Pb/^{235}U$	± (Ma)	$^{206}Pb/^{207}Pb$	± (Ma)	Best age (¥) (Ma)	± (Ma)
CPV-12-39-86	91	30.312	1.2	19.5309	9.6	0.2847	9.9	0.0403	2.5	0.25	254.9	6.3	254.4	22.3	249.9	221.4	254.9	6.3
CPV-12-39-87	90	20.254	1.7	21.0382	14.8	0.3003	15.0	0.0458	2.3	0.15	288.9	6.5	266.7	35.2	76.0	353.8	288.9	6.5
CPV-12-39-88	122	36.750	0.9	19.6868	9.1	0.3113	9.3	0.0444	2.1	0.22	280.3	5.7	275.2	22.5	231.5	210.1	280.3	5.7
CPV-12-39-89	299	137.925	1.2	19.0766	3.9	0.2746	4.2	0.0380	1.3	0.32	240.4	3.1	246.4	9.1	303.8	90.0	240.4	3.1
CPV-12-39-90	146	10.786	1.1	18.3406	10.1	0.2934	10.3	0.0390	2.0	0.19	246.8	4.8	261.2	23.7	392.7	227.2	246.8	4.8
CPV-12-39-91	102	35.785	1.0	19.3364	10.1	0.2772	10.3	0.0389	2.1	0.20	245.9	5.0	248.4	22.7	272.9	231.2	245.9	5.0
CPV-12-39-92	419	106.841	2.2	19.0185	3.1	0.2944	3.2	0.0406	0.7	0.23	256.6	1.8	262.0	7.3	310.7	70.0	256.6	1.8
CPV-12-39-93	136	43.012	1.6	19.7983	13.7	0.3183	13.9	0.0457	2.5	0.18	288.1	7.0	280.6	34.2	218.5	318.6	288.1	7.0
CPV-12-39-94	128	57.445	0.8	19.2675	5.5	0.3384	5.7	0.0473	1.6	0.27	297.9	4.5	296.0	14.7	281.1	125.8	297.9	4.5
CPV-12-39-95	103	28.925	1.3	20.9628	14.1	0.2499	14.2	0.0380	1.9	0.13	240.4	4.5	226.5	28.8	84.6	335.2	240.4	4.5
CPV-12-39-96	67	25.294	0.5	19.8117	16.4	0.3304	16.7	0.0475	2.6	0.16	299.0	7.7	289.9	42.0	217.0	382.9	299.0	7.7
CPV-12-39-97	140	34.586	0.9	19.6466	5.4	0.3156	5.8	0.0450	2.1	0.37	283.5	5.9	278.5	14.0	236.3	123.6	283.5	5.9
CPV-12-39-98	145	15.034	1.4	17.0663	13.6	0.3625	13.7	0.0449	1.4	0.10	282.9	3.9	314.1	37.0	552.1	298.3	282.9	3.9
CPV-12-39-99	278	145.971	1.1	19.4119	2.8	0.3359	2.9	0.0473	0.8	0.27	297.9	2.3	294.1	7.5	263.9	64.7	297.9	2.3
CPV-12-39-100	80	23.858	1.1	19.3228	17.1	0.3059	17.9	0.0429	5.4	0.30	270.6	14.2	271.0	42.7	274.5	394.7	270.6	14.2

(¥) The best age considered these $^{206}Pb/^{207}Pb$ values for zircons older than 1 Ga and $^{206}Pb/^{238}U$ ages values for zircons younger than 1 Ga (Nemchin and Cawood, 2005).

Nemchin, A.A.; Cawood, P.A. 2005. Discordance of the U-Pb system in detrital zircons: Implication for provenance studies of sedimentary rocks. Sedimentary Geology 182 (1-4): 143-162. doi: 10.1016/j.sedgeo.2005.07.011.

SAMPLE CPV-12-50.

Analysis	U (ppm)	$^{206}Pb/^{204}Pb$	U/Th	Isotope ratios							Apparent ages (Ma)							
				$^{206}Pb/^{207}Pb$	± (%)	$^{207}Pb/^{235}U$	± (%)	$^{206}Pb/^{238}U$	± (%)	error corr.	$^{206}Pb/^{238}U$	± (Ma)	$^{207}Pb/^{235}U$	± (Ma)	$^{206}Pb/^{207}Pb$	± (Ma)	Best age (¥) (Ma)	± (Ma)
CPV-12-50-1	289	302.703	1.2	19.6386	4.8	0.3223	5.0	0.0459	1.3	0.25	289.3	3.6	283.7	12.4	237.2	111.5	289.3	3.6
CPV-12-50-2	100	38.998	1.1	19.3924	13.2	0.3335	13.3	0.0469	1.7	0.13	295.5	4.9	292.2	33.7	266.2	303.1	295.5	4.9
CPV-12-50-3	73	21.680	1.7	17.5495	15.7	0.3656	15.9	0.0465	2.5	0.16	293.2	7.2	316.4	43.3	490.8	348.3	293.2	7.2
CPV-12-50-4	455	163.433	1.3	19.2452	2.9	0.3392	2.9	0.0473	0.4	0.14	298.2	1.2	296.6	7.5	283.7	66.1	298.2	1.2
CPV-12-50-5	189	72.097	1.2	18.7419	5.1	0.3500	5.2	0.0476	1.1	0.21	299.6	3.2	304.7	13.8	344.0	115.6	299.6	3.2
CPV-12-50-6	182	94.813	0.9	19.8509	5.5	0.3267	5.6	0.0470	1.3	0.23	296.3	3.7	287.1	14.0	212.3	126.6	296.3	3.7
CPV-12-50-7	257	63.063	1.5	18.9671	3.1	0.3843	3.2	0.0529	0.6	0.18	332.1	1.9	330.2	9.0	316.9	71.1	332.1	1.9
CPV-12-50-8	423	210.344	1.2	19.1885	1.4	0.3499	2.0	0.0487	1.4	0.71	306.5	4.2	304.6	5.2	290.4	31.8	306.5	4.2
CPV-12-50-9	169	95.646	1.0	19.4740	8.3	0.3337	8.4	0.0471	1.3	0.16	296.9	3.9	292.4	21.3	256.6	190.5	296.9	3.9
CPV-12-50-10	275	114.451	1.0	19.6308	2.5	0.3200	2.6	0.0456	0.5	0.19	287.2	1.4	281.9	6.3	238.1	57.9	287.2	1.4
CPV-12-50-11	70	31.278	1.3	20.3436	17.1	0.3217	17.7	0.0475	4.7	0.27	299.0	13.8	283.2	43.8	155.3	402.2	299.0	13.8
CPV-12-50-12	308	84.149	1.2	19.0292	3.8	0.3402	3.9	0.0469	0.8	0.20	295.8	2.2	297.3	10.0	309.4	86.3	295.8	2.2
CPV-12-50-13	179	76.050	0.4	19.9790	9.7	0.2731	10.1	0.0396	2.5	0.25	250.2	6.2	245.2	21.9	197.4	226.5	250.2	6.2
CPV-12-50-14	187	43.723	3.2	19.8459	10.0	0.2859	10.1	0.0411	1.3	0.13	260.0	3.4	255.3	22.8	212.9	232.0	260.0	3.4
CPV-12-50-15	144	46.389	1.2	18.9485	8.0	0.3795	8.1	0.0521	1.2	0.15	327.7	3.8	326.6	22.7	319.1	182.7	327.7	3.8
CPV-12-50-16	72	35.906	1.0	22.9102	13.0	0.2704	13.5	0.0449	3.5	0.26	283.3	9.8	243.0	29.1	-130.5	322.7	283.3	9.8
CPV-12-50-17	192	7.000	1.0	14.8476	23.9	0.4346	24.5	0.0468	5.3	0.22	294.8	15.4	366.4	75.5	848.6	504.3	294.8	15.4
CPV-12-50-18	188	50.303	1.4	19.4141	4.4	0.2902	4.6	0.0409	1.1	0.24	258.2	2.8	258.7	10.5	263.7	102.0	258.2	2.8
CPV-12-50-19	105	45.011	1.2	18.7614	11.4	0.3426	11.5	0.0466	1.5	0.13	293.7	4.3	299.2	29.9	341.6	259.4	293.7	4.3
CPV-12-50-20	197	70.433	1.3	19.3585	3.6	0.3278	3.7	0.0460	1.1	0.28	290.1	3.0	287.9	9.3	270.2	81.9	290.1	3.0
CPV-12-50-21	161	46.968	0.8	20.0792	9.8	0.3156	9.9	0.0460	1.4	0.14	289.6	3.9	278.5	24.2	185.8	229.6	289.6	3.9
CPV-12-50-22	217	97.736	1.8	19.6877	4.5	0.3274	4.7	0.0468	1.3	0.28	294.6	3.8	287.6	11.7	231.4	103.2	294.6	3.8
CPV-12-50-24	596	297.147	1.0	18.9857	2.1	0.3421	2.2	0.0471	0.6	0.28	296.7	1.8	298.8	5.7	314.7	47.7	296.7	1.8
CPV-12-50-25	109	29.948	1.3	19.1276	9.5	0.3287	9.7	0.0456	2.2	0.22	287.5	6.1	288.6	24.4	297.7	216.5	287.5	6.1
CPV-12-50-26	549	196.999	0.9	19.0304	1.9	0.3387	1.9	0.0467	0.4	0.21	294.5	1.2	296.1	4.9	309.3	42.2	294.5	1.2
CPV-12-50-27	110	53.572	1.3	18.3425	13.0	0.3447	13.2	0.0459	2.3	0.18	289.1	6.6	300.8	34.3	392.5	292.1	289.1	6.6
CPV-12-50-28	197	38.065	1.4	18.7774	4.6	0.3437	4.8	0.0468	1.3	0.27	294.9	3.8	300.0	12.5	339.7	104.7	294.9	3.8

Sample CPV-12-50 continued.

Analysis	U (ppm)	$^{206}Pb/^{204}Pb$	U/Th	Isotope ratios							Apparent ages (Ma)							
				$^{206}Pb/^{207}Pb$	± (%)	$^{207}Pb/^{235}U$	± (%)	$^{206}Pb/^{238}U$	± (%)	error corr.	$^{206}Pb/^{238}U$	± (Ma)	$^{207}Pb/^{235}U$	± (Ma)	$^{206}Pb/^{207}Pb$	± (Ma)	Best age (¥) (Ma)	± (Ma)
CPV-12-50-29	159	45.964	0.4	19.8373	4.9	0.2721	5.3	0.0391	2.0	0.38	247.5	4.8	244.3	11.4	214.0	112.8	247.5	4.8
CPV-12-50-30	137	52.102	1.0	18.7246	6.1	0.3476	7.0	0.0472	3.4	0.49	297.4	9.9	303.0	18.2	346.1	137.2	297.4	9.9
CPV-12-50-31	138	42.850	0.8	19.7135	7.9	0.3264	8.1	0.0467	2.0	0.24	294.0	5.7	286.8	20.4	228.5	182.8	294.0	5.7
CPV-12-50-32	202	69.708	0.9	19.2558	9.9	0.3399	10.4	0.0475	3.1	0.30	299.0	9.0	297.1	26.7	282.5	226.9	299.0	9.0
CPV-12-50-33	207	136.516	1.5	18.9840	5.1	0.3802	5.2	0.0523	1.0	0.19	328.9	3.2	327.2	14.6	314.9	116.9	328.9	3.2
CPV-12-50-34	194	64.613	1.0	8.8786	0.2	5.1354	0.5	0.3307	0.5	0.91	1,841.7	7.2	1,842.0	4.2	1,842.3	3.7	1,842.3	3.7
CPV-12-50-35	264	165.551	1.2	18.5465	5.1	0.3484	5.3	0.0469	1.4	0.26	295.2	4.1	303.5	14.0	367.6	115.8	295.2	4.1
CPV-12-50-36	119	43.854	2.0	19.6606	9.6	0.3663	9.7	0.0522	1.5	0.15	328.2	4.7	316.9	26.3	234.7	221.1	328.2	4.7
CPV-12-50-37	128	39.237	1.0	20.2228	10.1	0.2807	10.2	0.0412	1.6	0.15	260.0	4.0	251.2	22.7	169.2	235.5	260.0	4.0
CPV-12-50-38	262	183.426	3.0	19.0997	5.2	0.3846	5.3	0.0533	0.4	0.08	334.6	1.3	330.4	14.8	301.0	119.7	334.6	1.3
CPV-12-50-39	147	40.014	0.8	20.5389	7.5	0.2705	7.6	0.0403	1.6	0.21	254.6	4.0	243.1	16.5	132.9	175.4	254.6	4.0
CPV-12-50-40	174	75.428	1.8	19.9136	7.1	0.3299	7.2	0.0476	1.3	0.19	300.0	3.9	289.5	18.2	205.0	164.7	300.0	3.9
CPV-12-50-41	38	17.144	1.2	29.2476	47.7	0.2293	48.4	0.0486	8.0	0.17	306.2	24.1	209.6	92.0	-774.1	1,414.6	306.2	24.1
CPV-12-50-42	318	256.178	1.3	19.2422	3.5	0.3381	3.6	0.0472	0.8	0.22	297.2	2.3	295.7	9.3	284.1	80.6	297.2	2.3
CPV-12-50-43	220	291.794	1.0	20.4517	3.2	0.3172	3.4	0.0470	1.0	0.28	296.4	2.8	279.7	8.3	142.8	76.1	296.4	2.8
CPV-12-50-44	83	44.864	2.0	19.1884	11.7	0.3798	11.8	0.0529	1.3	0.11	332.1	4.3	326.9	33.0	290.4	269.0	332.1	4.3
CPV-12-50-45	155	36.712	0.8	18.8717	6.5	0.2904	6.8	0.0398	1.8	0.26	251.3	4.4	258.9	15.5	328.4	148.3	251.3	4.4
CPV-12-50-46	204	123.383	0.8	19.1157	4.7	0.3304	4.9	0.0458	1.2	0.25	288.7	3.4	289.8	12.2	299.1	107.3	288.7	3.4
CPV-12-50-47	56	35.154	1.9	21.8688	13.7	0.3352	14.3	0.0532	3.8	0.27	333.9	12.4	293.5	36.4	-16.7	333.5	333.9	12.4
CPV-12-50-48	243	73.243	0.5	18.8867	5.7	0.2865	5.9	0.0392	1.7	0.29	248.2	4.1	255.8	13.3	326.5	128.4	248.2	4.1
CPV-12-50-49	416	94.623	0.9	18.6932	2.3	0.3499	2.3	0.0474	0.6	0.24	298.8	1.6	304.6	6.2	349.9	51.6	298.8	1.6
CPV-12-50-50	177	61.639	0.9	19.7526	6.6	0.3224	6.7	0.0462	1.1	0.16	291.1	3.0	283.7	16.5	223.8	152.5	291.1	3.0
CPV-12-50-51	185	28.642	0.9	19.3998	6.8	0.2810	6.9	0.0395	1.2	0.17	250.0	2.9	251.4	15.4	265.4	156.0	250.0	2.9
CPV-12-50-52	210	115.548	0.7	18.4094	6.7	0.3529	6.7	0.0471	0.6	0.10	296.8	1.9	306.9	17.8	384.3	150.1	296.8	1.9
CPV-12-50-53	96	2.428	0.9	16.5841	14.9	0.4151	15.7	0.0499	4.9	0.31	314.1	15.0	352.5	46.7	614.3	322.8	314.1	15.0
CPV-12-50-54	267	100.277	1.0	19.3360	3.9	0.2880	4.2	0.0404	1.4	0.34	255.2	3.5	257.0	9.4	272.9	89.6	255.2	3.5
CPV-12-50-55	141	38.776	0.7	17.9441	7.2	0.3620	7.4	0.0471	1.7	0.23	296.7	4.8	313.7	20.0	441.6	160.7	296.7	4.8

Sample CPV-12-50 continued.

Analysis	U (ppm)	$^{206}Pb/^{204}Pb$	U/Th	Isotope ratios							Apparent ages (Ma)							
				$^{206}Pb/^{207}Pb$	± (%)	$^{207}Pb/^{235}U$	± (%)	$^{206}Pb/^{238}U$	± (%)	error corr.	$^{206}Pb/^{238}U$	± (Ma)	$^{207}Pb/^{235}U$	± (Ma)	$^{206}Pb/^{207}Pb$	± (Ma)	Best age (¥) (Ma)	± (Ma)
CPV-12-50-56	112	41.805	1.2	20.4986	7.9	0.3130	8.1	0.0465	1.4	0.18	293.2	4.1	276.5	19.5	137.5	186.7	293.2	4.1
CPV-12-50-57	103	45.428	1.0	18.1449	10.9	0.3638	11.2	0.0479	2.6	0.23	301.5	7.6	315.0	30.4	416.7	244.2	301.5	7.6
CPV-12-50-58	298	196.585	1.2	19.2794	3.7	0.3366	3.8	0.0471	0.9	0.24	296.5	2.6	294.6	9.7	279.7	84.5	296.5	2.6
CPV-12-50-59	413	213.856	1.3	18.8258	2.1	0.3420	2.2	0.0467	0.8	0.36	294.2	2.3	298.7	5.7	333.9	46.7	294.2	2.3
CPV-12-50-60	121	61.281	1.2	19.2291	7.2	0.3371	7.5	0.0470	1.8	0.24	296.1	5.3	295.0	19.1	285.6	165.5	296.1	5.3
CPV-12-50-62	134	20.178	0.7	19.5769	9.8	0.2813	10.4	0.0399	3.5	0.33	252.5	8.6	251.7	23.2	244.5	226.8	252.5	8.6
CPV-12-50-63	489	116.911	1.2	18.6864	2.0	0.3508	2.1	0.0475	0.6	0.30	299.4	1.9	305.3	5.6	350.7	46.2	299.4	1.9
CPV-12-50-64	399	18.427	0.7	17.8026	4.2	0.4191	4.4	0.0541	1.4	0.32	339.7	4.6	355.4	13.1	459.2	92.1	339.7	4.6
CPV-12-50-65	182	92.430	1.1	19.9394	8.6	0.3239	8.8	0.0468	1.8	0.21	295.1	5.3	284.9	21.9	202.0	200.4	295.1	5.3
CPV-12-50-66	197	47.464	0.4	19.8532	7.5	0.2718	7.6	0.0391	1.0	0.13	247.4	2.3	244.1	16.4	212.1	174.4	247.4	2.3
CPV-12-50-67	476	143.415	1.4	19.9133	2.6	0.3012	2.6	0.0435	0.6	0.23	274.5	1.6	267.3	6.2	205.1	59.8	274.5	1.6
CPV-12-50-68	94	26.547	1.5	18.4637	13.1	0.3382	13.2	0.0453	1.5	0.11	285.6	4.1	295.8	33.8	377.7	295.1	285.6	4.1
CPV-12-50-69	175	78.921	1.1	19.4356	10.7	0.2912	11.1	0.0411	2.9	0.26	259.3	7.3	259.5	25.4	261.1	247.1	259.3	7.3
CPV-12-50-70	145	60.674	1.4	19.4652	7.7	0.3358	7.8	0.0474	1.5	0.19	298.6	4.3	294.0	20.0	257.6	176.8	298.6	4.3
CPV-12-50-71	347	168.283	1.5	19.5522	3.6	0.3326	3.7	0.0472	1.0	0.27	297.1	3.0	291.5	9.4	247.4	82.6	297.1	3.0
CPV-12-50-72	111	64.884	1.6	18.8496	11.1	0.3425	11.4	0.0468	2.7	0.23	295.0	7.7	299.1	29.6	331.0	252.7	295.0	7.7
CPV-12-50-73	304	107.486	2.6	19.1123	4.6	0.3417	4.8	0.0474	1.0	0.22	298.3	3.0	298.4	12.3	299.5	105.9	298.3	3.0
CPV-12-50-74	364	159.878	1.1	19.1321	2.6	0.3416	2.8	0.0474	1.1	0.38	298.6	3.1	298.4	7.2	297.2	58.9	298.6	3.1
CPV-12-50-75	254	71.423	1.1	18.4014	5.7	0.3561	5.7	0.0475	0.9	0.16	299.3	2.7	309.3	15.3	385.3	127.1	299.3	2.7
CPV-12-50-76	559	27.738	1.4	18.6648	2.2	0.3486	2.4	0.0472	0.7	0.30	297.2	2.1	303.7	6.2	353.3	50.8	297.2	2.1
CPV-12-50-77	527	104.966	1.4	19.0760	2.5	0.3493	3.7	0.0483	2.7	0.73	304.2	7.9	304.2	9.6	303.9	57.4	304.2	7.9
CPV-12-50-78	240	95.083	1.0	18.6926	4.9	0.3474	5.0	0.0471	1.3	0.26	296.7	3.8	302.8	13.2	350.0	109.8	296.7	3.8
CPV-12-50-79	368	193.921	1.7	18.4835	2.7	0.3509	2.9	0.0470	0.9	0.31	296.4	2.6	305.4	7.6	375.3	61.3	296.4	2.6
CPV-12-50-80	132	11.134	0.8	17.0387	13.7	0.3802	14.5	0.0470	4.7	0.32	296.0	13.5	327.2	40.5	555.6	300.0	296.0	13.5
CPV-12-50-81	86	65.005	1.2	18.7449	9.2	0.3388	9.3	0.0461	1.7	0.18	290.3	4.8	296.3	24.0	343.6	208.0	290.3	4.8
CPV-12-50-82	282	77.741	1.1	19.1390	3.0	0.3814	3.2	0.0529	0.8	0.27	332.5	2.7	328.0	8.8	296.3	69.3	332.5	2.7
CPV-12-50-83	543	139.221	1.7	18.7033	1.9	0.3467	2.1	0.0470	0.8	0.38	296.3	2.3	302.2	5.4	348.7	43.2	296.3	2.3

Sample CPV-12-50 continued.

Analysis	U (ppm)	$^{206}Pb/^{204}Pb$	U/Th	Isotope ratios							Apparent ages (Ma)							
				$^{206}Pb/^{207}Pb$	± (%)	$^{207}Pb/^{235}U$	± (%)	$^{206}Pb/^{238}U$	± (%)	error corr.	$^{206}Pb/^{238}U$	± (Ma)	$^{207}Pb/^{235}U$	± (Ma)	$^{206}Pb/^{207}Pb$	± (Ma)	Best age (¥) (Ma)	± (Ma)
CPV-12-50-84	278	59.076	1.3	19.0516	5.2	0.3702	5.4	0.0511	1.4	0.26	321.6	4.4	319.8	14.9	306.8	119.2	321.6	4.4
CPV-12-50-85	119	48.549	1.0	18.2283	6.1	0.3421	6.5	0.0452	2.2	0.34	285.1	6.1	298.7	16.8	406.5	136.6	285.1	6.1
CPV-12-50-86	105	36.618	2.0	19.0267	8.9	0.3850	9.1	0.0531	2.0	0.22	333.7	6.5	330.7	25.7	309.7	202.9	333.7	6.5
CPV-12-50-87	412	203.582	1.1	18.8392	2.4	0.3795	2.5	0.0519	0.7	0.28	325.9	2.2	326.7	7.0	332.2	54.6	325.9	2.2
CPV-12-50-88	58	9.704	1.4	16.4875	18.1	0.4430	18.5	0.0530	3.8	0.21	332.8	12.5	372.4	57.7	626.9	393.1	332.8	12.5
CPV-12-50-89	78	32.241	0.9	18.3324	13.6	0.3591	13.8	0.0477	2.4	0.17	300.7	7.0	311.6	37.1	393.7	307.0	300.7	7.0
CPV-12-50-90	256	152.937	1.2	20.0924	3.5	0.3237	3.6	0.0472	0.8	0.21	297.2	2.2	284.8	9.0	184.2	82.2	297.2	2.2
CPV-12-50-91	157	46.203	1.7	18.6519	9.9	0.3662	10.2	0.0495	2.5	0.25	311.7	7.7	316.8	27.7	354.9	223.0	311.7	7.7
CPV-12-50-92	114	24.727	0.9	20.6088	11.9	0.2650	12.0	0.0396	1.8	0.15	250.4	4.4	238.7	25.5	124.8	280.2	250.4	4.4
CPV-12-50-93	402	111.690	1.1	18.7564	1.5	0.3470	1.8	0.0472	0.9	0.50	297.4	2.6	302.5	4.6	342.2	34.7	297.4	2.6
CPV-12-50-94	386	220.083	1.1	18.7431	1.8	0.3935	1.8	0.0535	0.4	0.23	335.9	1.4	336.9	5.3	343.8	40.5	335.9	1.4
CPV-12-50-95	110	41.658	1.3	19.8848	10.2	0.2782	10.6	0.0401	2.7	0.26	253.6	6.8	249.3	23.4	208.4	237.8	253.6	6.8
CPV-12-50-96	493	153.475	0.6	19.3961	2.3	0.2911	2.7	0.0410	1.5	0.55	258.7	3.8	259.4	6.3	265.8	52.6	258.7	3.8
CPV-12-50-97	214	13.976	1.0	18.3804	5.8	0.3449	5.9	0.0460	1.2	0.19	289.8	3.3	300.9	15.5	387.9	131.1	289.8	3.3
CPV-12-50-98	253	101.076	1.6	18.6589	4.1	0.3490	4.3	0.0472	1.4	0.32	297.5	4.0	304.0	11.4	354.0	93.0	297.5	4.0
CPV-12-50-99	141	39.290	1.0	18.9235	9.5	0.3978	11.6	0.0546	6.7	0.58	342.7	22.4	340.1	33.5	322.1	215.6	342.7	22.4
CPV-12-50-100	175	32.406	1.0	19.3621	5.7	0.2927	5.8	0.0411	1.4	0.23	259.7	3.5	260.7	13.4	269.8	130.4	259.7	3.5

(¥) The best age considered these $^{206}Pb/^{207}Pb$ values for zircons older than 1 Ga and $^{206}Pb/^{238}U$ ages values for zircons younger than 1 Ga (Nemchin and Cawood, 2005).

Nemchin, A.A; Cawood, P.A. 2005. Discordance of the U-Pb system in detrital zircons: Implication for provenance studies of sedimentary rocks. Sedimentary Geology 182 (1-4): 143-162. doi: 10.1016/j.sedgeo.2005.07.011.

SAMPLE CPV-12-88X.

Analysis	U (ppm)	$^{206}Pb/^{204}Pb$	U/Th	Isotope ratios							Apparent ages (Ma)							
				$^{206}Pb^{207}Pb$	± (%)	$^{207}Pb/^{235}U$	± (%)	$^{206}Pb/^{238}U$	± (%)	error corr.	$^{206}Pb/^{238}U$	± (Ma)	$^{207}Pb/^{235}U$	± (Ma)	$^{206}Pb/^{207}Pb$	± (Ma)	Best age (¥) (Ma)	± (Ma)
CPV-12-88X-84	143	124.223	0.7	18.9045	9.3	0.2823	9.5	0.0387	2.3	0.24	244.8	5.5	252.4	21.3	324.4	210.8	244.8	5.5
CPV-12-88X-52	106	53.805	0.7	18.2817	24.1	0.3067	24.8	0.0407	6.2	0.25	257.0	15.5	271.6	59.2	399.9	546.0	257.0	15.5
CPV-12-88X-69	101	97.743	0.8	29.9425	30.1	0.1942	30.5	0.0422	5.0	0.16	266.3	13.0	180.2	50.5	-840.9	878.4	266.3	13.0
CPV-12-88X-70	65	172.744	0.7	21.7653	30.6	0.2674	31.1	0.0422	5.7	0.18	266.5	14.8	240.6	66.8	-5.3	754.1	266.5	14.8
CPV-12-88X-3	89	112.061	0.8	18.3461	22.6	0.3172	23.1	0.0422	4.6	0.20	266.5	12.1	279.8	56.5	392.1	513.5	266.5	12.1
CPV-12-88X-88	117	63.904	0.9	19.9510	15.2	0.2933	15.5	0.0424	3.5	0.22	267.9	9.1	261.1	35.8	200.7	353.6	267.9	9.1
CPV-12-88X-40	574	754.061	3.0	19.4745	2.4	0.3007	2.6	0.0425	1.1	0.40	268.1	2.8	266.9	6.2	256.5	55.4	268.1	2.8
CPV-12-88X-51	256	182.547	1.2	18.4624	4.3	0.3202	4.8	0.0429	2.1	0.43	270.7	5.5	282.1	11.8	377.9	97.5	270.7	5.5
CPV-12-88X-33	200	305.136	1.1	18.9005	5.9	0.3173	6.2	0.0435	2.1	0.34	274.5	5.6	279.8	15.3	324.9	133.4	274.5	5.6
CPV-12-88X-39	206	167.655	1.1	17.3940	8.3	0.3465	10.6	0.0437	6.6	0.62	275.8	17.8	302.1	27.7	510.4	182.7	275.8	17.8
CPV-12-88X-48	177	149.057	0.9	18.1839	6.9	0.3315	7.1	0.0437	1.4	0.20	275.9	3.8	290.7	17.9	411.9	155.0	275.9	3.8
CPV-12-88X-11	114	87.345	1.0	17.5675	18.7	0.3442	20.4	0.0439	8.1	0.40	276.7	21.9	300.4	53.1	488.6	416.5	276.7	21.9
CPV-12-88X-95	92	91.551	0.8	23.7641	37.3	0.2552	37.6	0.0440	5.2	0.14	277.5	14.1	230.8	77.9	-221.7	966.8	277.5	14.1
CPV-12-88X-59	96	104.484	1.1	15.6358	12.0	0.3894	13.1	0.0442	5.2	0.40	278.6	14.1	333.9	37.3	740.2	255.1	278.6	14.1
CPV-12-88X-81	104	134.671	1.0	21.2366	17.7	0.2867	17.8	0.0442	2.2	0.12	278.6	5.9	256.0	40.3	53.7	424.2	278.6	5.9
CPV-12-88X-60	336	400.617	0.7	19.2923	4.3	0.3163	5.4	0.0443	3.1	0.59	279.2	8.6	279.1	13.1	278.1	99.4	279.2	8.6
CPV-12-88X-38	148	160.263	1.2	19.3125	11.6	0.3168	11.7	0.0444	2.0	0.17	279.9	5.5	279.4	28.7	275.7	265.8	279.9	5.5
CPV-12-88X-37	123	124.889	0.8	20.9371	15.5	0.2926	15.8	0.0444	3.0	0.19	280.2	8.2	260.6	36.3	87.5	369.1	280.2	8.2
CPV-12-88X-87	257	364.531	0.7	19.4596	7.5	0.3156	7.6	0.0445	1.3	0.17	280.9	3.6	278.5	18.6	258.3	172.8	280.9	3.6
CPV-12-88X-36	313	134.301	1.0	19.2665	8.2	0.3205	8.3	0.0448	1.2	0.14	282.4	3.3	282.3	20.4	281.2	187.3	282.4	3.3
CPV-12-88X-44	75	92.332	1.0	20.3069	22.5	0.3056	22.8	0.0450	4.0	0.17	283.8	11.1	270.8	54.3	159.5	531.7	283.8	11.1
CPV-12-88X-21	217	229.020	1.2	17.8283	6.6	0.3495	7.0	0.0452	2.3	0.32	284.9	6.3	304.3	18.3	455.9	146.6	284.9	6.3
CPV-12-88X-86	81	107.620	1.3	18.2948	24.6	0.3413	25.3	0.0453	6.2	0.24	285.5	17.2	298.2	65.6	398.3	558.5	285.5	17.2
CPV-12-88X-46	355	415.937	0.9	18.4295	4.6	0.3389	4.7	0.0453	1.1	0.23	285.6	3.1	296.3	12.1	381.9	103.2	285.6	3.1
CPV-12-88X-15	182	135.192	1.1	20.7001	5.6	0.3021	7.4	0.0454	4.8	0.65	285.9	13.4	268.0	17.3	114.4	131.7	285.9	13.4
CPV-12-88X-1	101	96.890	1.6	19.0145	22.6	0.3297	22.9	0.0455	3.4	0.15	286.7	9.7	289.4	57.7	311.2	520.8	286.7	9.7
CPV-12-88X-56	153	162.051	1.1	19.4861	10.6	0.3219	11.0	0.0455	2.9	0.26	286.8	8.1	283.4	27.2	255.2	244.1	286.8	8.1

Sample CPV-12-88X continued.

Analysis	U (ppm)	$^{206}Pb/^{204}Pb$	U/Th	Isotope ratios							Apparent ages (Ma)							
				$^{206}Pb/^{207}Pb$	± (%)	$^{207}Pb/^{235}U$	± (%)	$^{206}Pb/^{238}U$	± (%)	error corr.	$^{206}Pb/^{238}U$	± (Ma)	$^{207}Pb/^{235}U$	± (Ma)	$^{206}Pb/^{207}Pb$	± (Ma)	Best age (¥) (Ma)	± (Ma)
CPV-12-88X-64	115	79.113	1.0	23.1067	19.7	0.2717	20.2	0.0455	4.2	0.21	287.0	11.7	244.0	43.8	-151.6	493.5	287.0	11.7
CPV-12-88X-26	80	63.192	1.2	18.3073	14.7	0.3433	15.0	0.0456	2.9	0.19	287.3	8.2	299.6	39.0	396.8	331.6	287.3	8.2
CPV-12-88X-50	141	187.886	0.9	19.9113	10.8	0.3158	10.9	0.0456	1.8	0.16	287.5	5.0	278.7	26.7	205.3	251.0	287.5	5.0
CPV-12-88X-28	89	135.912	1.1	17.3838	12.6	0.3628	13.5	0.0457	4.8	0.36	288.3	13.5	314.3	36.4	511.7	277.7	288.3	13.5
CPV-12-88X-24	113	139.985	0.8	23.4412	28.8	0.2692	29.5	0.0458	6.4	0.22	288.5	18.0	242.1	63.7	-187.4	733.2	288.5	18.0
CPV-12-88X-22	164	146.433	1.6	17.8479	8.9	0.3537	10.6	0.0458	5.8	0.54	288.6	16.3	307.5	28.2	453.5	198.1	288.6	16.3
CPV-12-88X-16	199	238.122	1.6	19.7414	10.3	0.3205	10.7	0.0459	2.8	0.26	289.2	8.0	282.3	26.4	225.2	239.2	289.2	8.0
CPV-12-88X-8	199	141.079	0.9	20.0726	9.7	0.3160	9.8	0.0460	1.1	0.11	290.0	3.2	278.8	23.9	186.5	227.0	290.0	3.2
CPV-12-88X-32	96	111.634	1.2	19.1306	14.3	0.3322	14.7	0.0461	3.3	0.22	290.5	9.3	291.3	37.3	297.3	328.7	290.5	9.3
CPV-12-88X-76	375	392.818	1.6	18.7507	3.9	0.3390	4.1	0.0461	1.3	0.32	290.5	3.7	296.4	10.5	342.9	87.7	290.5	3.7
CPV-12-88X-96	139	113.008	1.0	20.3967	15.8	0.3119	16.5	0.0461	4.7	0.28	290.8	13.3	275.6	39.9	149.1	373.2	290.8	13.3
CPV-12-88X-54	234	208.496	2.1	18.5745	6.1	0.3425	6.3	0.0461	1.6	0.26	290.8	4.6	299.1	16.4	364.2	137.8	290.8	4.6
CPV-12-88X-75	44	31.119	1.5	8.3462	213.1	0.7630	213.3	0.0462	8.7	0.04	291.1	24.7	575.8	1.633.4	1.953.5	233.2	291.1	24.7
CPV-12-88X-67	298	338.255	0.9	20.2371	8.4	0.3150	8.5	0.0462	1.3	0.16	291.3	3.8	278.0	20.7	167.5	196.7	291.3	3.8
CPV-12-88X-89	167	181.872	1.0	20.0577	11.6	0.3179	11.7	0.0462	1.5	0.13	291.4	4.4	280.3	28.5	188.3	269.6	291.4	4.4
CPV-12-88X-82	626	320.607	1.3	18.8456	2.1	0.3394	2.7	0.0464	1.8	0.66	292.3	5.1	296.7	7.0	331.5	46.6	292.3	5.1
CPV-12-88X-19	184	289.530	1.6	19.7412	9.8	0.3249	10.0	0.0465	2.2	0.22	293.1	6.4	285.7	25.0	225.2	226.2	293.1	6.4
CPV-12-88X-68	112	132.064	1.7	23.1860	15.1	0.2772	15.5	0.0466	3.2	0.21	293.7	9.2	248.4	34.1	-160.1	378.1	293.7	9.2
CPV-12-88X-30	39	30.699	1.2	23.3031	33.9	0.2766	35.0	0.0468	8.9	0.25	294.6	25.5	248.0	77.2	-172.7	865.2	294.6	25.5
CPV-12-88X-53	316	501.226	1.6	19.1623	7.8	0.3366	8.1	0.0468	2.2	0.27	294.7	6.3	294.6	20.6	293.6	177.2	294.7	6.3
CPV-12-88X-62	61	110.663	0.9	18.0587	35.1	0.3589	35.9	0.0470	7.6	0.21	296.1	22.0	311.4	96.6	427.4	805.5	296.1	22.0
CPV-12-88X-29	151	117.378	1.1	19.0650	17.3	0.3401	17.5	0.0470	2.6	0.15	296.3	7.6	297.3	45.1	305.2	396.9	296.3	7.6
CPV-12-88X-55	47	37.832	0.9	15.8262	41.7	0.4110	42.4	0.0472	8.0	0.19	297.1	23.3	349.6	126.2	714.5	924.5	297.1	23.3
CPV-12-88X-7	97	69.250	1.1	18.8874	28.7	0.3450	28.7	0.0473	2.1	0.07	297.7	6.1	301.0	75.0	326.4	662.7	297.7	6.1
CPV-12-88X-35	128	204.359	1.2	20.6563	13.6	0.3156	13.7	0.0473	1.7	0.12	297.8	5.0	278.5	33.4	119.4	321.4	297.8	5.0
CPV-12-88X-6	97	127.115	1.6	22.0365	21.1	0.2960	21.5	0.0473	4.2	0.20	298.0	12.4	263.3	49.9	-35.2	516.1	298.0	12.4
CPV-12-88X-13	309	472.139	1.4	18.7741	6.3	0.3489	6.4	0.0475	1.4	0.22	299.2	4.1	303.9	16.9	340.1	142.2	299.2	4.1

Sample CPV-12-88X continued.

Analysis	U (ppm)	$^{206}Pb/^{204}Pb$	U/Th	Isotope ratios							Apparent ages (Ma)							
				$^{206}Pb/^{207}Pb$	± (%)	$^{207}Pb/^{235}U$	± (%)	$^{206}Pb/^{238}U$	± (%)	error corr.	$^{206}Pb/^{238}U$	± (Ma)	$^{207}Pb/^{235}U$	± (Ma)	$^{206}Pb/^{207}Pb$	± (Ma)	Best age (¥) (Ma)	± (Ma)
CPV-12-88X-77	74	41.712	1.4	17.0906	12.6	0.3835	13.4	0.0475	4.6	0.34	299.4	13.5	329.6	37.8	549.0	276.0	299.4	13.5
CPV-12-88X-90	177	107.674	1.6	21.1280	17.6	0.3104	17.8	0.0476	2.5	0.14	299.5	7.4	274.5	42.8	65.9	421.6	299.5	7.4
CPV-12-88X-25	105	92.436	1.4	21.1730	12.9	0.3102	13.7	0.0476	4.6	0.33	299.9	13.5	274.3	33.0	60.9	309.4	299.9	13.5
CPV-12-88X-61	56	51.266	1.1	34.5563	96.8	0.1902	96.9	0.0477	5.3	0.05	300.2	15.6	176.8	158.5	NA	NA	300.2	15.6
CPV-12-88X-78	66	67.048	1.2	19.0514	34.2	0.3454	35.1	0.0477	7.6	0.22	300.5	22.3	301.2	91.7	306.8	801.5	300.5	22.3
CPV-12-88X-34	95	239.104	1.9	18.9603	10.6	0.3472	10.9	0.0477	2.7	0.24	300.6	7.8	302.6	28.6	317.7	241.5	300.6	7.8
CPV-12-88X-2	171	232.923	1.1	18.1309	6.5	0.3633	7.8	0.0478	4.2	0.55	300.8	12.5	314.6	21.0	418.5	145.0	300.8	12.5
CPV-12-88X-23	194	282.108	0.9	19.1154	8.3	0.3449	8.6	0.0478	2.2	0.26	301.1	6.4	300.8	22.3	299.1	189.4	301.1	6.4
CPV-12-88X-9	378	391.046	1.1	17.9909	3.8	0.3665	4.0	0.0478	1.1	0.27	301.1	3.2	317.0	10.9	435.8	85.4	301.1	3.2
CPV-12-88X-49	120	110.672	1.6	19.7510	23.0	0.3338	23.3	0.0478	3.8	0.16	301.1	11.2	292.5	59.4	224.0	538.9	301.1	11.2
CPV-12-88X-17	216	120.398	0.8	19.5594	12.0	0.3376	12.3	0.0479	2.8	0.23	301.5	8.3	295.3	31.6	246.5	276.7	301.5	8.3
CPV-12-88X-79	141	158.465	1.7	21.7394	14.2	0.3043	15.8	0.0480	7.0	0.44	302.1	20.6	269.7	37.4	-2.4	343.0	302.1	20.6
CPV-12-88X-80	85	86.095	1.2	21.6646	27.4	0.3055	27.7	0.0480	4.1	0.15	302.2	12.0	270.7	66.0	5.9	671.2	302.2	12.0
CPV-12-88X-20	83	731.970	0.9	15.6635	12.1	0.4231	12.5	0.0481	3.3	0.26	302.7	9.7	358.3	37.8	736.4	256.3	302.7	9.7
CPV-12-88X-14	174	131.128	1.4	19.4683	11.4	0.3405	11.5	0.0481	1.6	0.14	302.7	4.8	297.5	29.7	257.3	263.0	302.7	4.8
CPV-12-88X-4	121	110.320	1.1	19.8550	16.7	0.3357	17.2	0.0483	4.1	0.24	304.3	12.2	293.9	44.0	211.9	390.1	304.3	12.2
CPV-12-88X-99	267	188.964	0.8	19.2635	11.0	0.3476	11.2	0.0486	2.2	0.20	305.7	6.7	302.9	29.3	281.5	251.8	305.7	6.7
CPV-12-88X-47	202	172.005	2.3	18.5341	8.8	0.3622	8.9	0.0487	0.9	0.10	306.4	2.6	313.8	23.9	369.1	199.0	306.4	2.6
CPV-12-88X-43	79	49.878	0.8	23.9241	32.2	0.2806	32.5	0.0487	4.9	0.15	306.5	14.7	251.2	72.5	-238.6	830.5	306.5	14.7
CPV-12-88X-93	105	81.509	1.7	20.7149	19.4	0.3243	19.7	0.0487	3.2	0.16	306.6	9.6	285.2	48.9	112.7	461.4	306.6	9.6
CPV-12-88X-27	263	342.605	1.8	19.1098	5.3	0.3525	5.6	0.0489	1.6	0.29	307.5	4.9	306.6	14.7	299.8	121.7	307.5	4.9
CPV-12-88X-42	367	402.431	1.7	19.7270	6.5	0.3416	6.6	0.0489	1.5	0.22	307.6	4.4	298.4	17.1	226.9	149.3	307.6	4.4
CPV-12-88X-92	111	89.511	1.4	17.6709	15.0	0.3836	15.7	0.0492	4.9	0.31	309.4	14.7	329.7	44.3	475.6	332.7	309.4	14.7
CPV-12-88X-58	77	332.138	1.2	21.2706	21.1	0.3206	21.7	0.0495	5.2	0.24	311.2	15.7	282.4	53.6	49.9	509.1	311.2	15.7
CPV-12-88X-18	138	150.668	1.1	18.8717	15.7	0.3628	16.0	0.0497	2.8	0.18	312.4	8.5	314.3	43.2	328.4	358.4	312.4	8.5
CPV-12-88X-65	47	66.373	1.2	21.6224	54.8	0.3205	55.6	0.0503	9.6	0.17	316.1	29.8	282.3	137.9	10.6	1,418.7	316.1	29.8

Sample CPV-12-88X continued.

Analysis	U (ppm)	$^{206}Pb/^{204}Pb$	U/Th	Isotope ratios							Apparent ages (Ma)							
				$^{206}Pb/^{207}Pb$	± (%)	$^{207}Pb/^{235}U$	± (%)	$^{206}Pb/^{238}U$	± (%)	error corr.	$^{206}Pb/^{238}U$	± (Ma)	$^{207}Pb/^{235}U$	± (Ma)	$^{206}Pb/^{207}Pb$	± (Ma)	Best age (¥) (Ma)	± (Ma)
CPV-12-88X-57	180	309.383	2.2	18.1248	10.8	0.3833	12.1	0.0504	5.4	0.44	316.9	16.6	329.5	34.0	419.2	241.9	316.9	16.6
CPV-12-88X-63	388	732.324	1.7	19.3939	5.1	0.3643	5.5	0.0512	2.2	0.39	322.1	6.8	315.4	15.0	266.1	116.8	322.1	6.8
CPV-12-88X-91	107	107.279	1.3	18.1048	16.7	0.3927	17.4	0.0516	4.7	0.27	324.2	14.8	336.4	49.7	421.7	375.4	324.2	14.8
CPV-12-88X-97	485	469.238	1.5	19.1748	3.7	0.3862	4.2	0.0537	2.0	0.47	337.3	6.5	331.6	12.0	292.1	85.3	337.3	6.5
CPV-12-88X-72	73	85.672	2.1	17.1967	24.6	0.4327	25.1	0.0540	5.1	0.20	338.9	16.8	365.1	77.2	535.5	546.2	338.9	16.8
CPV-12-88X-12	687	1.082.248	2.1	17.7425	1.6	0.5572	2.7	0.0717	2.2	0.80	446.4	9.4	449.7	9.9	466.6	36.4	446.4	9.4
CPV-12-88X-45	542	1.395.733	2.2	17.7302	2.5	0.5906	2.6	0.0759	0.8	0.32	471.9	3.8	471.3	9.9	468.2	54.9	471.9	3.8
CPV-12-88X-73	127	184.963	1.3	16.9671	6.5	0.6405	6.7	0.0788	1.7	0.25	489.1	7.9	502.6	26.7	564.8	142.4	489.1	7.9
CPV-12-88X-71	44	63.097	0.8	18.0169	17.4	0.6146	18.5	0.0803	6.3	0.34	498.0	30.3	486.5	71.5	432.5	389.4	498.0	30.3
CPV-12-88X-10	656	942.173	4.3	16.4800	1.2	0.7959	1.3	0.0951	0.4	0.35	585.8	2.5	594.5	5.8	627.9	26.0	585.8	2.5
CPV-12-88X-85	137	555.594	0.8	16.8428	5.9	0.8029	6.1	0.0981	1.7	0.28	603.1	9.7	598.4	27.5	580.8	127.2	603.1	9.7
CPV-12-88X-41	67	330.263	1.7	14.4099	5.1	1.4751	5.4	0.1542	1.8	0.34	924.2	15.6	920.2	32.6	910.5	104.5	910.5	104.5
CPV-12-88X-82	121	1.349.992	2.1	11.7518	3.1	2.3609	4.9	0.2012	3.8	0.78	1,181.9	40.8	1,230.9	34.8	1,317.6	59.7	1,317.6	59.7
CPV-12-88X-100	27	379.422	2.1	5.1276	2.0	14.8129	2.6	0.5509	1.6	0.62	2,828.8	36.6	2,803.3	24.5	2,785.0	33.1	2,785.0	33.1

(¥) The best age considered these $^{206}Pb/^{207}Pb$ values for zircons older than 1 Ga and $^{206}Pb/^{238}U$ ages values for zircons younger than 1 Ga (Nemchin and Cawood. 2005).
Nemchin. A.A.; Cawood. P.A. 2005. Discordance of the U-Pb system in detrital zircons: Implication for provenance studies of sedimentary rocks. Sedimentary Geology 182 (1-4): 143-162. doi: 10.1016/j.sedgeo.2005.07.011.

SAMPLE CPV-12-90.

Analysis	U (ppm)	$^{206}Pb/^{204}Pb$	U/Th	Isotope ratios							Apparent ages (Ma)							
				$^{206}Pb/^{207}Pb$	± (%)	$^{207}Pb/^{235}U$	± (%)	$^{206}Pb/^{238}U$	± (%)	error corr.	$^{206}Pb/^{238}U$	± (Ma)	$^{207}Pb/^{235}U$	± (Ma)	$^{206}Pb/^{207}Pb$	± (Ma)	Best age (¥) (Ma)	± (Ma)
CPV-12-90-19T	131	9.168	1.4	19.3868	19.5	0.2322	20.2	0.0327	5.4	0.27	207.1	11.0	212.0	38.7	266.9	450.6	207.1	11.0
CPV-12-90-8C	299	13.050	1.1	21.3917	10.9	0.2125	11.1	0.0330	1.8	0.16	209.1	3.6	195.6	19.7	36.3	262.0	209.1	3.6
CPV-12-90-7C	424	22.496	1.0	19.2050	6.8	0.2408	7.0	0.0335	1.6	0.23	212.7	3.3	219.1	13.8	288.5	155.6	212.7	3.3
CPV-12-90-18T	1.897	77.037	2.1	19.6095	2.7	0.2360	3.0	0.0336	1.3	0.43	212.8	2.7	215.1	5.8	240.6	62.5	212.8	2.7
CPV-12-90-20T	151	5.858	1.4	26.1357	27.8	0.1777	28.2	0.0337	4.6	0.16	213.5	9.6	166.1	43.2	-467.0	746.5	213.5	9.6
CPV-12-90-6C	1.452	42.467	2.0	19.8880	2.4	0.2375	5.5	0.0343	4.9	0.90	217.1	10.6	216.4	10.7	208.0	54.9	217.1	10.6
CPV-12-90-3C	152	3.251	2.0	17.0867	11.9	0.3788	12.8	0.0469	4.8	0.37	295.7	13.7	326.1	35.7	549.4	260.3	295.7	13.7
CPV-12-90-13C	226	20.242	0.6	17.7914	5.5	0.5781	9.4	0.0746	7.6	0.81	463.8	33.8	463.2	34.8	460.5	122.5	463.8	33.8
CPV-12-90-4C	274	56.171	4.5	17.6221	6.0	0.6176	6.1	0.0789	1.3	0.21	489.7	6.2	488.3	23.6	481.7	131.6	489.7	6.2
CPV-12-90-16T	345	32.873	3.1	17.6631	3.0	0.6223	5.6	0.0797	4.7	0.85	494.4	22.6	491.3	21.8	476.6	66.1	494.4	22.6
CPV-12-90-22T	215	17.160	0.4	16.3987	4.1	0.7086	4.9	0.0843	2.7	0.55	521.6	13.7	543.9	20.8	638.6	88.5	521.6	13.7
CPV-12-90-12C	549	125.272	1.8	17.0688	1.5	0.7570	3.9	0.0937	3.6	0.93	577.5	19.9	572.3	17.0	551.8	32.1	577.5	19.9
CPV-12-90-10C	2.049	13.334	40.6	16.7398	1.0	0.7783	3.1	0.0945	2.9	0.94	582.1	16.3	584.5	13.8	594.1	22.1	582.1	16.3
CPV-12-90-14C	132	26.880	0.5	16.7184	7.9	0.7863	8.9	0.0953	4.0	0.45	587.0	22.3	589.1	39.6	596.9	172.0	587.0	22.3
CPV-12-90-23T	187	7.366	7.6	17.0383	4.1	0.7805	5.0	0.0965	2.8	0.56	593.6	15.7	585.8	22.1	555.7	90.2	593.6	15.7
CPV-12-90-24T	500	30.764	5.6	16.1956	1.3	0.8648	6.7	0.1016	6.6	0.98	623.7	39.0	632.7	31.5	665.3	27.5	623.7	39.0
CPV-12-90-17T	693	70.508	21.7	16.0378	3.5	0.9487	9.1	0.1103	8.4	0.92	674.8	54.1	677.4	45.1	686.2	74.1	674.8	54.1
CPV-12-90-5C	543	188.872	3.5	14.5113	0.9	1.2409	2.5	0.1306	2.4	0.93	791.3	17.6	819.3	14.2	896.1	18.6	791.3	17.6
CPV-12-90-2C	212	43.072	3.0	13.3648	1.6	1.7525	4.5	0.1699	4.3	0.94	1,011.4	39.8	1,028.1	29.4	1,063.8	31.9	1,063.8	31.9
CPV-12-90-9C	104	155.242	3.9	12.8718	2.9	2.1735	7.3	0.2029	6.7	0.92	1,190.9	72.7	1,172.6	50.7	1,139.0	57.8	1,139.0	57.8

(¥) The best age considered these $^{206}Pb/^{207}Pb$ values for zircons older than 1 Ga and $^{206}Pb/^{238}U$ ages values for zircons younger than 1 Ga (Nemchin and Cawood. 2005).

Nemchin. A.A.; Cawood. P.A. 2005. Discordance of the U-Pb system in detrital zircons: Implication for provenance studies of sedimentary rocks. Sedimentary Geology 182 (1-4): 143-162. doi: 10.1016/j.sedgeo.2005.07.011.

Supplementary material 2

U-Pb Methodology

Zircons were extracted from the rock samples by crushing, milling, gravitational separation and heavy liquids treatment. Crystals were randomly selected (regardless of their size, form or colour) using a stereomicroscope and then mounted in 25 mm epoxy and polished. U-Pb geochronology of zircons was attained by laser ablation multicollector inductively coupled plasma mass spectrometry at the Arizona LaserChron Center (Gehrels *et al*., 2008). The analyses involved ablation of zircon with a New Wave/Lambda Physik DUV193 Excimer laser (operating at a wavelength of 193 nm) using a spot diameter of 25 or 35 µm. The ablated material was carried with helium gas into the plasma source of a GV Instruments Isoprobe equipped with a flight tube of sufficient width that U, Th and Pb isotopes were measured simultaneously. All measurements were made in static mode, using Faraday detectors for ^{238}U and ^{232}Th, an ion-counting channel for ^{204}Pb, and either Faraday collectors or ion counting channels for $^{208\text{-}206}$Pb. Ion yields were *ca.* 1 mV ppm^{-1}. Each analysis consisted of one 20 s integration on peaks with the laser off (for backgrounds), twenty 1 s integrations with the laser firing, and a 30 s delay to purge the previous sample and to prepare for the next analysis. The ablation pit was *ca.* 15 µm in depth. For each analysis, the errors in determining ^{206}Pb/^{238}U and ^{206}Pb/^{204}Pb result in a measurement error of *ca.* 1% (at 2σ level) in the ^{206}Pb/^{238}U age. The errors in measurement of ^{206}Pb/^{207}Pb and ^{206}Pb/^{204}Pb also result in *ca.* 1% (2σ) uncertainty in age for grains that are >1.0 Ga, but are substantially larger for younger grains owing to low intensity of the ^{207}Pb signal. For most analyses, the crossover in precision of ^{206}Pb/^{238}U and ^{206}Pb/^{207}Pb ages occurs at *ca.* 1.0 Ga. Common Pb correction was accomplished by using the measured ^{204}Pb and assuming an initial Pb composition from Stacey and Kramers (1975) (with uncertainties of 1.0 for ^{206}Pb/^{204}Pb and 0.3 for ^{207}Pb/^{204}Pb). The measurement of ^{204}Pb is unaffected by the presence of ^{204}Hg because backgrounds are measured on peaks (thereby subtracting any background ^{204}Hg and ^{204}Pb), and because very little Hg is present in the argon gas. Interelement fractionation of Pb/U is generally *ca.* 20%, whereas fractionation of Pb isotopes is generally <2%. In-run analysis of fragments of a large Sri Lankan zircon crystal (generally every fifth measurement) with known age of 564±4 Ma (2σ error) was used to correct for this fractionation (see Gehrels *et al.*, 2008). The uncertainty resulting from the calibration correction is generally *ca.* 1% (2σ) for both ^{206}Pb/^{207}Pb and ^{206}Pb/^{238}U ages. The reported ages are determined either by the "unmix" algorithm or from the weighted mean of the ^{206}Pb/^{238}U ages of the concordant and overlapping analyses (Ludwig, 2003).

Specification for each sample. The reported uncertainty is based on the scatter and precision of the set of ^{206}Pb/^{238}U or ^{206}Pb/^{207}Pb ages, weighted according to their measurement errors (shown at 1σ). The systematic error, which includes contributions from the standard calibration, age of the calibration standard and composition of common Pb and U decay constants, is generally *ca.* 1-2% (2σ).

References

Gehrels, G.E.; Valencia, V.A.; Ruiz, J. 2008. Enhanced precision, accuracy, efficiency, and spatial resolution of U/Pb ages by laser ablation multicollector inductively coupled plasma mass spectrometry. Geochemistry, Geophysics, Geosystems 9 (3): 13 p. doi: 10.1029/2007GC001805.

Ludwig, K.R. 2003. User's manual for Isoplot 3.00: A geochronological toolkit for Microsoft Excel. Berkeley Geochronological Center, Special Publication 4: 70 p.

Stacey, J.S.; Kramers, J.D. 1975. Approximation of terrestrial lead isotope evolution by a two-stage model. Earth and Planetary Science Letters 26: 207-221.